

CERN-EP-2018-322
2019/04/24

CMS-SMP-18-002

Measurements of the $pp \rightarrow WZ$ inclusive and differential production cross sections and constraints on charged anomalous triple gauge couplings at $\sqrt{s} = 13$ TeV

The CMS Collaboration*

Abstract

The WZ production cross section is measured in proton-proton collisions at a centre-of-mass energy $\sqrt{s} = 13$ TeV using data collected with the CMS detector, corresponding to an integrated luminosity of 35.9 fb^{-1} . The inclusive cross section is measured to be $\sigma_{\text{tot}}(pp \rightarrow WZ) = 48.09_{-0.96}^{+1.00} \text{ (stat)}_{-0.37}^{+0.44} \text{ (theo)}_{-2.17}^{+2.39} \text{ (syst)} \pm 1.39 \text{ (lumi) pb}$, resulting in a total uncertainty of $-2.78/+2.98 \text{ pb}$. Fiducial cross section and ratios of charge-dependent cross section measurements are provided. Differential cross section measurements are also presented with respect to three variables: the Z boson transverse momentum p_T , the leading jet p_T , and the $M(WZ)$ variable, defined as the invariant mass of the system composed of the three leptons and the missing transverse momentum. Differential measurements with respect to the W boson p_T , separated by charge, are also shown. Results are consistent with standard model predictions, favouring next-to-next-to-leading-order predictions over those at next-to-leading order. Constraints on anomalous triple gauge couplings are derived via a binned maximum likelihood fit to the $M(WZ)$ variable.

Published in the Journal of High Energy Physics as doi:10.1007/JHEP04(2019)122.

1 Introduction

The measurement of the diboson production cross section is sensitive to the self-interaction between gauge bosons via triple gauge couplings (TGCs) and is therefore an important test of the standard model (SM). Such couplings directly result from the nonabelian $SU(2) \times U(1)$ gauge symmetry of the SM. In the SM, the values of the couplings are fully determined by the structure of the Lagrangian; any deviation of the observed diboson production strength from the SM prediction, typically manifested as a change in the cross section, would indicate new physics. The expected change would lead to an overall increase of the cross section, although in some portions of phase space there will be a negative interference between the SM and new physics beyond the SM (BSM).

Associated WZ production is particularly interesting, as it is the only process directly sensitive to the WWZ coupling with a Z boson in the final state. Furthermore, WZ production is a major background to searches for new physics in multilepton final states; a precise determination of its cross section is crucial to improve the sensitivity of these searches. In addition, initial state radiation can be used as a probe of the boost of the WZ system through a differential study of the leading jet transverse momentum, since an initial state particle can radiate a jet and this jet will recoil against the WZ system.

In the SM at leading order (LO) in perturbative quantum chromodynamics (QCD), WZ production in proton-proton (pp) collisions proceeds via quark-antiquark interactions in the s -, t -, and u -channels. Figure 1 shows the tree-level production diagrams for each channel. The s -channel, which proceeds through the WWZ TGC, is the only channel sensitive to anomalous values of this coupling.

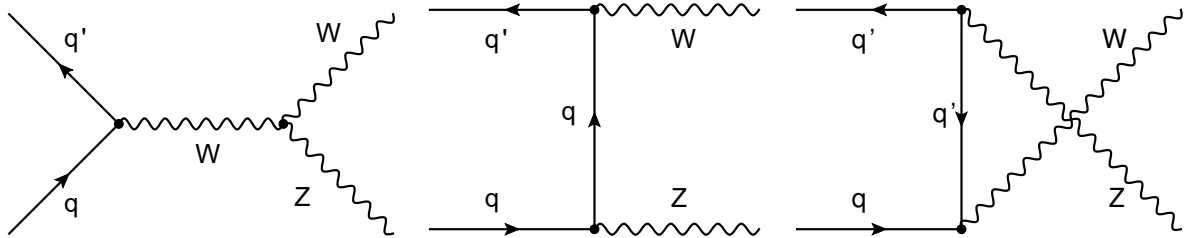


Figure 1: Feynman diagrams for WZ production at leading order in perturbative QCD in proton-proton collisions for the s -channel (left), t -channel (middle), and u -channel (right). The contribution from s -channel proceeds through TGC.

After a first inconclusive observation of candidate events for WZ production at UA1 [1], standard model WZ production has been studied at $\sqrt{s} = 1.96$ TeV at the Fermilab Tevatron [2, 3] and also in pp collisions at the CERN LHC by the ATLAS [4–10] and CMS [11–16] Collaborations. The most relevant of these results to this paper is the CMS analysis reporting the $pp \rightarrow WZ$ production cross section at $\sqrt{s} = 7$ and 8 TeV as well as a search for anomalous TGCs (aTGCs) at $\sqrt{s} = 8$ TeV in the multilepton final state using the full 2011 and 2012 data sets [15]. The ATLAS Collaboration has similarly analyzed the full 8 TeV data set [7], measured the inclusive and differential cross section, and set limits on aTGCs. The inclusive $pp \rightarrow WZ$ production cross section at $\sqrt{s} = 13$ TeV was measured in the multilepton final state by the ATLAS [8] and CMS [14] Collaborations, using the full 2015 data set.

This paper presents a new analysis of $pp \rightarrow WZ$ production at $\sqrt{s} = 13$ TeV using multilepton final states in which the Z boson decays into a pair of electrons or muons, and the W boson decays into a neutrino and either an electron or a muon. Compared to the previous results, the inclusive and differential cross sections are measured with increased precision (the overall

uncertainty in the inclusive cross section is reduced by half), and more stringent confidence intervals on aTGCs are set, yielding the current best limits in two of the parameters.

This paper is organized as follows: the detector is described in Section 2; the data and Monte Carlo (MC) simulated samples are described in Section 3; the object definition and the event selection are described in Section 4 and Section 5, respectively; the background estimation is described in Section 6, and the systematic uncertainties affecting the analysis are described in Section 7. Finally, the inclusive cross section measurement is presented in Section 8, the differential cross section measurement is presented in Section 9, and the confidence regions for aTGCs are presented in Section 10. A summary of the results is shown in Section 11.

2 The CMS Detector

The central feature of the CMS apparatus is a superconducting solenoid of 6 m internal diameter, providing a magnetic field of 3.8 T. Within the solenoid volume are a silicon pixel and strip tracker, a lead tungstate crystal electromagnetic calorimeter (ECAL), and a brass and scintillator hadron calorimeter (HCAL), each composed of a barrel and two endcap sections. Forward calorimeters extend the pseudorapidity coverage provided by the barrel and endcap detectors. Muons are detected in gas-ionization chambers embedded in the steel flux-return yoke outside the solenoid.

Events of interest are selected using a two-tiered trigger system [17]. The first level (L1), composed of custom hardware processors, uses information from the calorimeters and muon detectors to select events at a rate of around 100 kHz within a time interval of less than 4 μ s. The second level, known as the high-level trigger (HLT), consists of a farm of processors running a version of the full event reconstruction software optimized for fast processing, and reduces the event rate to around 1 kHz before data storage.

A more detailed description of the CMS detector, together with a definition of the coordinate system used and the relevant kinematic variables, can be found in Ref. [18].

3 Data and simulated samples

This study is performed using proton-proton (pp) collisions at a centre-of-mass energy of 13 TeV at the LHC. Data taken in 2016 with the CMS detector are analyzed, corresponding to a total integrated luminosity of 35.9 fb⁻¹. The data are filtered to remove detector noise and unphysical events.

Event generators based on the MC method are used to simulate the behaviour of signal and background processes. The POWHEG v2.0 [19, 20] software is used to generate both the WZ signal and the ZZ background samples without additional partons besides the ones included in the matrix element calculations at next-to-leading order (NLO) in perturbative QCD. The rest of the SM background samples are produced with the MADGRAPH5_aMC@NLO v2.3.3 generator [21] at LO or NLO accuracy, including up to one or two additional partons in the matrix element calculations. The procedure for accounting correctly for parton multiplicities larger than one is referred to as the merging scheme; where applicable, the FxFx merging scheme [22] is used for the NLO samples, and the MLM merging scheme [23] is used for the LO samples. The modelling of the aTGCs is done by applying the matrix element reweighting method [24] at LO accuracy to a signal sample generated with the MADGRAPH5_aMC@NLO v2.3.3 generator [21] at NLO accuracy. The procedure is applied to a set of samples produced for different ranges of the Z boson transverse momentum (p_T^Z) such that the statistical power of the

MC at higher energies, where anomalous couplings are expected to dominate, is enhanced. The NNPDF3.0LO (NNPDF3.0NLO) [25] parton distribution functions (PDFs) are used for the simulated samples generated at LO (NLO). The computations are interfaced with the PYTHIA v8.205 generator [26] to include the effects of parton showering and hadronization using the CUETP8M1 tune [27, 28].

The effect of additional interactions in the same or adjacent bunch crossing (referred to as pileup) is accounted for by simulating additional minimum bias interactions for each hard scattering event. Simulated events are then reweighted so that the pileup distribution matches that observed in data, which is characterized by an average of 23 collisions per bunch crossing. The generated events are interfaced with a model of the CMS detector response implemented using the GEANT4 package [29] and reconstructed using the same software as the real data.

4 Event reconstruction and object selection

4.1 Event Reconstruction

Events are reconstructed using the particle-flow (PF) algorithm [30] by matching information from all CMS subdetectors to obtain a global description of the event. The resulting objects are classified into mutually exclusive categories: charged hadrons, neutral hadrons, photons, electrons, and muons.

Interaction vertices are identified by grouping tracks consistent with originating from the same location in the beam interaction region. The reconstructed vertex with the largest value of summed physics-object p_T^2 is taken to be the primary pp interaction vertex. The aforementioned physics objects are the jets, clustered using the jet finding algorithm [31, 32] with the tracks assigned to the vertex as inputs, and the associated missing transverse momentum, taken as the negative vector sum of the p_T of those jets. More details are given in Section 9.4.1 of Ref. [33].

Photons are identified as ECAL energy clusters not linked to the extrapolation of any charged particle trajectory to the ECAL, but are not used in this analysis. Electrons are identified as a primary charged particle accompanied by potentially many ECAL energy clusters [34]; such clusters are matched to the extrapolation of this track to the ECAL and to possible bremsstrahlung photons emitted along the way through the tracker material. Muons are identified as a track in the central tracker consistent with either a track or several hits in the muon system, in association with an energy deficit in the calorimeters. Charged hadrons are identified as charged particle tracks neither identified as electrons, nor as muons. Finally, neutral hadrons are identified as HCAL energy clusters not linked to any charged-hadron trajectory, or as ECAL and HCAL energy excesses with respect to the expected charged-hadron energy deposit. The energy of photons is directly obtained from the ECAL measurement, corrected for zero-suppression effects. The energy of electrons is determined from a combination of the track momentum at the main interaction vertex, the corresponding ECAL cluster energy, and the energy sum of all bremsstrahlung photons attached to the track. The energy of muons is obtained from the corresponding track momentum. The energy of charged hadrons is determined from a combination of the track momentum and the corresponding ECAL and HCAL energy, corrected for zero-suppression effects and for the response function of the calorimeters to hadronic showers. Finally, the energy of neutral hadrons is obtained from the corresponding corrected ECAL and HCAL energy.

4.2 Electrons and muons

In this analysis, leptons [35] coming from the primary vertex play a prominent role amongst all reconstructed event objects because of the very distinct trilepton (3ℓ) signature of the signal process. *Prompt signal leptons* are defined as the light leptons (electrons or muons) from the decays of particles in the signal processes, such as those coming from W and Z boson and τ lepton decays. Leptons originating from hadrons, primarily b hadron decays, are referred to as *nonprompt leptons*.

Electrons are reconstructed as described in Section 4.1; candidates are further required to have $|\eta| < 2.5$, to be within the tracking acceptance, and to have $p_T > 7\text{ GeV}$. The identification is performed using a multivariate discriminant with inputs related to the shower shape and to the tracking and track-cluster matching. Additional identification criteria are applied for electrons with $p_T > 30\text{ GeV}$ to mimic the identification applied at trigger level described in Section 5; this ensures consistency between the *measurement* region and *application* region of the misidentification rate estimate.

Muon candidates are reconstructed as described in Section 4.1 by combining the information from both the silicon tracker and the muon spectrometer in a global fit [36]. Candidates are identified by checking the quality of the geometrical matching between the tracker and the muon system measurements. Only candidates within the muon system acceptance $|\eta| < 2.4$ and with $p_T > 5\text{ GeV}$ are considered.

The energy scale of the leptons is corrected to account for mismeasurements in the tracker and muon systems, and in the ECAL. For both electrons and muons, the average difference between the corrected and uncorrected energies is zero; however, a spread is induced in the lepton p_T of about 1% that is assigned as a systematic uncertainty in the energy of each lepton.

In order to improve the rejection of pileup and misreconstructed tracks and, more importantly, to reject background leptons from b hadron decays, loose selections are applied to variables related to the track impact parameter, as described in Refs. [37, 38].

The charged leptons produced in decays of heavy particles, such as W and Z bosons, are typically spatially isolated from the hadronic activity in the event, whereas the leptons produced in the decays of hadrons or misidentified leptons are usually spatially embedded in jets. For high-energy W and Z bosons the decay products tend to be collimated (a boosted system) and this distinction based on a simple definition of isolation is not effective anymore.

Therefore, the PF-based isolation definition used in the $\sqrt{s} = 8\text{ TeV}$ analysis [15], which included all the photons and the neutral and charged hadrons in a cone of $\Delta R = \sqrt{(\eta^\ell - \eta^i)^2 + (\phi^\ell - \phi^i)^2} < 0.3$ (where i indicates the hadrons and ℓ the lepton) around the leptons, is improved [39, 40] by using a p_T -dependent cone size given by the formula:

$$\Delta R(p_T(\ell)) = \frac{10\text{ GeV}}{\min[\max(p_T(\ell), 50\text{ GeV}), 200\text{ GeV}]}. \quad (1)$$

The discrimination between prompt leptons and nonprompt leptons is improved by exploiting the differences in isolation-related variables and in impact-parameter-related variables between the two categories of leptons (prompt and nonprompt). An identification algorithm, based on a multivariate analysis (MVA) using boosted decision trees (BDTs), is trained to discriminate signal leptons (from W and Z decays) from background leptons (mostly b hadron decays). The resulting classifier is referred to as the *lepton MVA discriminator*, and was trained using a sample of $t\bar{t}Z$ events: signal leptons originate from leptonic $t\bar{t}Z$ decays, and background

leptons originate mostly from b hadron decays. Further details on the lepton MVA discriminator can be found in Refs. [37, 38]. The efficiencies have a high dependence on the lepton p_T and η ; typical values for electrons are 3–7% misidentification efficiency and 20/40/80/90% identification efficiency for low p_T electrons in the endcap, low p_T electrons in the barrel, high p_T electrons in the endcap, and high p_T electrons in the barrel, respectively. For muons, typical values are 2–10% misidentification efficiency and 80–100% identification efficiencies where higher values correspond to higher p_T muons.

Throughout the analysis, leptons passing a high threshold on the lepton MVA discriminator are referred to as *tight* leptons.

4.3 Jets

Jets are reconstructed by clustering PF candidates using the anti- k_T algorithm [31, 32] with a distance parameter of 0.4. The jet momentum is determined as the vector sum of all particle momenta in the jet, and is estimated from simulation to be within 5–10% of the true momentum over the whole p_T spectrum and detector acceptance [41]. Charged hadrons not originating from the primary vertex are subtracted from the PF candidates considered in the clustering; this procedure is referred to as charged-hadron subtraction. Jet energy corrections are derived from simulation to bring the measured response of jets to that of particle level jets on average, and are applied to the energy of the jet as a function of the jet p_T and η . In situ measurements of the momentum balance in dijet, photon+jet, Z +jet, and multijet events are used to correct for any residual differences in jet energy scale between data and simulation [42]. The jet energy resolution amounts typically to 15% at 10 GeV, 8% at 100 GeV, and 4% at 1 TeV. Additional selection criteria are applied to each jet to remove jets potentially dominated by anomalous contributions from various subdetector components or reconstruction failures [43]. Jets with a minimum $p_T > 30$ GeV are required to be separated from any lepton candidate passing the minimal lepton selection by selecting $\Delta R = \sqrt{(\eta^\ell - \eta^{jet})^2 + (\phi^\ell - \phi^{jet})^2} > 0.4$.

The combined secondary vertex (CSV) b tagging algorithm [44] is used to identify jets that are likely to originate from the hadronization of bottom quarks (referred to as b jets). This algorithm combines both secondary vertex information and track impact parameter information together in a likelihood discriminant with output values ranging from zero to one. A jet is tagged as a b jet if the CSV discriminator output exceeds a threshold value, referred to as the *working point*. This analysis uses the medium working point corresponding to requiring that $CSV > 0.8$. This working point gives approximately 70% efficiency for tagging b jets and 1.5% efficiency for mistakenly tagging jets coming from light quarks or gluons [44]. Jets that pass the medium CSV working point and have a minimum $p_T > 30$ GeV are defined in this analysis as b jets.

Corrections accounting for differences in the b tagging performance between data and simulation are derived by applying weights dependent on the jet p_T , η , b tagging discriminator, and flavour to each simulated jet [44]. The jet flavour is defined as the flavour of the object originating the jet, which is known in simulation. The weights are derived from $t\bar{t}$ and Z+jets events. The per-event weight is defined as the product of the per-jet weights, including the weights of the jets overlapping with leptons. Uncertainties in the weights are propagated throughout the analysis as systematic uncertainties.

4.4 Missing transverse momentum

The missing transverse momentum vector is computed as the negative vector p_T sum of all PF objects identified in the event. The magnitude of this vector is referred to as p_T^{miss} . The jet

energy corrections, introduced previously, are propagated to the estimation of p_T^{miss} .

5 Event selection

Events with contributions from beam halo processes or calorimeter noise are rejected using dedicated filters [45, 46]. The remaining events are required to pass one of several triggers involving either a single loosely isolated light lepton or a pair of them with any flavour composition. For the single-lepton cases, the p_T threshold is 27 (24) GeV for electrons (muons). The lower p_T thresholds for the same-flavour dilepton triggers are 23 (17) GeV for the leading and 12 (8) GeV for the subleading electron (muon). The cross-flavour triggers require a leading lepton p_T of 23 GeV and a subleading lepton p_T of 8 GeV.

The baseline selection is defined by the presence of at least three tight leptons with at least one opposite-sign same-flavour (OSSF) pair. To exploit the specific kinematic properties of the process, each of the three leading leptons is tentatively assigned to its most likely parent boson. The first stage of the algorithm assigns the OSSF pair of leptons with an invariant mass closest to the Z boson mass [47], m_Z , to the Z boson. These two leptons are denoted as ℓ_{Z1} (leading) and ℓ_{Z2} (subleading), ranked by p_T . The remaining lepton is assigned to the W boson and is denoted as ℓ_W . The performance of the algorithm is studied by using simulated events and comparing the assigned parent particle with MC generator level truth; this algorithm properly assigns the leptons in about 95% of cases.

The baseline selection includes additional requirements on the p_T of each lepton: $p_T(\ell_{Z1}) > 25$ GeV, $p_T(\ell_{Z2}) > 10$ GeV, and $p_T(\ell_W) > 25$ GeV. The total efficiency of the set of triggers used to record the data is measured to be close to 99% with respect to this baseline selection; this is because all the trigger paths can be triggered by more than one object, yielding a very high efficiency for the combined set of triggers even if the efficiency of the individual triggers is lower. The baseline selection is split, on the basis of the flavour composition of the leptonic triplet, into four categories denoted as: eee , $ee\mu$, $e\mu\mu$, and $\mu\mu\mu$.

The signal region (SR) is defined by applying to the baseline selection additional requirements that are designed to increase the purity of the region by reducing specific background contributions. Consistency with the Z boson mass peak is enforced by requiring the invariant mass of the two leptons assigned to the Z boson to be close to m_Z , $|M(\ell_{Z1}\ell_{Z2}) - m_Z| < 15$ GeV. This requirement greatly reduces the contribution from nonresonant multilepton production processes such as $t\bar{t}$ production. A requirement that $p_T^{\text{miss}} > 30$ GeV is found to greatly reduce the Z+jets background contribution; in the following, residual events are included in the contribution labelled *nonprompt*. A large reduction in the number of events that include both a $t\bar{t}$ pair and a Z boson is obtained by rejecting events that contain one or more b-tagged jets. The invariant mass of the tripleton system $M(\ell_{Z1}\ell_{Z2}\ell_W)$ is required to exceed 100 GeV. Finally, contributions from tetrileptonic decays in ZZ events are reduced by rejecting any event with an additional fourth lepton that passes a looser lepton selection. Generator-level requirements for the signal, designed to avoid infrared divergences, are matched at reconstruction level by vetoing events that do not contain a lepton pair passing a minimum invariant mass requirement of $M(\ell\ell') > 4$ GeV. This requirement also has the desirable effect of reducing the contribution from low-mass resonance processes. The distribution of the key observables used in the definition of the signal region after the signal extraction fit is displayed in Fig. 2.

Multiple control regions (CRs) are defined to cross-check or estimate the different background processes. Each of them follows the same selection as the signal region, except that individual specific selection criteria are inverted in order to increase the fraction of the targeted back-

ground process in the region. A summary of the three orthogonal control regions used in the analysis is presented in Table 1. The control regions are labelled according to the expected dominant background process in each region. A detailed explanation of their use is given in the next section.

Table 1: Requirements for the definition of the signal region of the analysis and the three different regions designed to estimate the main background sources.

Region	N_ℓ	$p_T\{\ell_{Z1}, \ell_{Z2}, \ell_W, \ell_4\}$ [GeV]	N_{OSSF}	$ M(\ell_{Z1}\ell_{Z2}) - m_Z $ [GeV]	p_T^{miss} [GeV]	$N_{\text{b tag}}$	$\min(M(\ell\ell'))$ [GeV]	$M(\ell_{Z1}\ell_{Z2}\ell_W)$ [GeV]
SR	=3	$>\{25, 10, 25\}$	≥ 1	< 15	> 30	=0	> 4	> 100
CR-top	=3	$>\{25, 10, 25\}$	≥ 1	> 5	> 30	> 0	> 4	> 100
CR-ZZ	=4	$>\{25, 10, 25, 10\}$	≥ 1	< 15	> 30	=0	> 4	> 100
CR-Conv	=3	$>\{25, 10, 25\}$	≥ 1	> 15	≤ 30	=0	> 4	< 100

6 Background estimation

The background contributions fall in two categories, depending on the origin of the final-state leptons. *Prompt* background sources consist of the SM processes where the leptons originate in the decay of an SM boson or τ lepton; the *nonprompt* backgrounds consist of SM processes where the leptons originate in the decay of b hadrons.

The nonprompt background contributions are heavily dominated by Z+jets production, with additional contributions from dileptonic $t\bar{t}$ decays. The total contribution of these processes to the signal region is estimated using the *tight-to-loose* method described in detail in Ref. [40]. The probability for a loose lepton to pass the tight criteria is measured in a single-lepton+jets signal region enriched in nonprompt leptons. For each specific selection, an application region is defined starting from the same requirements and additionally requesting that at least one of the leptons passes the loose selection but fails the tight selection. Depending on the p_T , $|\eta|$, and multiplicity of the failing leptons, the extrapolation from the control region to the application region is derived for each event as a transfer factor, based on the previously measured probability. The contamination of the application region due to the prompt contribution is estimated from simulation and its effect is subtracted from the total nonprompt estimation in the selection, using the same transfer factors. Uncertainties in the determination of the nonprompt contribution are estimated with simulated events by comparing the prediction of the method and the one derived directly from simulation; they are found to be dominated by the statistical uncertainty due to the limited amount of simulated events, and estimated to be about 30%. An additional source of systematic uncertainty is estimated to range between 5 and 30% from the differences observed amongst a number of methods used for the subtraction of the prompt background processes in the signal region.

The leading SM prompt background comes from the tetraleptonic decay of ZZ pairs when one of the produced leptons is too soft or does not pass the quality requirements of the identification selection. Our estimation of the contribution of this process is based on MC simulation. To validate the behaviour of this simulation we use a dedicated sideband region (CR-ZZ) that requires exactly four leptons in the final state; the resulting selection is dominated by ZZ production, therefore no additional ZZ-specific constraint is applied. To illustrate the behaviour of this associated control region, the key observables used in the different measurements of the analysis are shown in Fig. 3. As a numerical cross-check, we estimate the possible variations over the simulated prediction in the four flavour-dependent categories. For each category, we subtract the predicted non-ZZ yields from the observed data and divide the result by the expected ZZ contribution. Statistical and normalization uncertainties are propagated to this measurement.

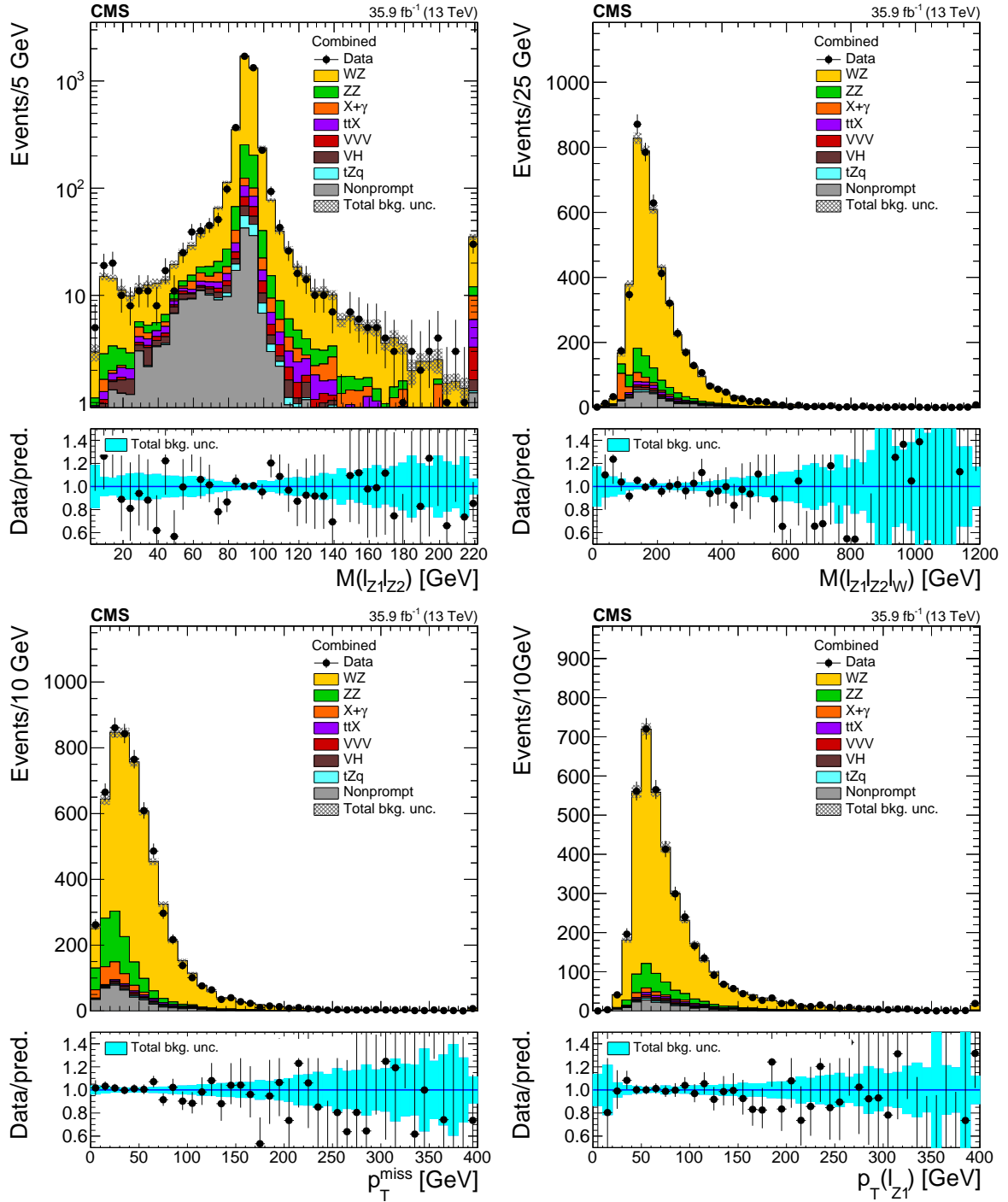


Figure 2: Distribution of key observables in the signal region after the signal extraction fit: invariant mass of the lepton pair assigned to the Z boson (top left), invariant mass of the three-lepton system (top right), missing transverse momentum (bottom left), and transverse momentum of the leading lepton assigned to the Z boson. For each distribution all the signal region requirements are applied except the requirement relating to the particular observable so that the effect of the requirement on that observable can be easily seen. The last bin contains the overflow. Vertical bars on the data points include the statistical uncertainty and shaded bands over the prediction include the contributions of the different sources of uncertainty at their values after the signal extraction fit.

The numerical values are consistent with unity for all categories and for the whole region, the value of the data minus the background divided by the predicted ZZ yield is $q_{ZZ} = 0.99 \pm 0.09$.

Top quark enriched prompt processes are dominated by $t\bar{t}Z$ and tZq production, where the Z boson and one of the top quarks decay leptonically. A procedure similar to the one used for the estimation of the ZZ background is performed in CR-top region. The key observables of the analysis in this sideband region are shown in Fig. 4. The estimation procedure results in good agreement across the different flavour categories; the global quotient of data minus background over the predicted $t\bar{t}Z$ plus tZq yields is consistent with unity, $q_{t\bar{t}Z+tZq} = 1.09 \pm 0.20$.

The last major background that contributes to our search is the production of asymmetrical final-state photon conversions. The production of $Z\gamma$ events makes up 99% of this contribution. The lepton assignment algorithm tends to match the electron originating from the photon to the W boson so the contribution in the eee and $e\mu\mu$ categories is highly enhanced. The procedure used for the prompt contributions is used to validate the behaviour of the simulated conversion processes in a region denoted as CR-conv and defined in Table 1.

Good agreement is found in the $e\mu\mu$ and eee categories, where sufficient statistical power is available. The normalization of the $X+\gamma$ background is estimated from the difference between the data and the other backgrounds, divided by the $X+\gamma$ ($X=t\bar{t}, V, t$) SM prediction; the result is $q_{X+\gamma} = 1.11 \pm 0.14$, consistent with unity. Validation plots for key observables used in the analysis are shown in Fig. 5.

Additional minor background contributions include the leptonic decays of multiboson production processes, dominated by VH and VVV production where V is either the Z or the W boson and H is the SM Higgs boson. Their contribution is estimated from simulation.

7 Systematic uncertainties

The major sources of systematic uncertainty can be grouped into three different categories: normalization uncertainties that are assigned to each of the background processes individually; global uncertainties related to the definition and energy measurement of the different physical objects, affecting both the background and signal acceptances; and a global uncertainty, correlated across all processes, that accounts for a possible mismeasurement of the total integrated luminosity.

As stated in Section 6, the contribution from prompt SM processes is estimated using MC samples and validated in appropriate control regions. The uncertainties in the normalization of such processes are taken from experimental measurements performed at a centre-of-mass energy of $\sqrt{s} = 13$ TeV, and correspond to assigning flat uncertainties of 7, 15, and 35% to the contributions of the ZZ, $t\bar{t}V$, and tZq background processes respectively [48–50]. The uncertainty in the normalization of the photon conversion background contribution is obtained from the observations in the dedicated control region, and estimated to be about 20%. The normalization uncertainties applied to the minor contributions of the multiboson production are estimated to be about 25% for the VH process and 50% for the VVV ones.

The nonprompt background estimation includes two different sources of systematic uncertainties. First, a 30% normalization uncertainty is applied to account for the observed variations in the performance of the method when applied to MC simulations. Second, a p_T - and η -dependent uncertainty that ranges between 5 and 30% is applied to account for the differences observed amongst different W/Z background subtraction procedures considered for the tight-to-loose method.

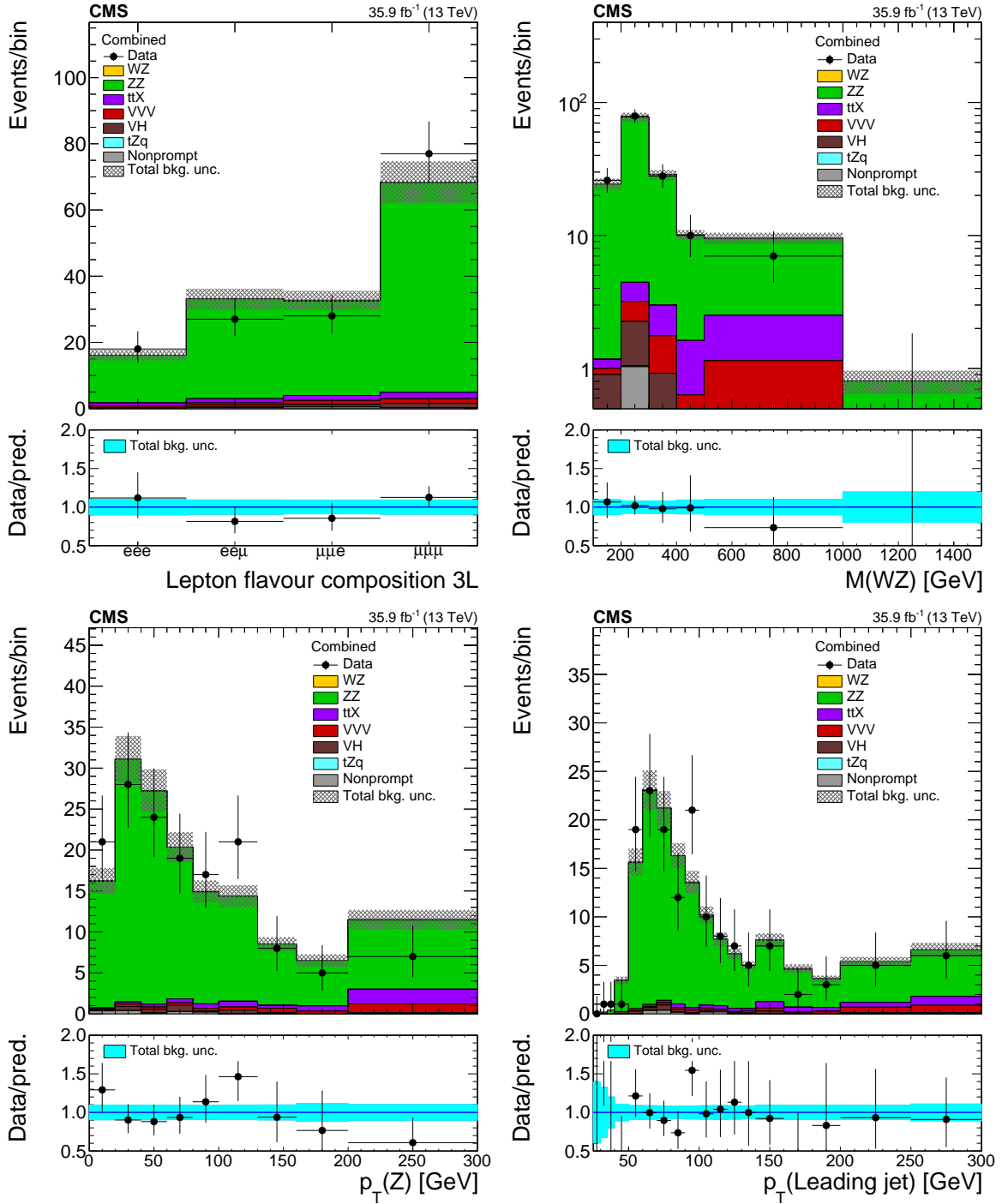


Figure 3: Distribution of key observables in the ZZ control region defined in Table 1: flavour composition of the three leading leptons (top left), invariant mass of the three leptons plus missing transverse momentum (top right), transverse momentum of the Z boson reconstructed from the p_T of the two leptons assigned to it (bottom left), and transverse momentum of the leading jet (bottom right). Vertical bars on the data points include the statistical uncertainty and shaded bands over the prediction include the contributions of the different sources of uncertainty evaluated after the signal extraction fit.

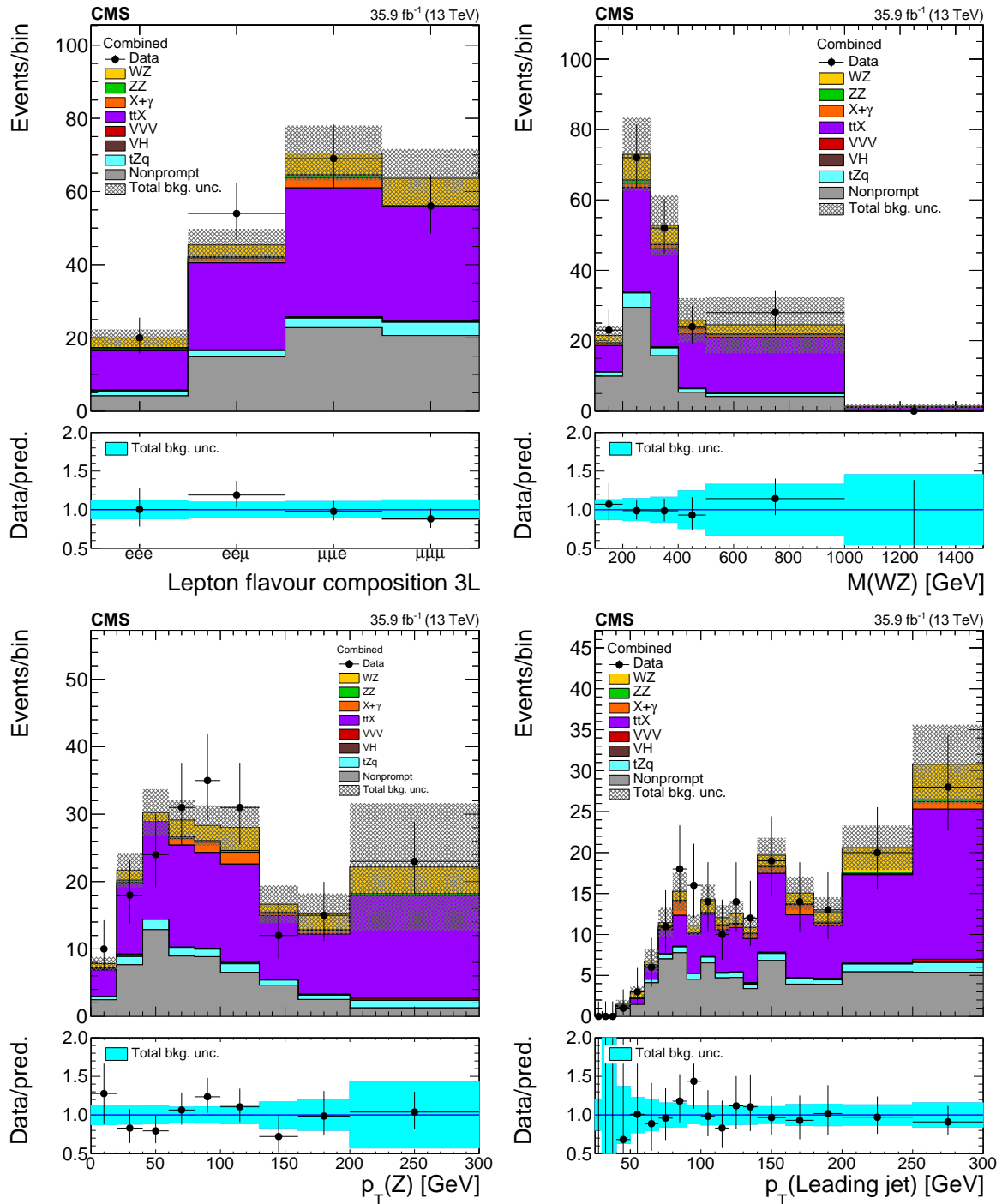


Figure 4: Distribution of key observables in the top enriched control region defined in Table 1: flavour composition of the three leading leptons (top left), invariant mass of the three lepton plus missing transverse momentum (top right), transverse momentum of the Z boson reconstructed from the p_T of the two leptons assigned to it (bottom left), and transverse momentum of the leading jet (bottom right). Vertical bars on the data points include the statistical uncertainty and shaded bands over the prediction include the contributions of the different sources of uncertainty evaluated after the signal extraction fit.

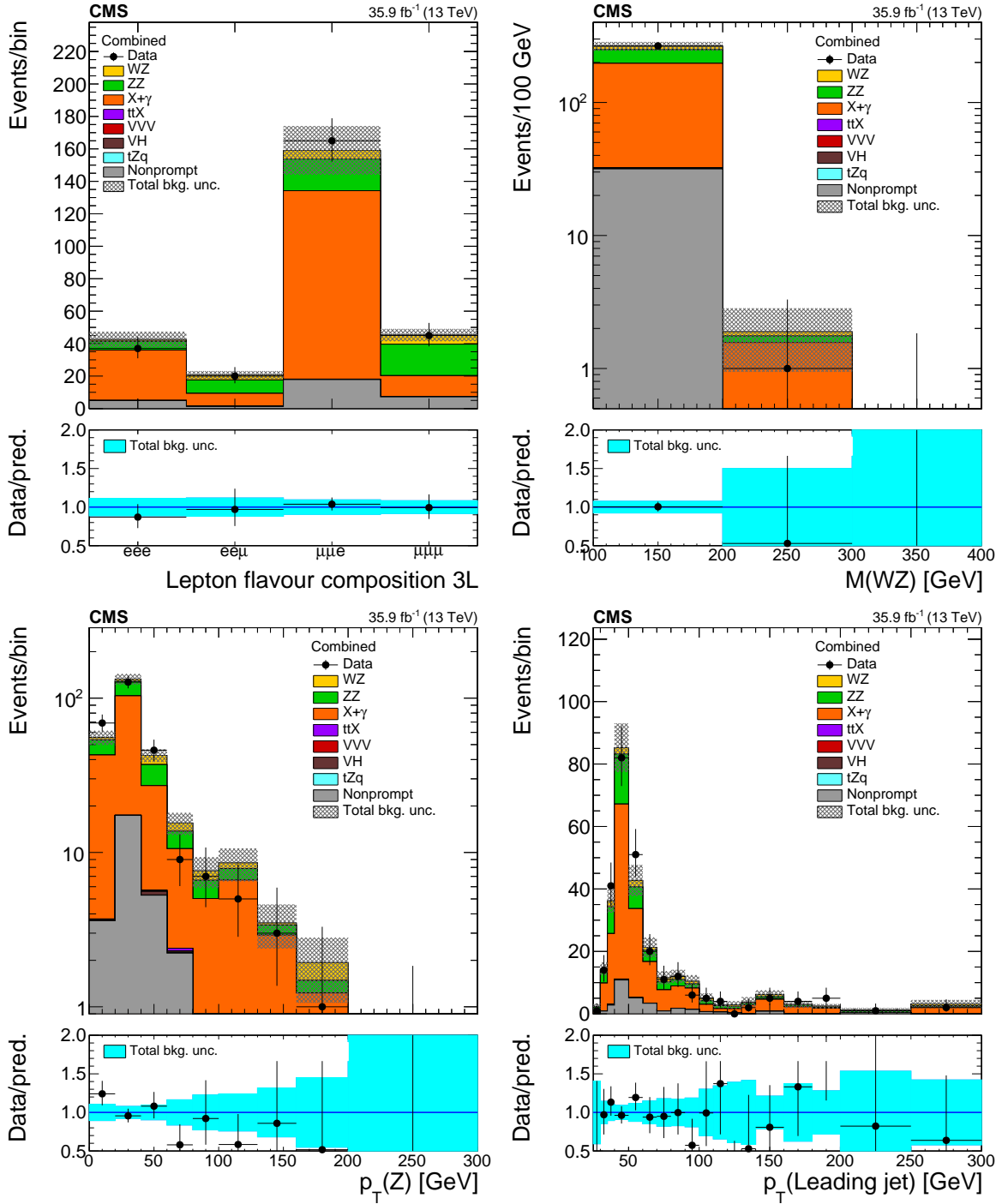


Figure 5: Distribution of key observables in the conversion control region defined in Table 1: flavour composition of the three leading leptons (top left), invariant mass of the three lepton plus missing transverse momentum (top right), transverse momentum of the Z boson reconstructed from the p_T of the two leptons assigned to it (bottom left), and transverse momentum of the leading jet (bottom right). Vertical bars on the data points include the statistical uncertainty and shaded bands over the prediction include the contributions of the different sources of uncertainty evaluated after the signal extraction fit.

Lepton identification and isolation introduce a sizeable uncertainty in the final measurement. Lepton efficiencies are computed using the tag-and-probe technique [11, 34, 51]. Since electron and muon identification efficiencies are computed separately, the uncertainty in their estimate is split by flavour and evaluated separately. The largest effects are in the eee category for the electron efficiency (about 5%) and in the $\mu\mu\mu$ category for the muon efficiency (about 3%). The uncertainty in the energy scale of the leptons is estimated to produce a variation of 1% in their p_T ; the reconstructed muon p_T is computed with a different method for high- p_T muons (above 200 GeV), thus a conservative 5% uncertainty is assigned to each high- p_T muon. The uncertainty in the lepton energy scale is assigned to each lepton—separately for electrons and muons—and propagated to the yields, with effects smaller than 1% in most cases.

A total trigger efficiency uncertainty is applied across all channels and processes to account for the differences observed between data and MC samples. Two different sources are considered for the estimation of this uncertainty. First, trigger efficiencies are measured in data and simulation samples, with the difference between the two being assigned as a systematic component of the trigger efficiency uncertainty. Second, the effect of limited statistical power in the data measurement is computed using Clopper–Pearson intervals [52], which is an estimation method that yields intervals in the physical region using an estimation that is statistically robust even when the efficiency is close to its extreme values—in this case the value 1—, and added quadratically to the first source. A final asymmetric flat uncertainty of -1.8 and $+1.4\%$ is applied.

The efficiency of the b tag veto is also corrected by comparing the measurements in data and simulation and propagated to each of the events. Separate uncertainty sources are considered for the b jet identification efficiency and the misidentification of light-flavour jets as b-tagged jets, with effects of up to 1.6 and 0.7% in the final signal acceptance, respectively.

Each of the reconstructed jets has an associated energy scale uncertainty of 2–10% depending on its p_T and η . The final measurement is sensitive to this kind of variation through the changes in acceptance that arise in the p_T^{miss} estimations and the b tag veto. The effect on the final signal acceptance amounts to about 1%.

The pileup modelling uncertainty is evaluated by varying the inelastic cross section up and down by 5% and propagating the effect to the final signal region, resulting in an uncertainty of up to 1.2%.

A fiducial region is defined by imposing requirements that mimic the lepton kinematic characteristics in the signal region. The acceptance \mathcal{A} is defined as the fraction of events in the total phase space that pass the requirements of the fiducial region. The efficiency ϵ is estimated as a transfer factor from the fiducial region to the signal region. Both acceptance and efficiency are estimated using generator-level information; details on the fiducial region, the acceptance, and the efficiency are provided in Section 8. Two sources of theoretical uncertainty in \mathcal{A} and ϵ are considered. Effects due to factorization (μ_F) and renormalization (μ_R) scale choices are evaluated with POWHEG by varying the scales up and down independently by a factor of two around the nominal value $\mu_0 = (m_Z + m_W)/2$, under the constraint $0.5 < \mu_F/\mu_R < 2.0$. The envelope of the set of variations is assigned as a systematic uncertainty on the yields. Parametric (PDF $+\alpha_S$) uncertainties are estimated using the PDF4LHC prescription [53] with the NNPDF3.0 set [25].

Finally, a 2.5% correlated normalization uncertainty is applied to all signal and background processes to account for the variations in the measurement of the total integrated luminosity [54].

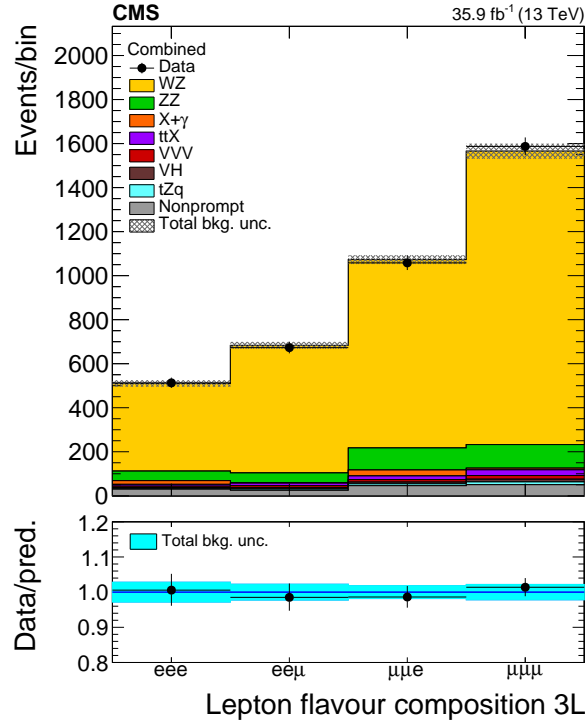


Figure 6: Distribution of expected and observed event yields in the four flavour categories used for the cross section measurement. Vertical bars on the data points include the statistical uncertainty and shaded bands over the prediction include the contributions of the different sources of uncertainty evaluated after the signal extraction fit.

8 Inclusive measurement

The inclusive WZ production cross section is measured by performing a simultaneous maximum likelihood fit to the total yields in the four flavour categories of the signal region, as presented in Fig. 6. The normalization of the WZ signal process is modelled via a parameter representing a multiplicative factor for the total NLO production cross section; the parameter is referred to as signal strength r_{WZ} and is a free parameter in the fit.

The contributions from the background processes are allowed to vary around the predicted yields, according to the systematic contributions described in Section 7. The systematic contributions are modelled in the likelihood as nuisance parameters with log-normal priors. The expected and observed yields for the processes involved in each of the flavour categories can be seen in Table 2. The final contribution of the different sources of uncertainty to the measurement is described in Table 3.

A fiducial region is defined by imposing requirements that mimic the lepton kinematic characteristics in the signal region. We require three light leptons located inside the detector acceptance, $|\eta^\ell| < 2.5(2.4)$ for electrons (muons), with at least one OSSF pair. Electrons and muons from $W/Z \rightarrow \tau + X \rightarrow \ell + X$ decays are included in this selection. These leptons are assigned to the W and Z bosons using the algorithm described in Section 5. Minimum transverse momenta requirements of $p_T(\ell_{Z1}) > 25$ GeV, $p_T(\ell_{Z2}) > 10$ GeV, and $p_T(\ell_W) > 25$ GeV are applied. We also apply the two additional criteria $M(\ell_{Z1}\ell_{Z2}\ell_W) > 100$ GeV and $|M(\ell_{Z1}\ell_{Z2}) - m_Z| < 15$ GeV. The total yields in the signal region for the expected background, N_{bkg} , and observed data, N_{obs} ,

Table 2: Expected and observed yields for each of the relevant processes and flavour categories. Combined statistical and systematic uncertainties are shown for each case except for the observed data yields for which only statistical uncertainties are presented. All expected yields correspond to quantities estimated after the maximum likelihood fit. Uncertainties are computed taking into account the full correlation matrix between sources of uncertainty, processes, and flavour categories.

Process	eee	ee μ	e $\mu\mu$	$\mu\mu\mu$	Total
Nonprompt	30.0 ± 12.4	25.0 ± 10.4	45.7 ± 20.7	50.3 ± 19.3	151 ± 63
ZZ	43.4 ± 4.1	44.4 ± 3.4	100.1 ± 9.2	107.1 ± 8.3	295 ± 24
X γ	16.8 ± 5.2	2.0 ± 0.7	26.9 ± 8.8	7.6 ± 2.0	53 ± 16
t \bar{t} V	8.5 ± 2.8	11.6 ± 4.1	16.8 ± 5.5	25.8 ± 9.0	63 ± 21
VVV	6.2 ± 2.5	8.6 ± 3.4	11.4 ± 4.6	16.9 ± 6.8	43 ± 17
VH	3.3 ± 0.8	6.4 ± 1.6	7.7 ± 1.9	12.1 ± 3.0	29.6 ± 7.2
tZq	3.9 ± 1.30	5.7 ± 1.9	8.4 ± 2.8	12.6 ± 4.3	31 ± 10
Total background	112 ± 15	104 ± 15	217 ± 28	233 ± 29	666 ± 45
WZ	398 ± 18	579 ± 21	856 ± 29	1333 ± 47	3166 ± 62
Data	513 ± 23	673 ± 26	1058 ± 32	1587 ± 40	3831 ± 62

are used to obtain the fiducial cross section of the WZ process through the expression:

$$\sigma_{\text{fid}}(\text{pp} \rightarrow \text{WZ}) = \frac{N_{\text{obs}} - N_{\text{bkg}}}{\epsilon \mathcal{L}}, \quad (2)$$

where the efficiency ϵ is estimated as a transfer factor from the fiducial region to the signal region using MC truth and the integrated luminosity \mathcal{L} amounts to 35.9 fb^{-1} . Scale and PDF uncertainties are considered in the computed efficiency and are propagated to the final cross section measurement. Table 4 summarizes the efficiencies and their uncertainties. Final state generator-level leptons are *dressed* by adding to their momenta those of generator-level photons within a cone of $\Delta R(\ell, \gamma) < 0.1$. The efficiency is estimated from simulation for each of the flavour channels separately, and for the inclusive case, as the ratio of expected reconstructed events in the signal region to the number of generated trilepton events in the fiducial region. The statistical uncertainty in the measurement of the efficiency, which originates from the limited number of simulated events, is below 1% and is added quadratically to the total sum of statistical uncertainties in the measurement. Theoretical uncertainties in the cross section measurements arise from renormalization and factorization scale and PDF uncertainties and are added quadratically to the experimental uncertainties. The results are presented in Table 5 and can be compared to the NLO prediction from POWHEG + PYTHIA of $\sigma_{\text{fid}}^{\text{POWHEG}} = 227.6_{-7.3}^{+8.8}$ (scale) ± 3.2 (PDF) fb; the NLO prediction is disfavoured by this measurement.

The phase space used for the computation of the total cross section is defined by having three generated light leptons that pass the requirement $60 \text{ GeV} < m_Z^{\text{OSSF}} < 120 \text{ GeV}$, where m_Z^{OSSF} is the mass closest to the Z boson mass among those computed with all possible OSSF lepton pairs. Light leptons originating from tau decay are included in the definition of the total region selection. The extrapolation to the total associated production cross section of WZ bosons is computed as:

$$\sigma_{\text{tot}}(\text{pp} \rightarrow \text{WZ}) = \frac{N_{\text{obs}} - N_{\text{bkg}}}{\mathcal{B}(W \rightarrow \ell + X) \mathcal{B}(Z \rightarrow \ell' \ell' + X) \mathcal{A} \epsilon \mathcal{L}'}, \quad (3)$$

where the leptonic branching ratios of the W and Z bosons, $\mathcal{B}(W \rightarrow \ell + X) = \mathcal{B}(W \rightarrow \ell + \nu) + \mathcal{B}(W \rightarrow \tau + \nu) \mathcal{B}(\tau \rightarrow \ell + 2\nu)$ and $\mathcal{B}(Z \rightarrow \ell' \ell' + X) = \mathcal{B}(Z \rightarrow \ell + \ell) + \mathcal{B}(Z \rightarrow \tau + \tau) \mathcal{B}(\tau \rightarrow \ell +$

Table 3: Summary of the total postfit impact of each uncertainty source on the uncertainty in the signal strength measurement, for the four flavour categories and their combination. Theoretical uncertainties are only included in the signal acceptance during the extrapolation to the total phase space, so they are not included in the likelihood fit. The values are percentages and correspond to half the difference between the up and down variation of each systematic uncertainty component.

Source	Combined	eee	ee μ	e $\mu\mu$	$\mu\mu\mu$
Electron efficiency	1.9	5.9	3.9	1.9	—
Electron energy scale	0.3	0.9	0.2	0.6	—
Muon efficiency	1.9	—	0.8	1.8	2.6
Muon momentum scale	0.5	—	0.7	0.3	0.9
Trigger efficiency	1.9	2.0	1.9	1.9	1.8
Jet energy scale	0.9	1.6	1.0	1.7	0.8
b-tagging (id.)	2.6	2.7	2.6	2.6	2.4
b-tagging (mis-id.)	0.9	1.0	0.9	1.0	0.7
Pileup	0.8	0.9	0.3	1.3	1.4
ZZ	0.6	0.7	0.4	0.8	0.5
Nonprompt norm.	1.2	2.0	1.2	1.5	1.0
Nonprompt (EWK subtr.)	1.0	1.5	1.0	1.3	0.8
VVV norm.	0.5	0.6	0.6	0.6	0.5
VH norm.	0.2	0.2	0.3	0.2	0.2
$t\bar{t}$ V norm.	0.5	0.5	0.5	0.5	0.5
tZq norm.	0.1	0.1	0.1	0.1	0.1
X+ γ norm.	0.3	0.8	< 0.1	0.7	< 0.1
Total systematic	4.7	7.8	5.8	5.4	4.6
Integrated luminosity	2.8	2.9	2.8	2.9	2.8
Statistical	2.1	6.0	4.8	4.1	3.1
Total experimental	6.0	10.8	8.0	7.5	6.3
Theoretical	0.9	0.9	0.9	0.9	0.9

Table 4: Efficiencies estimated as transfer factors from the fiducial region to the signal region using generator-level information, for an integrated luminosity \mathcal{L} of 35.9 fb^{-1} . Statistical, scale, and PDF uncertainties are later propagated to the final cross section measurement.

Category	ϵ
eee	0.1754 ± 0.0003 (stat) $^{+0.0017}_{-0.0015}$ (scale, PDF)
ee μ	0.2618 ± 0.0004 (stat) $^{+0.0025}_{-0.0021}$ (scale, PDF)
e $\mu\mu$	0.3764 ± 0.0006 (stat) $^{+0.0035}_{-0.0030}$ (scale, PDF)
$\mu\mu\mu$	0.5625 ± 0.0009 (stat) $^{+0.0047}_{-0.0040}$ (scale, PDF)
Combined:	0.3453 ± 0.0005 (stat) $^{+0.0031}_{-0.0027}$ (scale, PDF)

Table 5: Measured fiducial cross sections and their corresponding uncertainties for each of the individual flavour categories, as well as for the combination of the four. The combined value is the result of a simultaneous fit to the four categories, therefore both the central value and its total uncertainty differ from the sum of the central values and the quadratic sum of the uncertainties respectively, because of correlations among sources of uncertainty in the categorized values.

Category	$\sigma_{\text{fid}}(\text{pp} \rightarrow \text{WZ})$ [fb]
eee	$63.7^{+3.8}_{-3.7}$ (stat) $^{+0.6}_{-0.6}$ (theo) $^{+5.3}_{-4.7}$ (syst) ± 1.9 (lumi)
ee μ	$61.6^{+3.0}_{-2.9}$ (stat) $^{+0.6}_{-0.5}$ (theo) $^{+3.7}_{-3.3}$ (syst) ± 1.9 (lumi)
e $\mu\mu$	$63.4^{+2.6}_{-2.6}$ (stat) $^{+0.6}_{-0.5}$ (theo) $^{+3.5}_{-3.2}$ (syst) ± 1.9 (lumi)
$\mu\mu\mu$	$67.1^{+2.1}_{-2.0}$ (stat) $^{+0.6}_{-0.5}$ (theo) $^{+3.3}_{-3.0}$ (syst) ± 1.9 (lumi)
Combined	$257.5^{+5.3}_{-5.0}$ (stat) $^{+2.3}_{-2.0}$ (theo) $^{+12.8}_{-11.6}$ (syst) ± 7.4 (lumi)

Table 6: Measured WZ production cross sections computed separately in each of the flavour categories.

Category	$\sigma_{\text{tot}}(\text{pp} \rightarrow \text{WZ})$ [pb]
eee	$47.11^{+5.01}_{-4.63}$ (total) = $47.11^{+2.88}_{-2.79}$ (stat) $^{+0.46}_{-0.41}$ (theo) $^{+3.89}_{-3.47}$ (syst) ± 1.41 (lumi)
ee μ	$47.16^{+3.87}_{-3.61}$ (total) = $47.16^{+2.31}_{-2.29}$ (stat) $^{+0.45}_{-0.38}$ (theo) $^{+2.83}_{-2.52}$ (syst) ± 1.33 (lumi)
e $\mu\mu$	$47.70^{+3.58}_{-3.55}$ (total) = $47.70^{+2.00}_{-1.96}$ (stat) $^{+0.45}_{-0.39}$ (theo) $^{+2.66}_{-2.61}$ (syst) ± 1.42 (lumi)
$\mu\mu\mu$	$49.00^{+3.18}_{-3.03}$ (total) = $49.00^{+1.57}_{-1.53}$ (stat) $^{+0.41}_{-0.35}$ (theo) $^{+2.42}_{-2.22}$ (syst) ± 1.39 (lumi)

$2\nu)^2$, are taken from the current world averages [47] and include both the direct leptonic decays of the W and Z bosons and their decays to leptonically decaying τ leptons. The acceptance \mathcal{A} accounts for the fraction of events in the total phase space that pass the requirements of the fiducial region and is estimated using generator-level information. The same procedure used in the fiducial measurement is applied to estimate the effect of theoretical uncertainties and the limited number of simulated events used in the measurement.

The results obtained for each flavour category are listed in Table 6. The combined measurement is defined as the measurement obtained from a simultaneous fit to the four categories; the resulting value is:

$$\sigma_{\text{tot}}(\text{pp} \rightarrow \text{WZ}) = 48.09^{+2.98}_{-2.78} \text{ pb} = 48.09^{+1.00}_{-0.96} \text{ (stat)}^{+0.44}_{-0.37} \text{ (theo)}^{+2.39}_{-2.17} \text{ (syst)} \pm 1.39 \text{ (lumi) pb},$$

which can be compared to theoretical predictions at parton level [55] using MATRIX [55] at NLO, $\sigma_{\text{NLO}}(\text{pp} \rightarrow \text{WZ}) = 45.09^{+4.9\%}_{-3.9\%}$ pb, and next-to-next-to-leading order (NNLO) [56], $\sigma_{\text{NNLO}}(\text{pp} \rightarrow \text{WZ}) = 49.98^{+2.2\%}_{-2.0\%}$, in perturbative QCD, as well as the prediction obtained with POWHEG + PYTHIA at NLO QCD, of $\sigma_{\text{Pow}}^{\text{NLO}} = 42.5^{+1.6}_{-1.4}$ (scale) ± 0.6 (PDF) pb. Uncertainties in the theoretical values are derived from scale variations.

8.1 Charge-dependent measurements

The signal process is further divided depending on the charge of the W boson in order to compute the W^+Z and W^-Z production cross sections and their ratio; the value obtained for the ratio is then compared with theoretical predictions. The procedure described in the previous

section is applied separately for the two categories classified according to the charge of the lepton associated with the W boson. The results are:

$$\begin{aligned}\sigma_{\text{tot}}(\text{pp} \rightarrow W^+Z) &= 28.91^{+0.63}_{-0.61} (\text{stat})^{+0.28}_{-0.25} (\text{theo})^{+1.43}_{-1.31} (\text{syst}) \pm 0.80 (\text{lumi}) \text{ pb}, \\ \sigma_{\text{tot}}(\text{pp} \rightarrow W^-Z) &= 19.55^{+0.45}_{-0.44} (\text{stat})^{+0.17}_{-0.15} (\text{theo})^{+0.97}_{-0.88} (\text{syst}) \pm 0.55 (\text{lumi}) \text{ pb}.\end{aligned}$$

The ratio between the charge-dependent production cross sections is calculated. Statistical uncertainties are treated as completely uncorrelated between the two values, while the other sources of uncertainty are considered completely correlated in their propagation to the ratio. The final effect is that most of the systematic uncertainties show a similar behaviour in both cases so they are greatly reduced when computing the ratio. The value obtained for the ratio is:

$$A_{WZ}^{+-} = \frac{\sigma_{\text{tot}}(\text{pp} \rightarrow W^+Z)}{\sigma_{\text{tot}}(\text{pp} \rightarrow W^-Z)} = 1.48 \pm 0.06 (\text{stat}) \pm 0.02 (\text{syst}) \pm 0.01 (\text{theo}),$$

which is compatible within the uncertainties with the POWHEG + PYTHIA prediction of $A_{WZ}^{+-}(NLO) = 1.43^{+0.06}_{-0.05}$. The same results, split by flavour category, are shown in Fig. 7.

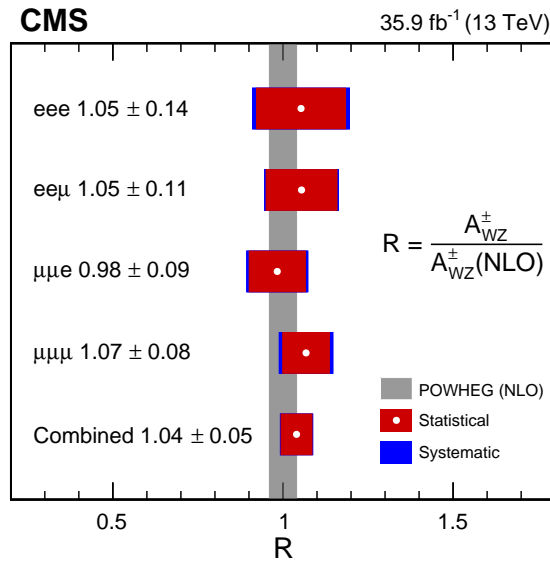


Figure 7: Measured ratio of cross sections for the two charge channels for each of the flavour categories and their combination. Values are normalized to the NLO prediction obtained with POWHEG. Coloured bands for each of the points include both systematic and statistical uncertainties. Shaded bands correspond to the MC prediction from the nominal POWHEG sample and its associated uncertainty.

9 Differential measurement

The differential WZ cross sections are measured in the full volume of the detector as a function of three observables. To better model the data, in the definition of such observables leptons are *dressed* in simulation by adding to their momenta those of all generator-level photons within a cone of $\Delta R(\ell, \gamma) < 0.1$.

The first observable is the p_T of the Z boson, defined as the transverse sum of the momenta of the two final-state leptons assigned to the Z boson decay. The second observable is the p_T

of the leading jet, which represents a probe for the boost of the WZ system recoiling against initial-state radiation. The generated leading jet is defined using the anti- k_T algorithm with a cone radius of 0.4, and by requiring a spatial separation of $\Delta R > 0.5$ from the leptons coming from the WZ decay. The third observable is the $M(\text{WZ})$ variable, defined as the invariant mass of the system composed of the three leptons and the p_T^{miss} . A general formula for the definition of the variable is:

$$M(\text{WZ})^2 = [p(\ell_1) + p(\ell_2) + p(\ell_3) + p(\nu)]^2, \quad (4)$$

where $p(\ell_i)$ is the measured four-momentum of each lepton. The four-momentum of the neutrino is defined in the (mass, p_T , η , ϕ) base as $p(\nu) = (0, p_T(p_T^{\text{miss}}), 0, \phi(p_T^{\text{miss}}))$. Slightly different choices (solving the $W \rightarrow \ell\nu$ system for $\eta(\nu)$ or setting the neutrino four-momentum to zero) were tested as well, giving similar results.

The reconstructed quantities are defined using the objects described in Section 4, and the pair of tight leptons most likely to come from the Z decay, as well as the tight lepton most likely to come from the W boson decay, are selected using the algorithm described in Section 5.

For these three measurements, events must pass the selection used for the inclusive cross section measurement, which is described in Section 5. The resulting reconstructed (*reco*) level distributions are shown in Fig. 8.

The differential WZ cross section is measured in the signal region of the inclusive measurement, here referred to as the inclusive final state, and in four exclusive categories corresponding to a classification by lepton flavour (eee, ee μ , e $\mu\mu$, and $\mu\mu\mu$), referred to as *exclusive* final states.

The reconstructed and generated distributions are assumed to differ by the effects of the detector response. This response can be modelled using a two-dimensional matrix that summarizes the bin migration effects induced by the detector on the target observables. Response matrices are obtained in the signal region for the inclusive and exclusive categories, using the POWHEG and MADGRAPH5_aMC@NLO NLO generators. These matrices are shown for the inclusive selection in Fig. 9, where the bin contents are normalized to the expected NLO yield for the integrated luminosity analyzed in this paper. The binning scheme is chosen such that for all the matrices the width of the diagonal bins in each dimension are larger than the standard deviation of the average of the bin content across the orthogonal axis.

The process of inverting the detector response matrix is known as *unfolding* [57], and several techniques are available in the literature for solving the problem [58], although in many cases it may be argued that the best strategy would be to perform any comparison in the reconstructed space. In the following, the space populated by reconstructed events (the reco-level distributions) is denoted as *folded space* (*folded distributions*), while the generator-level space (distributions) is denoted as *unfolded space* (*unfolded distributions*).

The unfolding procedure consists of performing a least-squares fit with optional Tikhonov regularization [59, 60], as implemented in the TUNFOLD software package [61]. The unfolding

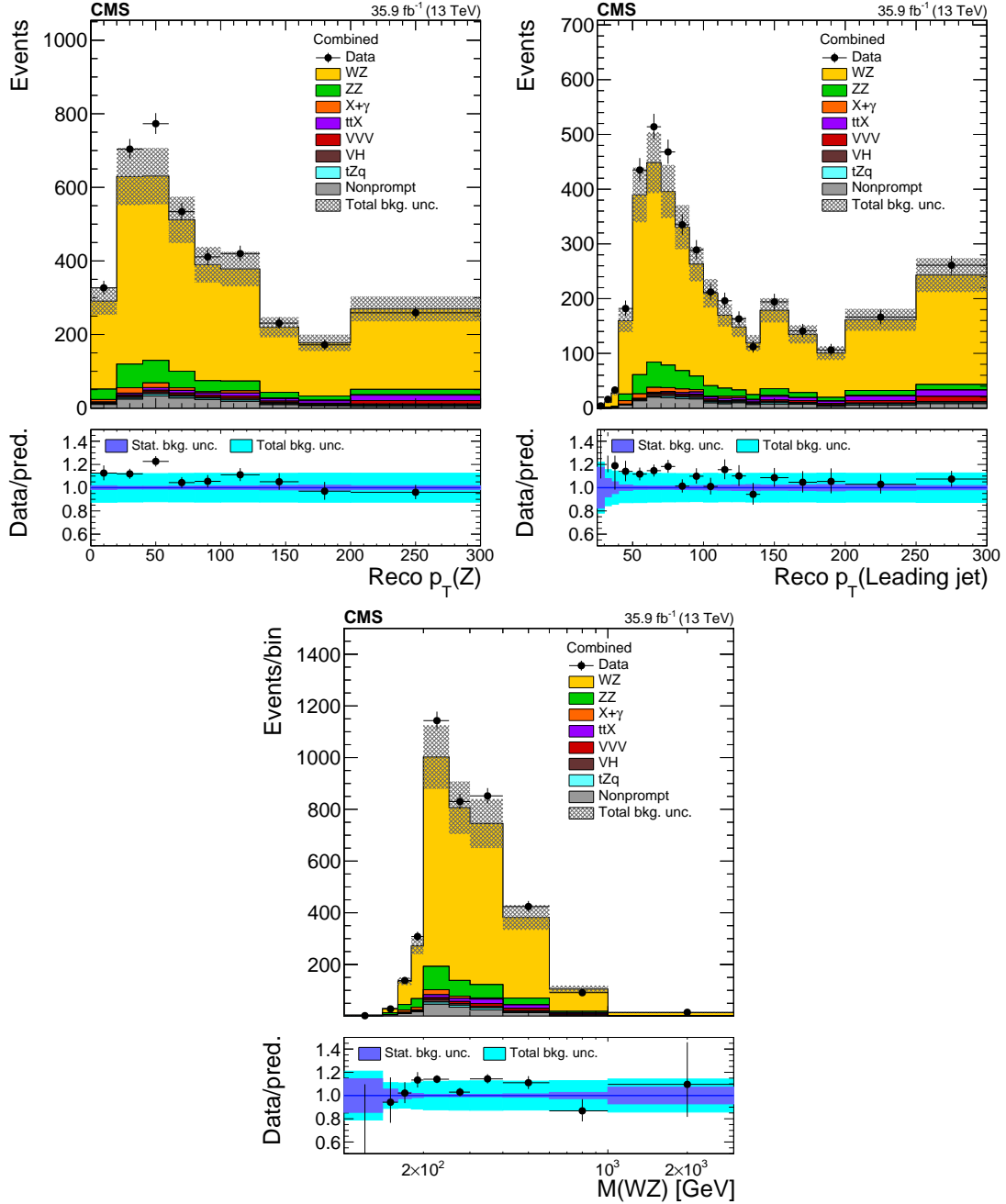


Figure 8: Prefit distributions of key observables in the signal region. The transverse momentum of the Z boson (top left), the transverse momentum of the leading jet (top right), and the mass of the WZ system (bottom). The last bin contains the overflow. Vertical bars on the data points include the statistical uncertainty and the shaded band over the MC prediction include both the statistical and the systematic uncertainties in the normalization of each of the background processes. An additional 15% uncertainty is assigned to the signal WZ process in the figures to account for the NLO/NNLO normalization differences.

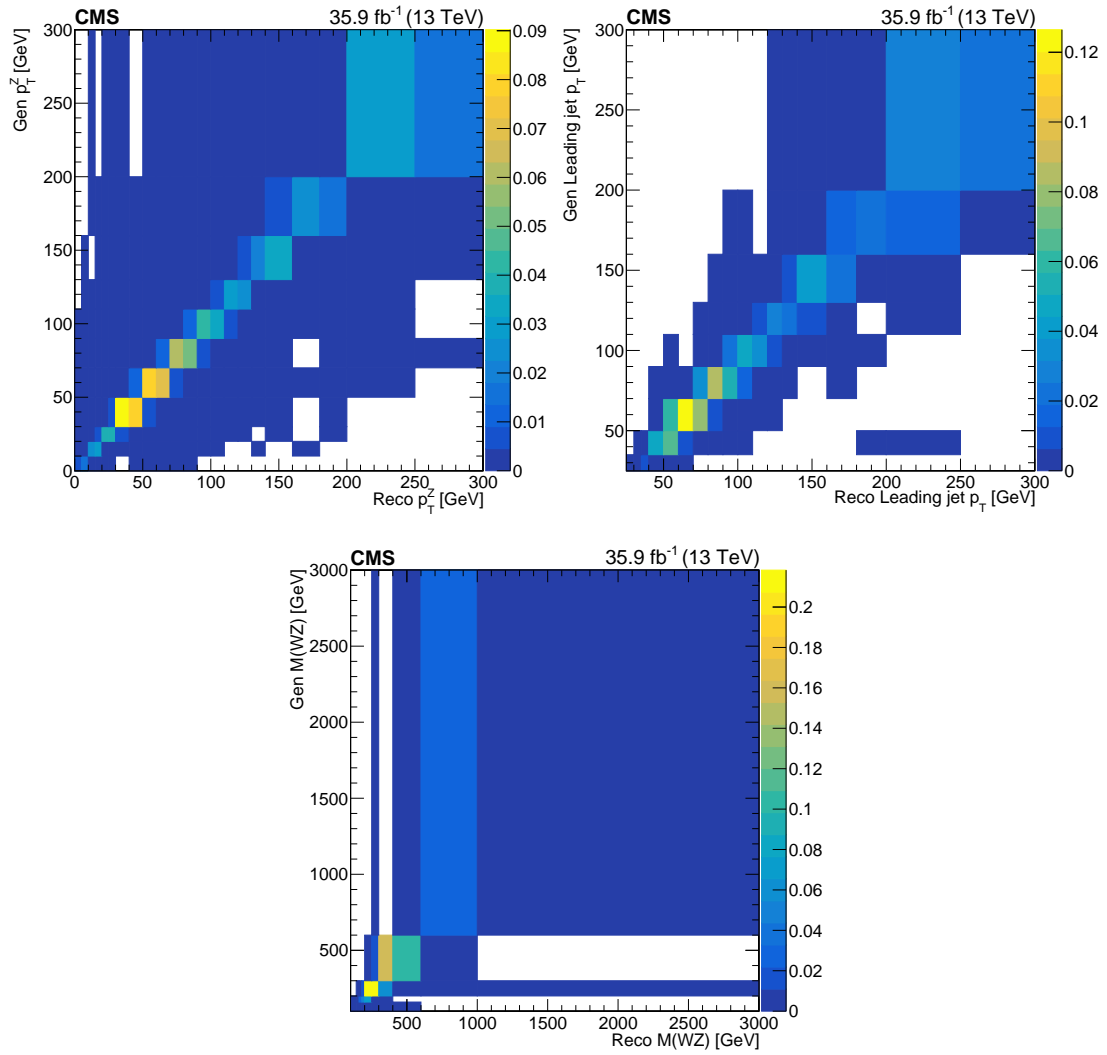


Figure 9: Response matrices obtained using NLO samples, simulated with the POWHEG generator and normalized to unity. The transverse momentum of the Z boson (top left), the leading jet transverse momentum (top right) and the mass of the WZ system (bottom) are shown.

problem, and the least-squares fit used to solve it, are modelled according to:

$$\begin{aligned}
\mathcal{L}(\mathbf{x}, \lambda) &= \mathcal{L}_1 + \mathcal{L}_2 + \mathcal{L}_3, \\
\mathcal{L}_1 &= (\mathbf{y} - \mathbf{A}\mathbf{x})^T \mathbf{V}_{\mathbf{y}\mathbf{y}} (\mathbf{y} - \mathbf{A}\mathbf{x}), \\
\mathcal{L}_2 &= \tau^2 (\mathbf{x} - f_b \mathbf{x}_0)^T (\mathbf{L}^T \mathbf{L}) (\mathbf{x} - f_b \mathbf{x}_0), \\
\mathcal{L}_3 &= \lambda (Y - \mathbf{e}^T \mathbf{x}), \\
Y &= \sum_i y_i, \\
e_j &= \sum_i A_{ij}.
\end{aligned} \tag{5}$$

Here \mathbf{y} is the vector of observed yields, \mathbf{A} is the response matrix, and \mathbf{x} is the unfolded result. \mathcal{L}_1 models the least-squares minimization, where $\mathbf{V}_{\mathbf{y}\mathbf{y}}$ is the covariance matrix of \mathbf{y} , with elements V_{ij} defined by the correlation coefficients obtained by rescaling each covariance e_{ij} by the variances e_{ii} and e_{jj} , $V_{ij} = e_{ij}/e_{ii}e_{jj}$. The regularization is described by \mathcal{L}_2 , which reduces the fluctuations in \mathbf{x} —induced by the statistical fluctuations of \mathbf{y} —via the regularization conditions defined in the matrix \mathbf{L} . The strength of the regularization is described by the parameter τ , and a bias vector $f_b \mathbf{x}_0$ defines the reference with respect to which large deviations are suppressed. An optional area constraint governs whether the normalization of the unfolded result is bound to the total yield in the folded space, as modelled by \mathcal{L}_3 .

To evaluate the performance of the algorithm, the data counts \mathbf{y} are substituted with a pseudodata distribution obtained by sampling from the signal plus background MC distributions. This distribution is then unfolded and folded back; the resulting distribution agrees with the MC truth in the unfolded space and the original sampled distribution, respectively, within uncertainties.

The default configuration for the unfolding performed in this paper is as follows. The POWHEG generator is used to model the response matrix and the area constraint is applied; such constraint accounts for the difference between the expected yields, from the NLO predictions, and the observed yields, which were shown by the inclusive measurement to be more compatible with the NNLO predictions. The bias vector is the generator-level distribution rescaled to the NNLO prediction by a bias scale of 1.13. By default, no regularization is performed. These settings are chosen following a series of checks using the pseudodata distributions, to evaluate the effect of the area constraint, the bias scale and vector, and the regularization scheme.

In particular, the effect of regularization has been checked by applying Tikhonov regularization to the curvature of the unfolded distribution \mathbf{x} . The best value for the regularization parameter τ is chosen using the well-established L-curve method [62]. The regularization process is applied for each of the variables and in no case is there an appreciable gain. No regularization is thus applied to obtain the final result.

Figure 10 shows the results in the inclusive final state for the Z boson p_T distribution (top left), leading jet p_T distribution (top right), and mass of the WZ system (bottom). Good agreement is found between the unfolded data distribution and the MC predictions at particle level, and is quantified by $\chi^2/NDOF$ values given in the plot legends. Results in the four different flavour channels are compatible. The results for the differential cross section in the inclusive and exclusive final states are expressed as a fraction of the total cross section and tabulated in Tables 7, 8, and 9 for the Z boson p_T , Tables 10 and 11 for the leading jet p_T , and Table 12 for the mass of the WZ system. The total cross section is constrained by the aforementioned area constraint. The *bottom line test* [63] is performed, in which goodness of fit tests are performed in the folded

and in the unfolded space to ensure that the agreement between the data and the model does not become worse after unfolding. The purpose is to check that the unfolding procedure is not enhancing the ability to reject incorrect models. The test shows a substantial agreement, giving further confidence in the unfolding procedure.

The results are derived using all the systematic uncertainties described in Section 7, including their effect on the response matrix. In addition, a systematic uncertainty due to the unfolding procedure is defined as the difference between the nominal result and the result obtained by unfolding the nominal shape using an alternative response matrix. Such alternative matrix is modelled using the MADGRAPH5.aMC@NLO generator. The effect of such uncertainty on the result is smaller than the effect of statistical fluctuation and of the background subtraction, and is included in the tables together with all the other sources of uncertainty within the *other syst* category.

Table 7: Differential cross section in bins of $p_T(Z)$. Values are expressed as a fraction of the total cross section. The $ee\bar{e}$ and $ee\mu$ final states are shown.

Bin $p_T(Z)$ [GeV]	Cross section [fraction of the total cross section]				
	Central value	(stat)	(bgr)	(other syst)	(total)
$ee\bar{e}$					
[0, 10]	0.024	± 0.016	± 0.002	± 0.005	(± 0.016)
[10, 20]	0.102	± 0.030	± 0.006	± 0.005	(± 0.031)
[20, 30]	0.169	± 0.039	± 0.010	± 0.007	(± 0.041)
[30, 50]	0.122	± 0.024	± 0.007	± 0.006	(± 0.025)
[50, 70]	0.180	± 0.027	± 0.006	± 0.005	(± 0.028)
[70, 90]	0.132	± 0.023	± 0.005	± 0.004	(± 0.024)
[90, 110]	0.092	± 0.020	± 0.006	± 0.004	(± 0.022)
[110, 130]	0.078	± 0.018	± 0.004	± 0.005	(± 0.019)
[130, 160]	0.053	± 0.012	± 0.002	± 0.004	(± 0.013)
[160, 200]	0.037	± 0.008	± 0.001	± 0.001	(± 0.008)
[200, 300]	0.010	± 0.003	± 0.000	± 0.001	(± 0.003)
$ee\mu$					
[0, 10]	0.033	± 0.013	± 0.002	± 0.005	(± 0.014)
[10, 20]	0.101	± 0.023	± 0.003	± 0.005	(± 0.024)
[20, 30]	0.177	± 0.030	± 0.004	± 0.005	(± 0.030)
[30, 50]	0.188	± 0.020	± 0.003	± 0.003	(± 0.021)
[50, 70]	0.148	± 0.019	± 0.003	± 0.003	(± 0.019)
[70, 90]	0.103	± 0.016	± 0.003	± 0.005	(± 0.017)
[90, 110]	0.080	± 0.015	± 0.003	± 0.003	(± 0.015)
[110, 130]	0.090	± 0.015	± 0.002	± 0.003	(± 0.015)
[130, 160]	0.049	± 0.009	± 0.001	± 0.002	(± 0.009)
[160, 200]	0.015	± 0.005	± 0.001	± 0.001	(± 0.005)
[200, 300]	0.015	± 0.003	± 0.000	± 0.000	(± 0.003)

9.1 Differential measurement split per W boson charge

The differential WZ cross section is computed as a function of the same observables as in Section 9 and categorized according to the sign of the charge of the lepton associated with the W boson. Additionally, the differential cross section is computed as a function of the momentum of the lepton that is assigned to the W boson using the procedure outlined in Section 5.

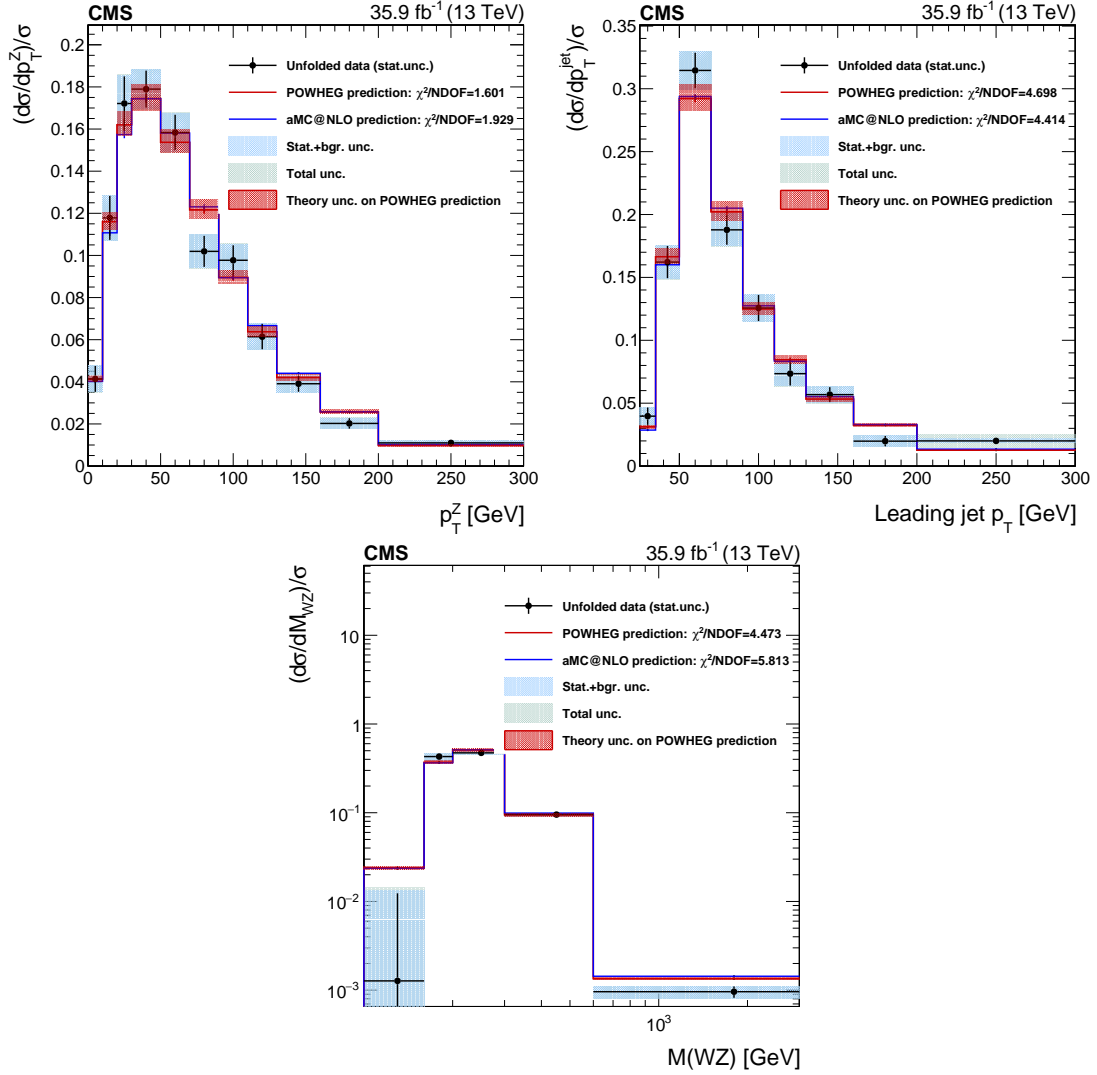


Figure 10: Differential distributions for the Z boson p_T (top left), leading jet p_T (top right), and mass of the WZ system (bottom). Data distributions are unfolded at the dressed leptons level and compared with the POWHEG, MADGRAPH5_aMC@NLO NLO generators, and PYTHIA predictions, as described in the text. The red band around the POWHEG prediction represents the theory uncertainty in it; the effect on the unfolded data of this uncertainty, through the unfolding matrix, is included in the shaded bands described in the legend.

Table 8: Differential cross section in bins of $p_T(Z)$. Values are expressed as a fraction of the total cross section. The $e\mu\mu$ and $\mu\mu\mu$ final states are shown.

Bin $p_T(Z)$ [GeV]	Cross section [fraction of the total cross section]				
	Central value	(stat)	(bgr)	(other syst)	(total)
$e\mu\mu$					
[0, 10]	0.052	± 0.012	± 0.001	± 0.003	(± 0.013)
[10, 20]	0.132	± 0.021	± 0.004	± 0.005	(± 0.021)
[20, 30]	0.175	± 0.024	± 0.005	± 0.007	(± 0.026)
[30, 50]	0.186	± 0.017	± 0.005	± 0.004	(± 0.018)
[50, 70]	0.149	± 0.015	± 0.005	± 0.002	(± 0.016)
[70, 90]	0.083	± 0.013	± 0.004	± 0.004	(± 0.014)
[90, 110]	0.108	± 0.014	± 0.004	± 0.006	(± 0.016)
[110, 130]	0.043	± 0.010	± 0.002	± 0.005	(± 0.011)
[130, 160]	0.041	± 0.008	± 0.002	± 0.003	(± 0.008)
[160, 200]	0.020	± 0.005	± 0.001	± 0.002	(± 0.005)
[200, 300]	0.010	± 0.002	± 0.000	± 0.001	(± 0.002)
$\mu\mu\mu$					
[0, 10]	0.039	± 0.009	± 0.001	± 0.003	(± 0.010)
[10, 20]	0.122	± 0.016	± 0.002	± 0.005	(± 0.017)
[20, 30]	0.171	± 0.020	± 0.002	± 0.004	(± 0.020)
[30, 50]	0.182	± 0.013	± 0.003	± 0.003	(± 0.014)
[50, 70]	0.165	± 0.013	± 0.003	± 0.007	(± 0.015)
[70, 90]	0.108	± 0.012	± 0.002	± 0.003	(± 0.012)
[90, 110]	0.102	± 0.011	± 0.001	± 0.002	(± 0.011)
[110, 130]	0.051	± 0.009	± 0.002	± 0.002	(± 0.009)
[130, 160]	0.031	± 0.006	± 0.001	± 0.001	(± 0.006)
[160, 200]	0.019	± 0.004	± 0.001	± 0.001	(± 0.004)
[200, 300]	0.011	± 0.001	± 0.000	± 0.001	(± 0.002)

Table 9: Differential cross section in bins of $p_T(Z)$. Values are expressed as a fraction of the total cross section. The inclusive final state is shown

Bin $p_T(Z)$ [GeV]	Cross section [fraction of the total cross section]				
	Central value	(stat)	(bgr)	(other syst)	(total)
Inclusive					
[0, 10]	0.041	± 0.006	± 0.001	± 0.001	(± 0.006)
[10, 20]	0.118	± 0.010	± 0.002	± 0.002	(± 0.011)
[20, 30]	0.172	± 0.013	± 0.003	± 0.004	(± 0.014)
[30, 50]	0.179	± 0.009	± 0.003	± 0.001	(± 0.009)
[50, 70]	0.158	± 0.008	± 0.003	± 0.003	(± 0.010)
[70, 90]	0.102	± 0.007	± 0.003	± 0.001	(± 0.008)
[90, 110]	0.098	± 0.007	± 0.002	± 0.002	(± 0.008)
[110, 130]	0.061	± 0.006	± 0.001	± 0.001	(± 0.006)
[130, 160]	0.039	± 0.004	± 0.001	± 0.002	(± 0.004)
[160, 200]	0.020	± 0.002	± 0.001	± 0.001	(± 0.003)
[200, 300]	0.011	± 0.001	± 0.000	± 0.001	(± 0.001)

Table 10: Differential cross section in bins of p_T (Leading jet). Values are expressed as a fraction of the total cross section. The eee , $ee\mu$, $e\mu\mu$, and $\mu\mu\mu$ final states are shown.

Bin p_T (Leading jet) p_T [GeV]	Cross section [fraction of the total cross section]				
	Central value	(stat)	(bgr)	(other syst)	(total)
eee					
[25, 35]	0.022	± 0.015	± 0.002	± 0.008	(± 0.017)
[35, 50]	0.189	± 0.038	± 0.008	± 0.006	(± 0.039)
[50, 70]	0.257	± 0.039	± 0.012	± 0.007	(± 0.041)
[70, 90]	0.194	± 0.035	± 0.010	± 0.011	(± 0.038)
[90, 110]	0.140	± 0.033	± 0.007	± 0.008	(± 0.034)
[110, 130]	0.109	± 0.030	± 0.005	± 0.006	(± 0.031)
[130, 160]	0.031	± 0.016	± 0.004	± 0.004	(± 0.017)
[160, 200]	0.035	± 0.013	± 0.002	± 0.003	(± 0.013)
[200, 300]	0.023	± 0.005	± 0.001	± 0.006	(± 0.007)
$ee\mu$					
[25, 35]	0.059	± 0.025	± 0.001	± 0.008	(± 0.026)
[35, 50]	0.146	± 0.031	± 0.003	± 0.011	(± 0.033)
[50, 70]	0.286	± 0.032	± 0.005	± 0.007	(± 0.033)
[70, 90]	0.224	± 0.028	± 0.005	± 0.006	(± 0.029)
[90, 110]	0.111	± 0.023	± 0.002	± 0.005	(± 0.024)
[110, 130]	0.083	± 0.022	± 0.004	± 0.007	(± 0.024)
[130, 160]	0.055	± 0.013	± 0.002	± 0.003	(± 0.014)
[160, 200]	0.017	± 0.009	± 0.001	± 0.002	(± 0.010)
[200, 300]	0.019	± 0.004	± 0.001	± 0.004	(± 0.006)
$e\mu\mu$					
[25, 35]	0.037	± 0.013	± 0.002	± 0.007	(± 0.015)
[35, 50]	0.166	± 0.026	± 0.005	± 0.009	(± 0.028)
[50, 70]	0.329	± 0.029	± 0.007	± 0.005	(± 0.030)
[70, 90]	0.181	± 0.024	± 0.007	± 0.006	(± 0.026)
[90, 110]	0.121	± 0.021	± 0.005	± 0.010	(± 0.024)
[110, 130]	0.067	± 0.019	± 0.005	± 0.009	(± 0.022)
[130, 160]	0.060	± 0.012	± 0.002	± 0.004	(± 0.013)
[160, 200]	0.015	± 0.008	± 0.001	± 0.003	(± 0.009)
[200, 300]	0.023	± 0.003	± 0.001	± 0.005	(± 0.006)
$\mu\mu\mu$					
[25, 35]	0.042	± 0.011	± 0.000	± 0.003	(± 0.011)
[35, 50]	0.155	± 0.019	± 0.002	± 0.008	(± 0.021)
[50, 70]	0.333	± 0.021	± 0.004	± 0.004	(± 0.022)
[70, 90]	0.176	± 0.017	± 0.004	± 0.006	(± 0.019)
[90, 110]	0.132	± 0.015	± 0.003	± 0.004	(± 0.016)
[110, 130]	0.062	± 0.013	± 0.002	± 0.004	(± 0.014)
[130, 160]	0.062	± 0.009	± 0.002	± 0.004	(± 0.010)
[160, 200]	0.020	± 0.006	± 0.001	± 0.003	(± 0.007)
[200, 300]	0.018	± 0.002	± 0.001	± 0.005	(± 0.006)

Table 11: Differential cross section in bins of p_T (Leading jet). Values are expressed as a fraction of the total cross section. The inclusive final state is shown.

Bin p_T (Leading jet) p_T [GeV]	Cross section [fraction of the total cross section]				
	Central value	(stat)	(bgr)	(other syst)	(total)
	Inclusive				
[25, 35]	0.040	± 0.007	± 0.001	± 0.002	(± 0.007)
[35, 50]	0.162	± 0.013	± 0.003	± 0.004	(± 0.014)
[50, 70]	0.315	± 0.014	± 0.005	± 0.003	(± 0.015)
[70, 90]	0.188	± 0.012	± 0.005	± 0.003	(± 0.013)
[90, 110]	0.126	± 0.010	± 0.003	± 0.003	(± 0.011)
[110, 130]	0.073	± 0.009	± 0.002	± 0.003	(± 0.010)
[130, 160]	0.057	± 0.006	± 0.001	± 0.003	(± 0.007)
[160, 200]	0.020	± 0.004	± 0.001	± 0.002	(± 0.004)
[200, 300]	0.020	± 0.002	± 0.001	± 0.005	(± 0.005)

The charge of the W boson is estimated using as a proxy the charge of the lepton associated to the W boson. Results are shown here for the inclusive final state, but similar results have been obtained in the four exclusive categories ($\mu\mu\mu$, $e\mu\mu$, $e\mu$, and eee).

Results for the leading jet p_T are shown in Fig. 11, results for the Z boson p_T are shown in Fig. 12, results for the mass of the WZ system are shown in Fig. 13, and results for the W boson p_T are shown in Fig. 14. The overall description of the data by the simulation is good. The agreement is quantified by $\chi^2/NDOF$ values that are given in the plot legends. As in the case of the measurement not split by charge, the total uncertainty is dominated by the statistical and background subtraction uncertainties. The remaining uncertainties include the one due to the unfolding procedure and are grouped into the *other syst.* category.

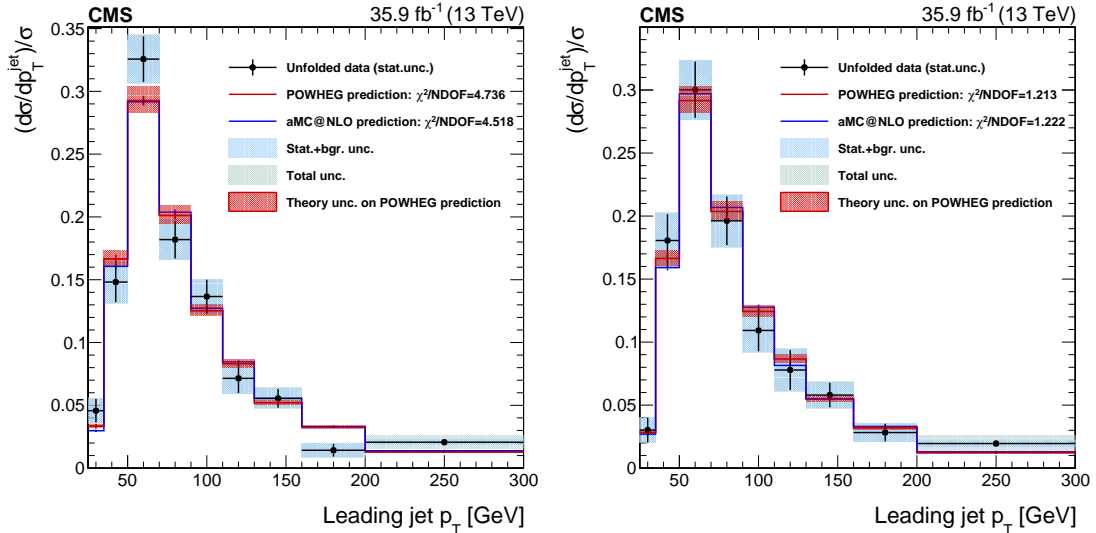


Figure 11: Differential distributions for W^+ (left) and W^- (right), in the full SR. The leading jet transverse momentum is unfolded at the dressed leptons level, as described in the text. The red band around the POWHEG prediction represents the theory uncertainty in it. The effect on the unfolded data of this uncertainty, through the unfolding matrix, is included in the shaded bands described in the legend.

Table 12: Differential cross section in bins of mass of the WZ system. Values are expressed as a fraction of the total cross section.

Bin $M(WZ)$ [GeV]	Cross section [fraction of the inclusive cross section]				
	Central value	(stat)	(bgr)	(other syst)	(total)
eee					
[100, 160]	0.000	± 0.035	± 0.011	± 0.010	(± 0.038)
[160, 200]	0.515	± 0.120	± 0.034	± 0.024	(± 0.127)
[200, 300]	0.370	± 0.050	± 0.013	± 0.009	(± 0.053)
[300, 600]	0.118	± 0.012	± 0.003	± 0.002	(± 0.012)
[600, 3000]	0.001	± 0.000	± 0.000	± 0.000	(± 0.000)
$ee\mu$					
[100, 160]	0.000	± 0.029	± 0.006	± 0.010	(± 0.031)
[160, 200]	0.458	± 0.097	± 0.014	± 0.037	(± 0.105)
[200, 300]	0.465	± 0.041	± 0.009	± 0.013	(± 0.044)
[300, 600]	0.083	± 0.009	± 0.002	± 0.002	(± 0.009)
[600, 3000]	0.001	± 0.000	± 0.000	± 0.000	(± 0.000)
$e\mu\mu$					
[100, 160]	0.006	± 0.024	± 0.006	± 0.014	(± 0.028)
[160, 200]	0.415	± 0.075	± 0.017	± 0.024	(± 0.081)
[200, 300]	0.489	± 0.035	± 0.013	± 0.008	(± 0.038)
[300, 600]	0.090	± 0.008	± 0.002	± 0.001	(± 0.008)
[600, 3000]	0.001	± 0.000	± 0.000	± 0.000	(± 0.000)
$\mu\mu\mu$					
[100, 160]	0.009	± 0.016	± 0.004	± 0.010	(± 0.019)
[160, 200]	0.384	± 0.056	± 0.010	± 0.021	(± 0.061)
[200, 300]	0.507	± 0.028	± 0.007	± 0.008	(± 0.030)
[300, 600]	0.099	± 0.006	± 0.002	± 0.002	(± 0.007)
[600, 3000]	0.001	± 0.000	± 0.000	± 0.000	(± 0.000)
Inclusive					
[100, 160]	0.001	± 0.011	± 0.005	± 0.005	(± 0.013)
[160, 200]	0.430	± 0.038	± 0.009	± 0.012	(± 0.041)
[200, 300]	0.473	± 0.018	± 0.009	± 0.005	(± 0.020)
[300, 600]	0.095	± 0.004	± 0.002	± 0.001	(± 0.004)
[600, 3000]	0.001	± 0.000	± 0.000	± 0.000	(± 0.000)

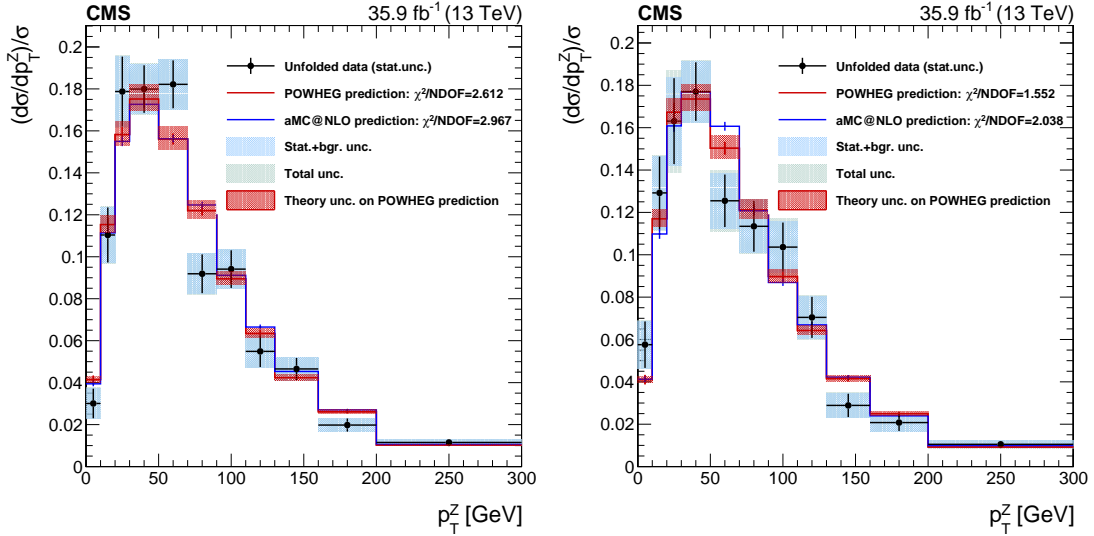


Figure 12: Differential distributions for W^+ (left) and W^- (right), in the full SR. The transverse momentum of the Z boson is unfolded at the dressed leptons level, as described in the text. The red band around the POWHEG prediction represents the theory uncertainty in it; the effect on the unfolded data of this uncertainty, through the unfolding matrix, is included in the shaded bands described in the legend.

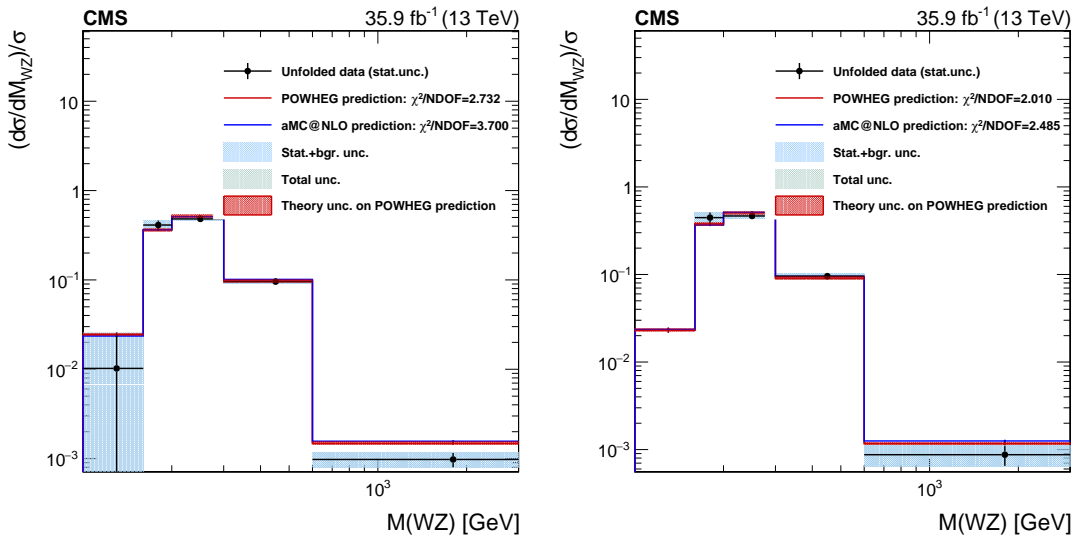


Figure 13: Differential distributions for W^+ (left) and W^- (right), in the full SR. The mass of the WZ system data distribution is unfolded at the dressed leptons level, as described in the text. The red band around the POWHEG prediction represents the theory uncertainty in it; the effect on the unfolded data of this uncertainty, through the unfolding matrix, is included in the shaded bands described in the legend.

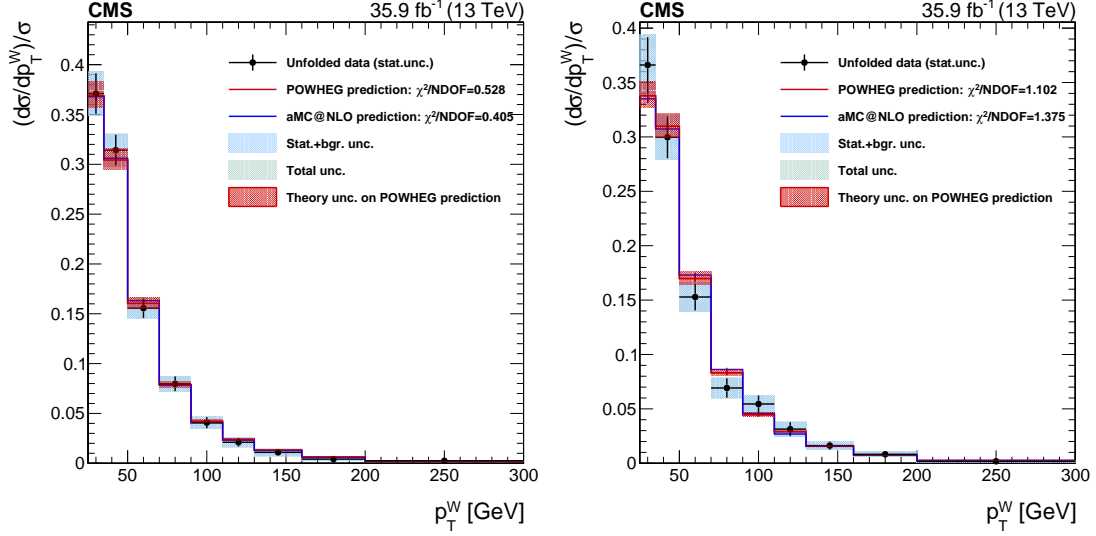


Figure 14: Differential distributions for W^+ (left) and W^- (right), in the full SR. The W boson transverse momentum is unfolded at the dressed leptons level, as described in the text. The red band around the POWHEG prediction represents the theory uncertainty in it; the effect on the unfolded data of this uncertainty, through the unfolding matrix, is included in the shaded bands described in the legend.

10 Confidence regions for anomalous triple gauge couplings

The WZ production process is sensitive to the presence of BSM physics through the presence of deviations from the SM predictions of the coupling constants between the SM vector bosons. Because of the dominant SM production modes, the process is expected to be particularly influenced by TGCs of the W and Z bosons. Such couplings are called *anomalous* when they assume values different from the SM predictions. The total set of allowed operators of dimension six can be summarized in three independent parameters [64]. Usually the choice of a basis for these parameters is based on the effective field theory (EFT) approach, where the anomalous coupling Lagrangian can be written as:

$$\delta\mathcal{L}_{AC} = \frac{c_{WWW}}{\Lambda^2} \text{Tr}[W_{\mu\nu} W^{\nu\rho} W_{\rho}^{\mu}] + \frac{c_W}{\Lambda^2} (D_{\mu}H)^{\dagger} W^{\mu\nu} (D_{\nu}H) + \frac{c_b}{\Lambda^2} (D_{\mu}H)^{\dagger} B^{\mu\nu} (D_{\nu}H), \quad (6)$$

where $W_{\mu\nu}^{\pm}$, $B_{\mu\nu}$ are the field strengths associated to the SM electroweak bosons and H is the SM Higgs field. The parameters representing different aTGC effects are noted as $\{c_W, c_{WWW}, c_b\}$. Values predicted by the SM are $c_W = c_{WWW} = c_b = 0$. The typical energy scale at which BSM physics are dominant is represented by Λ^2 and it is usually absorbed in the definition of the aTGC parameters.

The behaviour of the SM prediction and those of different configurations of anomalous couplings values are compared in Fig. 15 for two different observables that aim to reconstruct the mass of a hypothetical BSM particle decaying to a WZ pair. The predictions corresponding to four different anomalous couplings are drawn for comparison to outline the behaviour of the most asymmetric one (c_{WWW}).

The $M(WZ)$ variable, defined in Section 9, is chosen to determine confidence regions for each of the anomalous parameters considered. A different behaviour as a function of this variable is expected at high energy values in the presence of anomalous couplings, because of the nature of the proper anomalous terms, which include the momenta of the bosons through the field strength terms.

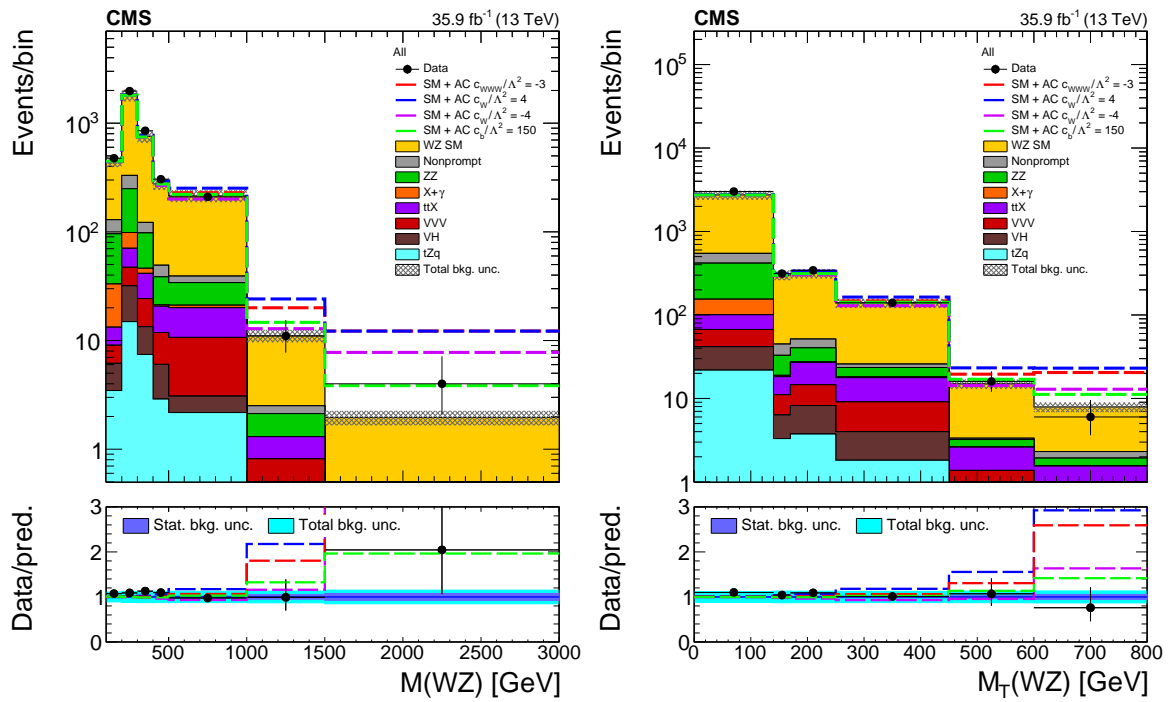


Figure 15: Distributions of discriminant observables in the anomalous triple gauge couplings searches, before the fit used to determine confidence regions on the couplings. The invariant mass of the three lepton and missing transverse momentum system (left) and the transverse mass of the same configuration (right). The dashed lines represent the total yields expected from the sum of the SM processes, with the total WZ yields for different values of the associated anomalous coupling (AC) parameters. The SM prediction for the WZ process is obtained from the aTGC simulated sample with the AC parameters set to 0.

Table 13: Expected and observed one-dimensional confidence intervals (CI) at 95% confidence level for each of the considered EFT parameters. Both the square matrix of the dimension-6 contribution and the interference term between the SM amplitude and the BSM one are accounted for. The one-dimensional intervals for each parameter are computed fixing the other two parameters to zero, the SM value.

Parameter	95% CI (expected) [TeV ⁻²]	95% CI (observed) [TeV ⁻²]
c_W/Λ^2	[-3.3, 2.0]	[-4.1, 1.1]
c_{WWW}/Λ^2	[-1.8, 1.9]	[-2.0, 2.1]
c_b/Λ^2	[-130, 170]	[-100, 160]

Table 14: Expected and observed one-dimensional confidence intervals (CI) at 95% confidence level for each of the considered EFT parameters, accounting only for the interference term between the SM amplitude and the BSM one. The one-dimensional intervals for each parameter are computed fixing the other two parameters to zero, the SM value.

Parameter	95% CI (expected) [TeV ⁻²]	95% CI (observed) [TeV ⁻²]
c_W/Λ^2	[-2.3, 3.4]	[-2.2, 2.7]
c_{WWW}/Λ^2	[-33.2, 28.6]	[-13.8, 41.2]
c_b/Λ^2	[-360, 300]	[-230, 390]

For each of the bins presented in Fig. 15 (left), a three-dimensional quadratic fit is performed to the predicted yields of the anomalous couplings in a grid of simulated points in order to extrapolate the prediction to the continuous space of parameter values. A binned likelihood function is built with the signal yields for each bin depending on the values of each of the three anomalous coupling parameters obtained from the fit. The uncertainties described in Section 7 are included as additional nuisance parameters correlated across the bins. Confidence regions for each parameter and each combination of two parameters are derived using a multidimensional likelihood fit to the relevant parameters, with the remaining ones set to the SM values. Nuisance parameters are profiled in the likelihood fit. Appropriate confidence levels (CL_s) are derived assuming the distribution of the log-likelihood function is half a χ^2 distribution with degrees of freedom equal to the number of free parameters.

The full procedure is applied to derive one-dimensional confidence intervals in each of the anomalous couplings parameters, fixing the other two parameters to zero—the SM value. The results are shown in Table 13. For each pair of parameters, a two-dimensional confidence region is derived, as shown in Fig. 16.

The procedure we described includes both the interference term between the SM amplitude and the BSM one, and for the square of the dimension-6 contribution. If the quadratic term used to build the statistical model is suppressed in the fit, the resulting confidence intervals include the interference term between the SM amplitude and the BSM one only, neglecting the square of the dimension-6 contributions. The results corresponding to this approximation are tabulated in Table 14.

Restricting the effect of the anomalous couplings to a given range in the invariant mass of the diboson system can be used to impose unitarity in the aTGC models. While no direct computation of the invariant mass is possible in the leptonic decay of the WZ channel, we use the $M(WZ)$ variable as a reasonable substitute. We compute the confidence interval for each parameter based on multiple cutoff values of the $M(WZ)$ value to obtain the results shown in Fig. 17.

No anomalous effect has been observed, and the confidence regions obtained represent a sig-

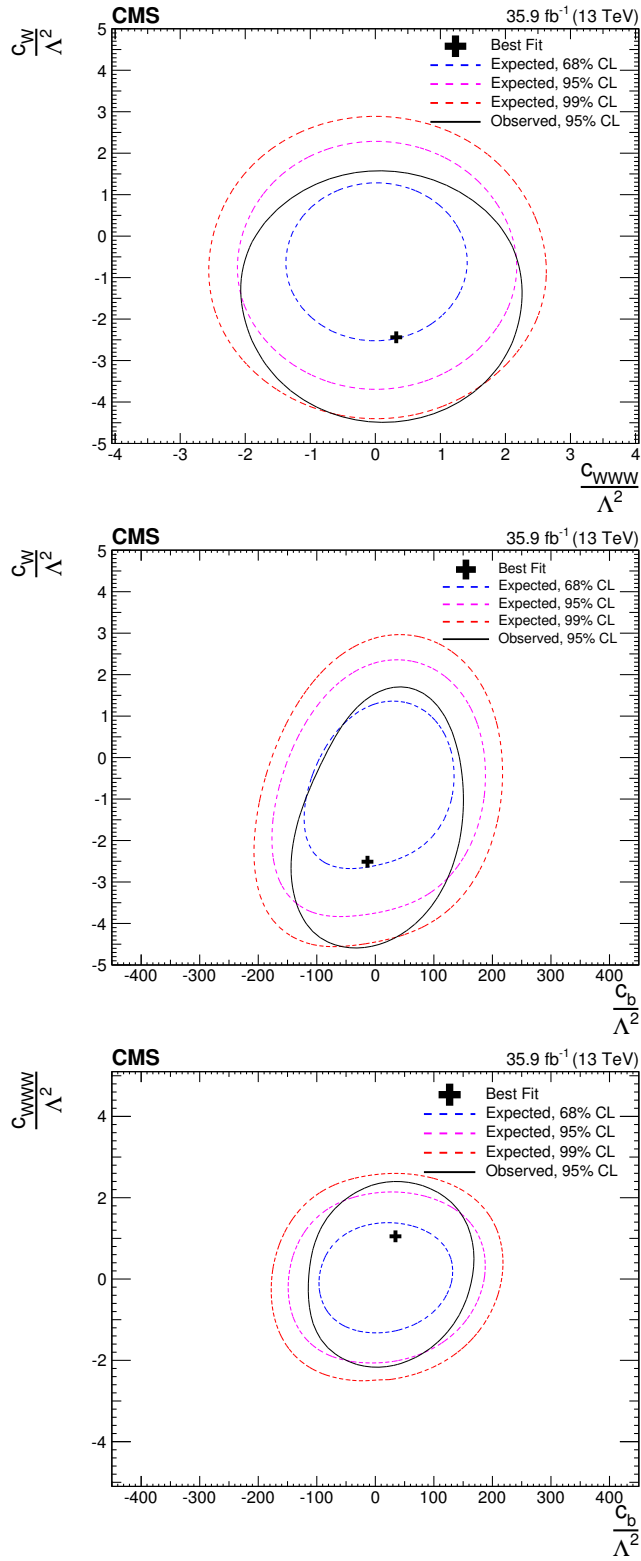


Figure 16: Two-dimensional confidence regions for each of the possible combinations of the considered aTGC parameters. The contours of the expected confidence regions for 68% and 95% confidence level are presented in each case. The parameters considered in each plot are $c_W - c_{WWW}$ (top), $c_W - c_b$ (middle) and $c_{WWW} - c_b$ (bottom).

nificant improvement with respect to previous searches performed by the ATLAS [65] and CMS [15, 16] Collaborations.

11 Summary

The production process $pp \rightarrow WZ$ is studied in the trilepton final state at $\sqrt{s} = 13$ TeV, using the full 2016 data set with a total integrated luminosity of 35.9 fb^{-1} collected with the CMS detector.

Fiducial results are obtained in each of the flavour categories (eee , $ee\mu$, $e\mu\mu$, and $\mu\mu\mu$) and in the combined category, and are extrapolated to the total WZ production cross section for $60 < m_Z^{OSSF} < 120$ GeV. The combined measurement yields a cross section of $\sigma_{\text{tot}}(pp \rightarrow WZ) = 48.09_{-0.96}^{+1.00}$ (stat) $_{-0.37}^{+0.44}$ (theo) $_{-2.17}^{+2.39}$ (syst) ± 1.39 (lumi) pb, for a total uncertainty of $+2.98$ and -2.78 pb. The result is in good agreement with the MATRIX next-to-next-to-leading-order (NNLO) prediction [55, 56], of $\sigma_{\text{NNLO}}(pp \rightarrow WZ) = 49.98_{-2.0\%}^{+2.2\%}$ pb. This result supersedes the result from the CMS Collaboration using data corresponding to a smaller integrated luminosity of 2.3 fb^{-1} [14]. A measurement in the fiducial region yields a value of $\sigma_{\text{fid}}(pp \rightarrow WZ) = 257.5_{-5.0}^{+5.3}$ (stat) $_{-2.0}^{+2.3}$ (theo) $_{-11.6}^{+12.8}$ (syst) ± 7.4 (lumi) fb, pointing to an excess over the POWHEG next-to-leading-order cross section $\sigma_{\text{fid}}^{\text{POWHEG}} = 227.6_{-8.0}^{+9.4}$ fb. The cross sections are also measured independently for the two possible values of the W boson charge, yielding a ratio of $A_{WZ}^{+-} = \sigma_{\text{tot}}(pp \rightarrow W^+Z) / \sigma_{\text{tot}}(pp \rightarrow W^-Z) = 1.48 \pm 0.06$, which is compatible within uncertainties with the POWHEG + PYTHIA prediction of $1.43_{-0.05}^{+0.06}$. Similar results are obtained when splitting by flavour category. All the measurements of this paper are compatible with the SM when the appropriate order of theoretical calculations is considered.

Differential cross sections are measured as a function of the transverse momentum of the Z boson, of the transverse momentum of the leading jet, and of an estimate of the mass of the WZ system; results are compared with predictions from the POWHEG and MADGRAPH5_aMC@NLO generators. Differential cross sections as a function of the transverse momentum of the leading jet are also measured for each sign of the W boson charge. Confidence intervals for anomalous triple gauge boson couplings are extracted for each of the possible one- and two-dimensional combinations of the anomalous couplings parameters, using the $M(WZ)$ variable in a maximum likelihood fit. The confidence intervals obtained represent the most stringent results on the anomalous WWZ triple gauge coupling to date.

Acknowledgments

We congratulate our colleagues in the CERN accelerator departments for the excellent performance of the LHC and thank the technical and administrative staffs at CERN and at other CMS institutes for their contributions to the success of the CMS effort. In addition, we gratefully acknowledge the computing centres and personnel of the Worldwide LHC Computing Grid for delivering so effectively the computing infrastructure essential to our analyses. Finally, we acknowledge the enduring support for the construction and operation of the LHC and the CMS detector provided by the following funding agencies: the Austrian Federal Ministry of Science, Research and Economy and the Austrian Science Fund; the Belgian Fonds de la Recherche Scientifique, and Fonds voor Wetenschappelijk Onderzoek; the Brazilian Funding Agencies (CNPq, CAPES, FAPERJ, FAPERGS, and FAPESP); the Bulgarian Ministry of Education and Science; CERN; the Chinese Academy of Sciences, Ministry of Science and Technology, and National Natural Science Foundation of China; the Colombian Funding Agency (COLCIENCIAS);

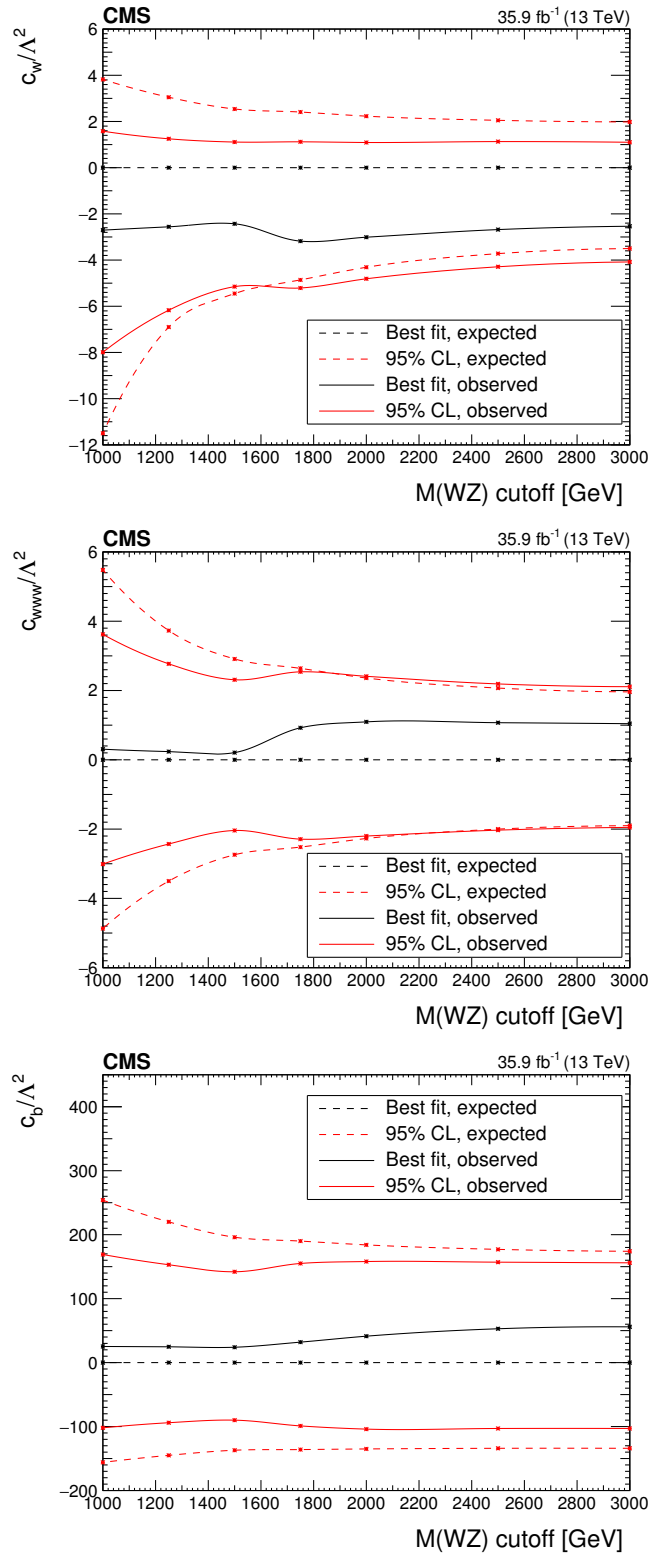


Figure 17: Evolution of the expected and observed confidence intervals of the EFT anomalous coupling parameters in terms of the cutoff scale given by different restrictions in the $M(WZ)$ variable. For each point and parameter, the confidence intervals are computed imposing the additional restriction of no anomalous coupling contribution over the given value of the $M(WZ)$ cutoff. The last point is equivalent to no cutoff requirement being imposed. The parameters considered are: c_W (top), c_{WWW} (middle) and c_b (bottom).

the Croatian Ministry of Science, Education and Sport, and the Croatian Science Foundation; the Research Promotion Foundation, Cyprus; the Secretariat for Higher Education, Science, Technology and Innovation, Ecuador; the Ministry of Education and Research, Estonian Research Council via IUT23-4 and IUT23-6 and European Regional Development Fund, Estonia; the Academy of Finland, Finnish Ministry of Education and Culture, and Helsinki Institute of Physics; the Institut National de Physique Nucléaire et de Physique des Particules / CNRS, and Commissariat à l'Énergie Atomique et aux Énergies Alternatives / CEA, France; the Bundesministerium für Bildung und Forschung, Deutsche Forschungsgemeinschaft, and Helmholtz-Gemeinschaft Deutscher Forschungszentren, Germany; the General Secretariat for Research and Technology, Greece; the National Research, Development and Innovation Fund, Hungary; the Department of Atomic Energy and the Department of Science and Technology, India; the Institute for Studies in Theoretical Physics and Mathematics, Iran; the Science Foundation, Ireland; the Istituto Nazionale di Fisica Nucleare, Italy; the Ministry of Science, ICT and Future Planning, and National Research Foundation (NRF), Republic of Korea; the Lithuanian Academy of Sciences; the Ministry of Education, and University of Malaya (Malaysia); the Ministry of Science of Montenegro; the Mexican Funding Agencies (BUAP, CINVESTAV, CONACYT, LNS, SEP, and UASLP-FAI); the Ministry of Business, Innovation and Employment, New Zealand; the Pakistan Atomic Energy Commission; the Ministry of Science and Higher Education and the National Science Centre, Poland; the Fundação para a Ciência e a Tecnologia, Portugal; JINR, Dubna; the Ministry of Education and Science of the Russian Federation, the Federal Agency of Atomic Energy of the Russian Federation, Russian Academy of Sciences, the Russian Foundation for Basic Research, and the National Research Center "Kurchatov Institute"; the Ministry of Education, Science and Technological Development of Serbia; the Secretaría de Estado de Investigación, Desarrollo e Innovación, Programa Consolider-Ingenio 2010, Plan Estatal de Investigación Científica y Técnica y de Innovación 2013-2016, Plan de Ciencia, Tecnología e Innovación 2013-2017 del Principado de Asturias, and Fondo Europeo de Desarrollo Regional, Spain; the Ministry of Science, Technology and Research, Sri Lanka; the Swiss Funding Agencies (ETH Board, ETH Zurich, PSI, SNF, UniZH, Canton Zurich, and SER); the Ministry of Science and Technology, Taipei; the Thailand Center of Excellence in Physics, the Institute for the Promotion of Teaching Science and Technology of Thailand, Special Task Force for Activating Research and the National Science and Technology Development Agency of Thailand; the Scientific and Technical Research Council of Turkey, and Turkish Atomic Energy Authority; the National Academy of Sciences of Ukraine, and State Fund for Fundamental Researches, Ukraine; the Science and Technology Facilities Council, UK; the US Department of Energy, and the US National Science Foundation.

Individuals have received support from the Marie-Curie programme and the European Research Council and Horizon 2020 Grant, contract No. 675440 (European Union); the Leventis Foundation; the A. P. Sloan Foundation; the Alexander von Humboldt Foundation; the Belgian Federal Science Policy Office; the Fonds pour la Formation à la Recherche dans l'Industrie et dans l'Agriculture (FRIA-Belgium); the Agentschap voor Innovatie door Wetenschap en Technologie (IWT-Belgium); the F.R.S.-FNRS and FWO (Belgium) under the "Excellence of Science - EOS" - be.h project n. 30820817; the Ministry of Education, Youth and Sports (MEYS) of the Czech Republic; the Lendület ("Momentum") Programme and the János Bolyai Research Scholarship of the Hungarian Academy of Sciences, the New National Excellence Program ÚNKP, the NKFI research grants 123842, 123959, 124845, 124850 and 125105 (Hungary); the Council of Scientific and Industrial Research, India; the HOMING PLUS programme of the Foundation for Polish Science, cofinanced from European Union, Regional Development Fund, the Mobility Plus programme of the Ministry of Science and Higher Education, the National Science Center (Poland), contracts Harmonia 2014/14/M/ST2/00428, Opus 2014/13/B/ST2/02543,

2014/15/B/ST2/03998, and 2015/19/B/ST2/02861, Sonata-bis 2012/07/E/ST2/01406; the National Priorities Research Program by Qatar National Research Fund; the Programa de Excelencia María de Maeztu, and the Programa Severo Ochoa del Principado de Asturias; the Thalys and Aristeia programmes cofinanced by EU-ESF, and the Greek NSRF; the Rachadapisek Sompot Fund for Postdoctoral Fellowship, Chulalongkorn University, and the Chulalongkorn Academic into Its 2nd Century Project Advancement Project (Thailand); the Welch Foundation, contract C-1845; and the Weston Havens Foundation (USA).

References

- [1] UA1 Collaboration, “Production of W 's with large transverse momentum at the CERN proton-antiproton collider”, *Physics Letters B* **193** (1987) 389, doi:10.1016/0370-2693(87)91257-3.
- [2] D0 Collaboration, “Measurement of the $WZ \rightarrow \ell\nu\ell\ell$ cross section and limits on anomalous triple gauge couplings in $\bar{t}t$ collisions at $\sqrt{s} = 1.96$ TeV”, *Phys. Lett. B* **695** (2011) 67, doi:10.1016/j.physletb.2010.10.047, arXiv:1006.0761.
- [3] CDF Collaboration, “Observation of WZ production”, *Phys. Rev. Lett* **98** (2007) 161801, doi:10.1103/PhysRevLett.98.161801, arXiv:hep-ex/0702027.
- [4] ATLAS Collaboration, “Measurement of the $W^{\pm}Z$ production cross section and limits on anomalous triple gauge couplings in proton-proton collisions at $\sqrt{s} = 7$ TeV with the ATLAS detector”, *Phys. Lett. B* **709** (2012) 341, doi:10.1016/j.physletb.2012.02.053, arXiv:1111.5570.
- [5] ATLAS Collaboration, “Measurement of WZ production in proton-proton collisions at $\sqrt{s} = 7$ TeV with the ATLAS detector”, *Eur. Phys. J. C* **72** (2012) 2173, doi:10.1140/epjc/s10052-012-2173-0, arXiv:1208.1390.
- [6] ATLAS Collaboration, “Measurement of the $WW + WZ$ cross section and limits on anomalous triple gauge couplings using final states with one lepton, missing transverse momentum, and two jets with the ATLAS detector at $\sqrt{s} = 7$ TeV”, *JHEP* **01** (2015) 049, doi:10.1007/JHEP01(2015)049, arXiv:1410.7238.
- [7] ATLAS Collaboration, “Measurements of $W^{\pm}Z$ production cross sections in pp collisions at $\sqrt{s} = 8$ TeV with the ATLAS detector and limits on anomalous gauge boson self-couplings”, *Phys. Rev. D* **93** (2016) 092004, doi:10.1103/PhysRevD.93.092004, arXiv:1603.02151.
- [8] ATLAS Collaboration, “Measurement of the $W^{\pm}Z$ boson pair-production cross section in pp collisions at $\sqrt{s} = 13$ TeV with the ATLAS Detector”, *Phys. Lett. B* **762** (2016) 1, doi:10.1016/j.physletb.2016.08.052, arXiv:1606.04017.
- [9] ATLAS Collaboration, “Search for anomalous electroweak production of WW/WZ in association with a high-mass dijet system in pp collisions at $\sqrt{s} = 8$ TeV with the ATLAS detector”, *Phys. Rev. D* **95** (2017) 032001, doi:10.1103/PhysRevD.95.032001, arXiv:1609.05122.
- [10] ATLAS Collaboration, “Measurement of $WW/WZ \rightarrow \ell\nu qq'$ production with the hadronically decaying boson reconstructed as one or two jets in pp collisions at $\sqrt{s} = 8$ TeV with ATLAS, and constraints on anomalous gauge couplings”, *Eur. Phys. J. C* **77** (2017) 563, doi:10.1140/epjc/s10052-017-5084-2, arXiv:1706.01702.

-
- [11] CMS Collaboration, “Study of the dijet mass spectrum in $pp \rightarrow W + \text{jets}$ events at $\sqrt{s} = 7$ TeV”, *Phys. Rev. Lett.* **109** (2012) 251801, doi:10.1103/PhysRevLett.109.251801, arXiv:1208.3477.
- [12] CMS Collaboration, “Measurement of the sum of WW and WZ production with W+dijet events in pp collisions at $\sqrt{s} = 7$ TeV”, *Eur. Phys. J. C* **73** (2013) 2283, doi:10.1140/epjc/s10052-013-2283-3, arXiv:1210.7544.
- [13] CMS Collaboration, “Measurement of WZ and ZZ production in pp collisions at $\sqrt{s} = 8$ TeV in final states with b-tagged jets”, *Eur. Phys. J. C* **74** (2014) 2973, doi:10.1140/epjc/s10052-014-2973-5, arXiv:1403.3047.
- [14] CMS Collaboration, “Measurement of the WZ production cross section in pp collisions at $\sqrt{s} = 13$ TeV”, *Phys. Lett. B* **766** (2017) 268, doi:10.1016/j.physletb.2017.01.011, arXiv:1607.06943.
- [15] CMS Collaboration, “Measurement of the WZ production cross section in pp collisions at $\sqrt{s} = 7$ and 8 TeV and search for anomalous triple gauge couplings at $\sqrt{s} = 8$ TeV”, *Eur. Phys. J. C* **77** (2017) 236, doi:10.1140/epjc/s10052-017-4730-z, arXiv:1609.05721.
- [16] CMS Collaboration, “Search for anomalous couplings in boosted WW/WZ $\rightarrow \ell\nu q\bar{q}$ production in proton-proton collisions at $\sqrt{s} = 8$ TeV”, *Phys. Lett. B* **772** (2017) 21, doi:10.1016/j.physletb.2017.06.009, arXiv:1703.06095.
- [17] CMS Collaboration, “The CMS trigger system”, *JINST* **12** (2017) P01020, doi:10.1088/1748-0221/12/01/P01020, arXiv:1609.02366.
- [18] CMS Collaboration, “The CMS experiment at the CERN LHC”, *JINST* **3** (2008) S08004, doi:10.1088/1748-0221/3/08/S08004.
- [19] T. Melia, P. Nason, R. Rontsch, and G. Zanderighi, “ W^+W^- , WZ and ZZ production in the POWHEG BOX”, *JHEP* **11** (2011) 078, doi:10.1007/JHEP11(2011)078, arXiv:1107.5051.
- [20] P. Nason and G. Zanderighi, “ W^+W^- , WZ and ZZ production in the POWHEG-BOX-V2”, *Eur. Phys. J. C* **74** (2014) 2702, doi:10.1140/epjc/s10052-013-2702-5, arXiv:1311.1365.
- [21] J. Alwall et al., “The automated computation of tree-level and next-to-leading order differential cross sections, and their matching to parton shower simulations”, *JHEP* **07** (2014) 079, doi:10.1007/JHEP07(2014)079, arXiv:1405.0301.
- [22] R. Frederix and S. Frixione, “Merging meets matching in MC@NLO”, *JHEP* **12** (2012) 061, doi:10.1007/JHEP12(2012)061, arXiv:1209.6215.
- [23] J. Alwall et al., “Comparative study of various algorithms for the merging of parton showers and matrix elements in hadronic collisions”, *Eur. Phys. J. C* **53** (2008) 473, doi:10.1140/epjc/s10052-007-0490-5, arXiv:0706.2569.
- [24] O. Mattelaer, “On the maximal use of Monte Carlo samples: re-weighting events at NLO accuracy”, *Eur. Phys. J. C* **76** (2016) 010, doi:10.1140/epjc/s10052-016-4533-7, arXiv:1607.00763.

- [25] NNPDF Collaboration, “Parton distributions for the LHC Run II”, *JHEP* **04** (2015) 040, doi:10.1007/JHEP04(2015)040, arXiv:1410.8849.
- [26] T. Sjöstrand et al., “An introduction to PYTHIA 8.2”, *Comput. Phys. Commun.* **191** (2015) 159, doi:10.1016/j.cpc.2015.01.024, arXiv:1410.3012.
- [27] P. Skands, S. Carrazza, and J. Rojo, “Tuning PYTHIA 8.1: the Monash 2013 tune”, *Eur. Phys. J. C* **74** (2014) 3024, doi:10.1140/epjc/s10052-014-3024-y, arXiv:1404.5630.
- [28] CMS Collaboration, “Event generator tunes obtained from underlying event and multiparton scattering measurements”, *Eur. Phys. J. C* **76** (2016) 155, doi:10.1140/epjc/s10052-016-3988-x, arXiv:1512.00815.
- [29] GEANT4 Collaboration, “GEANT4—a simulation toolkit”, *Nucl. Instrum. Meth. A* **506** (2003) 250, doi:10.1016/S0168-9002(03)01368-8.
- [30] CMS Collaboration, “Particle-flow reconstruction and global event description with the CMS detector”, *JINST* **12** (2017) P10003, doi:10.1088/1748-0221/12/10/P10003, arXiv:1706.04965.
- [31] M. Cacciari, G. P. Salam, and G. Soyez, “The anti- k_T jet clustering algorithm”, *JHEP* **04** (2008) 063, doi:10.1088/1126-6708/2008/04/063, arXiv:0802.1189.
- [32] M. Cacciari, G. P. Salam, and G. Soyez, “FastJet user manual”, *Eur. Phys. J. C* **72** (2012) 1896, doi:10.1140/epjc/s10052-012-1896-2, arXiv:1111.6097.
- [33] CMS Collaboration, “Technical proposal for the phase-II upgrade of the compact muon solenoid”, CMS Technical proposal CMS-TDR-15-02, CERN, 2015.
- [34] CMS Collaboration, “Performance of electron reconstruction and selection with the CMS detector in proton-proton collisions at $\sqrt{s} = 8$ TeV”, *JINST* **10** (2015) P06005, doi:10.1088/1748-0221/10/06/P06005, arXiv:1502.02701.
- [35] S. Weinberg, “A model of leptons”, *Phys. Rev. Lett.* **19** (Nov, 1967) 1264, doi:10.1103/PhysRevLett.19.1264.
- [36] CMS Collaboration, “Performance of the CMS muon detector and muon reconstruction with proton-proton collisions at $\sqrt{s} = 13$ TeV”, *JINST* **13** (2018) P06015, doi:10.1088/1748-0221/13/06/P06015.
- [37] CMS Collaboration, “Search for electroweak production of charginos and neutralinos in multilepton final states in proton-proton collisions at $\sqrt{s} = 13$ TeV”, *JHEP* **03** (2018) 166, doi:10.1007/JHEP03(2018)166, arXiv:1709.05406.
- [38] CMS Collaboration, “Evidence for associated production of a Higgs boson with a top quark pair in final states with electrons, muons, and hadronically decaying τ leptons at $\sqrt{s} = 13$ TeV”, *JHEP* **08** (2018) 066, doi:10.1007/JHEP08(2018)066, arXiv:1803.05485.
- [39] K. Rehermann and B. Tweedie, “Efficient identification of boosted semileptonic top quarks at the LHC”, *JHEP* **03** (2011) 059, doi:10.1007/JHEP03(2011)059, arXiv:1007.2221.

-
- [40] CMS Collaboration, “Search for new physics in same-sign dilepton events in proton-proton collisions at $\sqrt{s} = 13$ TeV”, *Eur. Phys. J. C* **76** (2016) 439, doi:10.1140/epjc/s10052-016-4261-z, arXiv:1605.03171.
- [41] CMS Collaboration, “Jet energy scale and resolution performances with 13 TeV data”, technical report, 2016.
- [42] CMS Collaboration, “Jet energy scale and resolution in the CMS experiment in pp collisions at 8 TeV”, *JINST* **12** (2017) P02014, doi:10.1088/1748-0221/12/02/P02014, arXiv:1607.03663.
- [43] CMS Collaboration, “Jet performance in pp collisions at $\sqrt{s}=7$ TeV”, CMS Physics Analysis Summary CMS-PAS-JME-10-003, 2010.
- [44] CMS Collaboration, “Identification of heavy-flavour jets with the CMS detector in pp collisions at 13 TeV”, *JINST* **13** (2018) P05011, doi:10.1088/1748-0221/13/05/P05011, arXiv:1712.07158.
- [45] CMS Collaboration, “Performance of the CMS missing transverse momentum reconstruction in ttdata at $\sqrt{s} = 8$ TeV”, *JINST* **10** (2015) P02006, doi:10.1088/1748-0221/10/02/P02006, arXiv:1411.0511.
- [46] CMS Collaboration, “Performance of missing energy reconstruction in 13 TeV pp collision data using the CMS detector”, CMS Physics Analysis Summary CMS-PAS-JME-16-004, 2016.
- [47] Particle Data Group, C. Patrignani et al., “Review of particle physics”, *Chin. Phys. C* **40** (2016) 100001, doi:10.1088/1674-1137/40/10/100001.
- [48] CMS Collaboration, “Measurements of the pp \rightarrow ZZ production cross section and the $Z \rightarrow 4\ell$ branching fraction, and constraints on anomalous triple gauge couplings at $\sqrt{s} = 13$ TeV”, *Eur. Phys. J. C* **78** (2018) 165, doi:10.1140/epjc/s10052-018-5567-9, arXiv:1709.08601. [Erratum: doi:10.1140/epjc/s10052-018-5769-1].
- [49] CMS Collaboration, “Measurement of the associated production of a single top quark and a Z boson in pp collisions at $\sqrt{s} = 13$ TeV”, *Phys. Lett. B* **779** (2018) 358, doi:10.1016/j.physletb.2018.02.025, arXiv:1712.02825.
- [50] CMS Collaboration, “Measurement of the cross section for top quark pair production in association with a W or Z boson in proton-proton collisions at $\sqrt{s} = 13$ TeV”, *JHEP* **08** (2018) 011, doi:10.1007/JHEP08(2018)011, arXiv:1711.02547.
- [51] CMS Collaboration, “Performance of CMS muon reconstruction in pp collision events at $\sqrt{s} = 7$ TeV”, *JINST* **7** (2012) P10002, doi:10.1088/1748-0221/7/10/P10002, arXiv:1206.4071.
- [52] C. J. Clopper and E. S. Pearson, “The use of confidence or fiducial limits illustrated in the case of the binomial”, *Biometrika* **26** (1934) 404, doi:10.1093/biomet/26.4.404.
- [53] J. Butterworth et al., “PDF4LHC recommendations for LHC Run II”, *J. Phys. G* **43** (2016) 023001, doi:10.1088/0954-3899/43/2/023001, arXiv:1510.03865.
- [54] CMS Collaboration, “CMS luminosity measurements for the 2016 data taking period”, CMS Physics Analysis Summary CMS-PAS-LUM-17-001, 2017.

- [55] M. Grazzini, S. Kallweit, D. Rathlev, and M. Wiesemann, “ $W^\pm Z$ production at hadron colliders in NNLO QCD”, *Phys. Lett. B* **761** (2016) 179, doi:10.1016/j.physletb.2016.08.017, arXiv:1604.08576.
- [56] M. Grazzini, S. Kallweit, and M. Wiesemann, “Fully differential NNLO computations with MATRIX”, *Eur. Phys. J. C* **78** (2018) 537, doi:10.1140/epjc/s10052-018-5771-7, arXiv:1711.06631.
- [57] G. Cowan, “Statistical data analysis”. Oxford University Press, Oxford, England, 1998. ISBN 978-0198501558.
- [58] S. Schmitt, “Data unfolding methods in high energy physics”, in *Proceedings, 12th Conference on Quark Confinement and the Hadron Spectrum (Confinement XII)*, p. 11008. Thessaloniki, Greece, 2017. arXiv:1611.01927. [Euro. Phys. J. Web Conf. 137, 11008]. doi:10.1051/epjconf/201713711008.
- [59] A. N. Tikhonov, A. Goncharsky, V. V. Stepanov, and A. G. Yagola, “Numerical methods for the solution of ill-posed problems”. Springer, 1995. MAIA, volume 328. doi:10.1007/978-94-015-8480-7, ISBN 978-0792335832.
- [60] A. E. Hoerl and R. W. Kennard, “Ridge regression: Biased estimation for nonorthogonal problems”, *Technometrics* **12** (1970) 55, doi:10.1080/00401706.1970.10488634.
- [61] S. Schmitt, “TUnfold: an algorithm for correcting migration effects in high energy physics”, *JINST* **7** (2012) T10003, doi:10.1088/1748-0221/7/10/T10003, arXiv:1205.6201.
- [62] P. C. Hansen, “The L-curve and its use in the numerical treatment of inverse problems”, in *Computational Inverse Problems in Electrocardiology (Advances in Computational Bioengineering)*, P. R. Johnston, ed., p. 119. WIT Press, Southampton, England, 2000.
- [63] R. D. Cousins, S. J. May, and Y. Sun, “Should unfolded histograms be used to test hypotheses?”, (2016). arXiv:1607.07038.
- [64] C. Degrande et al., “Effective field theory: A modern approach to anomalous couplings”, *Annals Phys.* **335** (2013) 21, doi:10.1016/j.aop.2013.04.016, arXiv:1205.4231.
- [65] ATLAS Collaboration, “Measurement of total and differential W^+W^- production cross sections in proton-proton collisions at $\sqrt{s} = 8$ TeV with the ATLAS detector and limits on anomalous triple-gauge-boson couplings”, *JHEP* **09** (2016) 029, doi:10.1007/JHEP09(2016)029, arXiv:1603.01702.

A The CMS Collaboration

Yerevan Physics Institute, Yerevan, Armenia

A.M. Sirunyan, A. Tumasyan

Institut für Hochenergiephysik, Wien, Austria

W. Adam, F. Ambrogio, E. Asilar, T. Bergauer, J. Brandstetter, M. Dragicevic, J. Erö, A. Escalante Del Valle, M. Flechl, R. Frühwirth¹, V.M. Ghete, J. Hrubec, M. Jeitler¹, N. Krammer, I. Krätschmer, D. Liko, T. Madlener, I. Mikulec, N. Rad, H. Rohringer, J. Schieck¹, R. Schöfbeck, M. Spanring, D. Spitzbart, A. Taurok, W. Waltenberger, J. Wittmann, C.-E. Wulz¹, M. Zarucki

Institute for Nuclear Problems, Minsk, Belarus

V. Chekhovsky, V. Mossolov, J. Suarez Gonzalez

Universiteit Antwerpen, Antwerpen, Belgium

E.A. De Wolf, D. Di Croce, X. Janssen, J. Lauwers, M. Pieters, H. Van Haevermaet, P. Van Mechelen, N. Van Remortel

Vrije Universiteit Brussel, Brussel, Belgium

S. Abu Zeid, F. Blekman, J. D'Hondt, J. De Clercq, K. Deroover, G. Flouris, D. Lontkovskyi, S. Lowette, I. Marchesini, S. Moortgat, L. Moreels, Q. Python, K. Skovpen, S. Tavernier, W. Van Doninck, P. Van Mulders, I. Van Parijs

Université Libre de Bruxelles, Bruxelles, Belgium

D. Beghin, B. Bilin, H. Brun, B. Clerboux, G. De Lentdecker, H. Delannoy, B. Dorney, G. Fasanella, L. Favart, R. Goldouzian, A. Grebenyuk, A.K. Kalsi, T. Lenzi, J. Luetic, N. Postiau, E. Starling, L. Thomas, C. Vander Velde, P. Vanlaer, D. Vannerom, Q. Wang

Ghent University, Ghent, Belgium

T. Cornelis, D. Dobur, A. Fagot, M. Gul, I. Khvastunov², D. Poyraz, C. Roskas, D. Trocino, M. Tytgat, W. Verbeke, B. Vermassen, M. Vit, N. Zaganidis

Université Catholique de Louvain, Louvain-la-Neuve, Belgium

H. Bakhshiansohi, O. Bondu, S. Brochet, G. Bruno, C. Caputo, P. David, C. Delaere, M. Delcourt, A. Giammanco, G. Krintiras, V. Lemaître, A. Magitteri, K. Piotrkowski, A. Saggio, M. Vidal Marono, P. Vischia, S. Wertz, J. Zobec

Centro Brasileiro de Pesquisas Físicas, Rio de Janeiro, Brazil

F.L. Alves, G.A. Alves, M. Correa Martins Junior, G. Correia Silva, C. Hensel, A. Moraes, M.E. Pol, P. Rebello Teles

Universidade do Estado do Rio de Janeiro, Rio de Janeiro, Brazil

E. Belchior Batista Das Chagas, W. Carvalho, J. Chinellato³, E. Coelho, E.M. Da Costa, G.G. Da Silveira⁴, D. De Jesus Damiao, C. De Oliveira Martins, S. Fonseca De Souza, H. Malbouisson, D. Matos Figueiredo, M. Melo De Almeida, C. Mora Herrera, L. Mundim, H. Nogima, W.L. Prado Da Silva, L.J. Sanchez Rosas, A. Santoro, A. Sznajder, M. Thiel, E.J. Tonelli Manganote³, F. Torres Da Silva De Araujo, A. Vilela Pereira

Universidade Estadual Paulista ^a, Universidade Federal do ABC ^b, São Paulo, Brazil

S. Ahuja^a, C.A. Bernardes^a, L. Calligaris^a, T.R. Fernandez Perez Tomei^a, E.M. Gregores^b, P.G. Mercadante^b, S.F. Novaes^a, SandraS. Padula^a

Institute for Nuclear Research and Nuclear Energy, Bulgarian Academy of Sciences, Sofia,

Bulgaria

A. Aleksandrov, R. Hadjiiska, P. Iaydjiev, A. Marinov, M. Misheva, M. Rodozov, M. Shopova, G. Sultanov

University of Sofia, Sofia, Bulgaria

A. Dimitrov, L. Litov, B. Pavlov, P. Petkov

Beihang University, Beijing, China

W. Fang⁵, X. Gao⁵, L. Yuan

Institute of High Energy Physics, Beijing, China

M. Ahmad, J.G. Bian, G.M. Chen, H.S. Chen, M. Chen, Y. Chen, C.H. Jiang, D. Leggat, H. Liao, Z. Liu, S.M. Shaheen⁶, A. Spiezia, J. Tao, Z. Wang, E. Yazgan, H. Zhang, S. Zhang⁶, J. Zhao

State Key Laboratory of Nuclear Physics and Technology, Peking University, Beijing, China

Y. Ban, G. Chen, A. Levin, J. Li, L. Li, Q. Li, Y. Mao, S.J. Qian, D. Wang

Tsinghua University, Beijing, China

Y. Wang

Universidad de Los Andes, Bogota, Colombia

C. Avila, A. Cabrera, C.A. Carrillo Montoya, L.F. Chaparro Sierra, C. Florez, C.F. González Hernández, M.A. Segura Delgado

University of Split, Faculty of Electrical Engineering, Mechanical Engineering and Naval Architecture, Split, Croatia

B. Courbon, N. Godinovic, D. Lelas, I. Puljak, T. Sculac

University of Split, Faculty of Science, Split, Croatia

Z. Antunovic, M. Kovac

Institute Rudjer Boskovic, Zagreb, Croatia

V. Brigljevic, D. Ferencek, K. Kadija, B. Mesic, A. Starodumov⁷, T. Susa

University of Cyprus, Nicosia, Cyprus

M.W. Ather, A. Attikis, M. Kolosova, G. Mavromanolakis, J. Mousa, C. Nicolaou, F. Ptochos, P.A. Razis, H. Rykaczewski

Charles University, Prague, Czech Republic

M. Finger⁸, M. Finger Jr.⁸

Escuela Politecnica Nacional, Quito, Ecuador

E. Ayala

Universidad San Francisco de Quito, Quito, Ecuador

E. Carrera Jarrin

Academy of Scientific Research and Technology of the Arab Republic of Egypt, Egyptian Network of High Energy Physics, Cairo, Egypt

M.A. Mahmoud^{9,10}, A. Mahrous¹¹, Y. Mohammed⁹

National Institute of Chemical Physics and Biophysics, Tallinn, Estonia

S. Bhowmik, A. Carvalho Antunes De Oliveira, R.K. Dewanjee, K. Ehataht, M. Kadastik, M. Raidal, C. Veelken

Department of Physics, University of Helsinki, Helsinki, Finland

P. Eerola, H. Kirschenmann, J. Pekkanen, M. Voutilainen

Helsinki Institute of Physics, Helsinki, Finland

J. Havukainen, J.K. Heikkilä, T. Järvinen, V. Karimäki, R. Kinnunen, T. Lampén, K. Lassila-Perini, S. Laurila, S. Lehti, T. Lindén, P. Luukka, T. Mäenpää, H. Siikonen, E. Tuominen, J. Tuominiemi

Lappeenranta University of Technology, Lappeenranta, Finland

T. Tuuva

IRFU, CEA, Université Paris-Saclay, Gif-sur-Yvette, France

M. Besancon, F. Couderc, M. Dejardin, D. Denegri, J.L. Faure, F. Ferri, S. Ganjour, A. Givernaud, P. Gras, G. Hamel de Monchenault, P. Jarry, C. Leloup, E. Locci, J. Malcles, G. Negro, J. Rander, A. Rosowsky, M.Ö. Sahin, M. Titov

Laboratoire Leprince-Ringuet, Ecole polytechnique, CNRS/IN2P3, Université Paris-Saclay, Palaiseau, France

A. Abdulsalam¹², C. Amendola, I. Antropov, F. Beaudette, P. Busson, C. Charlot, R. Granier de Cassagnac, I. Kucher, A. Lobanov, J. Martin Blanco, C. Martin Perez, M. Nguyen, C. Ochando, G. Ortona, P. Paganini, P. Pigard, J. Rembser, R. Salerno, J.B. Sauvan, Y. Sirois, A.G. Stahl Leiton, A. Zabi, A. Zghiche

Université de Strasbourg, CNRS, IPHC UMR 7178, Strasbourg, France

J.-L. Agram¹³, J. Andrea, D. Bloch, J.-M. Brom, E.C. Chabert, V. Cherepanov, C. Collard, E. Conte¹³, J.-C. Fontaine¹³, D. Gelé, U. Goerlach, M. Jansová, A.-C. Le Bihan, N. Tonon, P. Van Hove

Centre de Calcul de l'Institut National de Physique Nucleaire et de Physique des Particules, CNRS/IN2P3, Villeurbanne, France

S. Gadrat

Université de Lyon, Université Claude Bernard Lyon 1, CNRS-IN2P3, Institut de Physique Nucléaire de Lyon, Villeurbanne, France

S. Beauceron, C. Bernet, G. Boudoul, N. Chanon, R. Chierici, D. Contardo, P. Depasse, H. El Mamouni, J. Fay, L. Finco, S. Gascon, M. Gouzevitch, G. Grenier, B. Ille, F. Lagarde, I.B. Laktineh, H. Lattaud, M. Lethuillier, L. Mirabito, S. Perries, A. Popov¹⁴, V. Sordini, G. Touquet, M. Vander Donckt, S. Viret

Georgian Technical University, Tbilisi, Georgia

T. Toriashvili¹⁵

Tbilisi State University, Tbilisi, Georgia

Z. Tsamalaidze⁸

RWTH Aachen University, I. Physikalisches Institut, Aachen, Germany

C. Autermann, L. Feld, M.K. Kiesel, K. Klein, M. Lipinski, M. Preuten, M.P. Rauch, C. Schomakers, J. Schulz, M. Teroerde, B. Wittmer

RWTH Aachen University, III. Physikalisches Institut A, Aachen, Germany

A. Albert, D. Duchardt, M. Erdmann, S. Erdweg, T. Esch, R. Fischer, S. Ghosh, A. Güth, T. Hebbeker, C. Heidemann, K. Hoepfner, H. Keller, L. Mastrolorenzo, M. Merschmeyer, A. Meyer, P. Millet, S. Mukherjee, T. Pook, M. Radziej, H. Reithler, M. Rieger, A. Schmidt, D. Teyssier, S. Thüer

RWTH Aachen University, III. Physikalisches Institut B, Aachen, Germany

G. Flügge, O. Hlushchenko, T. Kress, T. Müller, A. Nehr Korn, A. Nowack, C. Pistone, O. Pooth, D. Roy, H. Sert, A. Stahl¹⁶

Deutsches Elektronen-Synchrotron, Hamburg, Germany

M. Aldaya Martin, T. Arndt, C. Asawatangtrakuldee, I. Babounikau, K. Beernaert, O. Behnke, U. Behrens, A. Bermúdez Martínez, D. Bertsche, A.A. Bin Anuar, K. Borras¹⁷, V. Botta, A. Campbell, P. Connor, C. Contreras-Campana, V. Danilov, A. De Wit, M.M. Defranchis, C. Diez Pardos, D. Domínguez Damiani, G. Eckerlin, T. Eichhorn, A. Elwood, E. Eren, E. Gallo¹⁸, A. Geiser, J.M. Grados Luyando, A. Grohsjean, M. Guthoff, M. Haranko, A. Harb, H. Jung, M. Kasemann, J. Keaveney, C. Kleinwort, J. Knolle, D. Krücker, W. Lange, A. Lelek, T. Lenz, J. Leonard, K. Lipka, W. Lohmann¹⁹, R. Mankel, I.-A. Melzer-Pellmann, A.B. Meyer, M. Meyer, M. Missiroli, G. Mittag, J. Mnich, V. Myronenko, S.K. Pflitsch, D. Pitzl, A. Raspereza, M. Savitskyi, P. Saxena, P. Schütze, C. Schwanenberger, R. Shevchenko, A. Singh, H. Tholen, O. Turkot, A. Vagnerini, G.P. Van Onsem, R. Walsh, Y. Wen, K. Wichmann, C. Wissing, O. Zenaiev

University of Hamburg, Hamburg, Germany

R. Aggleton, S. Bein, L. Benato, A. Benecke, V. Blobel, T. Dreyer, A. Ebrahimi, E. Garutti, D. Gonzalez, P. Gunnellini, J. Haller, A. Hinzmann, A. Karavdina, G. Kasieczka, R. Klanner, R. Kogler, N. Kovalchuk, S. Kurz, V. Kutzner, J. Lange, D. Marconi, J. Multhaupt, M. Niedziela, C.E.N. Niemeyer, D. Nowatschin, A. Perieanu, A. Reimers, O. Rieger, C. Scharf, P. Schleper, S. Schumann, J. Schwandt, J. Sonneveld, H. Stadie, G. Steinbrück, F.M. Stober, M. Stöver, A. Vanhoefer, B. Vormwald, I. Zoi

Karlsruher Institut fuer Technologie, Karlsruhe, Germany

M. Akbiyik, C. Barth, M. Baselga, S. Baur, E. Butz, R. Caspart, T. Chwalek, F. Colombo, W. De Boer, A. Dierlamm, K. El Morabit, N. Faltermann, B. Freund, M. Giffels, M.A. Harrendorf, F. Hartmann¹⁶, S.M. Heindl, U. Husemann, I. Katkov¹⁴, S. Kudella, S. Mitra, M.U. Mozer, Th. Müller, M. Musich, M. Plagge, G. Quast, K. Rabbertz, M. Schröder, I. Shvetsov, H.J. Simonis, R. Ulrich, S. Wayand, M. Weber, T. Weiler, C. Wöhrmann, R. Wolf

Institute of Nuclear and Particle Physics (INPP), NCSR Demokritos, Aghia Paraskevi, Greece

G. Anagnostou, G. Daskalakis, T. Gerasis, A. Kyriakis, D. Loukas, G. Paspalaki

National and Kapodistrian University of Athens, Athens, Greece

A. Agapitos, G. Karathanasis, P. Kontaxakis, A. Panagiotou, I. Papavergou, N. Saoulidou, E. Tziaferi, K. Vellidis

National Technical University of Athens, Athens, Greece

K. Kousouris, I. Papakrivopoulos, G. Tsipolitis

University of Ioánnina, Ioánnina, Greece

I. Evangelou, C. Foudas, P. Giannelis, P. Katsoulis, P. Kokkas, S. Mallios, N. Manthos, I. Papadopoulos, E. Paradas, J. Strolagos, F.A. Triantis, D. Tsitsonis

MTA-ELTE Lendület CMS Particle and Nuclear Physics Group, Eötvös Loránd University, Budapest, Hungary

M. Bartók²⁰, M. Csanad, N. Filipovic, P. Major, M.I. Nagy, G. Pasztor, O. Surányi, G.I. Veres

Wigner Research Centre for Physics, Budapest, Hungary

G. Bencze, C. Hajdu, D. Horvath²¹, Á. Hunyadi, F. Sikler, T.Á. Vámi, V. Veszpremi, G. Vesztergombi[†]

Institute of Nuclear Research ATOMKI, Debrecen, Hungary

N. Beni, S. Czellar, J. Karancsi²⁰, A. Makovec, J. Molnar, Z. Szillasi

Institute of Physics, University of Debrecen, Debrecen, Hungary

P. Raics, Z.L. Trocsanyi, B. Ujvari

Indian Institute of Science (IISc), Bangalore, India

S. Choudhury, J.R. Komaragiri, P.C. Tiwari

National Institute of Science Education and Research, HBNI, Bhubaneswar, IndiaS. Bahinipati²³, C. Kar, P. Mal, K. Mandal, A. Nayak²⁴, D.K. Sahoo²³, S.K. Swain**Panjab University, Chandigarh, India**

S. Bansal, S.B. Beri, V. Bhatnagar, S. Chauhan, R. Chawla, N. Dhingra, R. Gupta, A. Kaur, M. Kaur, S. Kaur, P. Kumari, M. Lohan, A. Mehta, K. Sandeep, S. Sharma, J.B. Singh, A.K. Viridi, G. Walia

University of Delhi, Delhi, India

A. Bhardwaj, B.C. Choudhary, R.B. Garg, M. Gola, S. Keshri, Ashok Kumar, S. Malhotra, M. Naimuddin, P. Priyanka, K. Ranjan, Aashaq Shah, R. Sharma

Saha Institute of Nuclear Physics, HBNI, Kolkata, IndiaR. Bhardwaj²⁵, M. Bharti²⁵, R. Bhattacharya, S. Bhattacharya, U. Bhawandeep²⁵, D. Bhowmik, S. Dey, S. Dutt²⁵, S. Dutta, S. Ghosh, K. Mondal, S. Nandan, A. Purohit, P.K. Rout, A. Roy, S. Roy Chowdhury, G. Saha, S. Sarkar, M. Sharan, B. Singh²⁵, S. Thakur²⁵**Indian Institute of Technology Madras, Madras, India**

P.K. Behera

Bhabha Atomic Research Centre, Mumbai, India

R. Chudasama, D. Dutta, V. Jha, V. Kumar, D.K. Mishra, P.K. Netrakanti, L.M. Pant, P. Shukla

Tata Institute of Fundamental Research-A, Mumbai, India

T. Aziz, M.A. Bhat, S. Dugad, G.B. Mohanty, N. Sur, B. Sutar, RavindraKumar Verma

Tata Institute of Fundamental Research-B, Mumbai, IndiaS. Banerjee, S. Bhattacharya, S. Chatterjee, P. Das, M. Guchait, Sa. Jain, S. Karmakar, S. Kumar, M. Maity²⁶, G. Majumder, K. Mazumdar, N. Sahoo, T. Sarkar²⁶**Indian Institute of Science Education and Research (IISER), Pune, India**

S. Chauhan, S. Dube, V. Hegde, A. Kapoor, K. Kothekar, S. Pandey, A. Rane, A. Rastogi, S. Sharma

Institute for Research in Fundamental Sciences (IPM), Tehran, IranS. Chenarani²⁷, E. Eskandari Tadavani, S.M. Etesami²⁷, M. Khakzad, M. Mohammadi Najafabadi, M. Naseri, F. Rezaei Hosseinabadi, B. Safarzadeh²⁸, M. Zeinali**University College Dublin, Dublin, Ireland**

M. Felcini, M. Grunewald

INFN Sezione di Bari ^a, Università di Bari ^b, Politecnico di Bari ^c, Bari, ItalyM. Abbrescia^{a,b}, C. Calabria^{a,b}, A. Colaleo^a, D. Creanza^{a,c}, L. Cristella^{a,b}, N. De Filippis^{a,c}, M. De Palma^{a,b}, A. Di Florio^{a,b}, F. Errico^{a,b}, L. Fiore^a, A. Gelmi^{a,b}, G. Iaselli^{a,c}, M. Ince^{a,b}, S. Lezki^{a,b}, G. Maggi^{a,c}, M. Maggi^a, G. Miniello^{a,b}, S. My^{a,b}, S. Nuzzo^{a,b}, A. Pompili^{a,b}, G. Pugliese^{a,c}, R. Radogna^a, A. Ranieri^a, G. Selvaggi^{a,b}, A. Sharma^a, L. Silvestris^a, R. Venditti^a, P. Verwilligen^a, G. Zito^a**INFN Sezione di Bologna ^a, Università di Bologna ^b, Bologna, Italy**G. Abbiendi^a, C. Battilana^{a,b}, D. Bonacorsi^{a,b}, L. Borgonovi^{a,b}, S. Braibant-Giacomelli^{a,b},

R. Campanini^{a,b}, P. Capiluppi^{a,b}, A. Castro^{a,b}, F.R. Cavallo^a, S.S. Chhibra^{a,b}, C. Ciocca^a, G. Codispoti^{a,b}, M. Cuffiani^{a,b}, G.M. Dallavalle^a, F. Fabbri^a, A. Fanfani^{a,b}, E. Fontanesi, P. Giacomelli^a, C. Grandi^a, L. Guiducci^{a,b}, F. Iemmi^{a,b}, S. Lo Meo^a, S. Marcellini^a, G. Masetti^a, A. Montanari^a, F.L. Navarra^{a,b}, A. Perrotta^a, F. Primavera^{a,b,16}, T. Rovelli^{a,b}, G.P. Siroli^{a,b}, N. Tosi^a

INFN Sezione di Catania^a, Università di Catania^b, Catania, Italy

S. Albergo^{a,b}, A. Di Mattia^a, R. Potenza^{a,b}, A. Tricomi^{a,b}, C. Tuve^{a,b}

INFN Sezione di Firenze^a, Università di Firenze^b, Firenze, Italy

G. Barbagli^a, K. Chatterjee^{a,b}, V. Ciulli^{a,b}, C. Civinini^a, R. D'Alessandro^{a,b}, E. Focardi^{a,b}, G. Latino, P. Lenzi^{a,b}, M. Meschini^a, S. Paoletti^a, L. Russo^{a,29}, G. Sguazzoni^a, D. Strom^a, L. Viliani^a

INFN Laboratori Nazionali di Frascati, Frascati, Italy

L. Benussi, S. Bianco, F. Fabbri, D. Piccolo

INFN Sezione di Genova^a, Università di Genova^b, Genova, Italy

F. Ferro^a, R. Mulargia^{a,b}, F. Ravera^{a,b}, E. Robutti^a, S. Tosi^{a,b}

INFN Sezione di Milano-Bicocca^a, Università di Milano-Bicocca^b, Milano, Italy

A. Benaglia^a, A. Beschi^b, F. Brivio^{a,b}, V. Ciriolo^{a,b,16}, S. Di Guida^{a,d,16}, M.E. Dinardo^{a,b}, S. Fiorendi^{a,b}, S. Gennai^a, A. Ghezzi^{a,b}, P. Govoni^{a,b}, M. Malberti^{a,b}, S. Malvezzi^a, D. Menasce^a, F. Monti, L. Moroni^a, M. Paganoni^{a,b}, D. Pedrini^a, S. Ragazzi^{a,b}, T. Tabarelli de Fatis^{a,b}, D. Zuolo^{a,b}

INFN Sezione di Napoli^a, Università di Napoli 'Federico II'^b, Napoli, Italy, Università della Basilicata^c, Potenza, Italy, Università G. Marconi^d, Roma, Italy

S. Buontempo^a, N. Cavallo^{a,c}, A. De Iorio^{a,b}, A. Di Crescenzo^{a,b}, F. Fabozzi^{a,c}, F. Fienga^a, G. Galati^a, A.O.M. Iorio^{a,b}, W.A. Khan^a, L. Lista^a, S. Meola^{a,d,16}, P. Paolucci^{a,16}, C. Sciacca^{a,b}, E. Voevodina^{a,b}

INFN Sezione di Padova^a, Università di Padova^b, Padova, Italy, Università di Trento^c, Trento, Italy

P. Azzi^a, N. Bacchetta^a, D. Bisello^{a,b}, A. Boletti^{a,b}, A. Bragagnolo, R. Carlin^{a,b}, P. Checchia^a, M. Dall'Osso^{a,b}, P. De Castro Manzano^a, T. Dorigo^a, U. Dosselli^a, F. Gasparini^{a,b}, U. Gasparini^{a,b}, A. Gozzelino^a, S.Y. Hoh, S. Lacaprara^a, P. Lujan, M. Margoni^{a,b}, A.T. Meneguzzo^{a,b}, J. Pazzini^{a,b}, M. Presilla^b, P. Ronchese^{a,b}, R. Rossin^{a,b}, F. Simonetto^{a,b}, A. Tiko, E. Torassa^a, M. Tosi^{a,b}, M. Zanetti^{a,b}, P. Zotto^{a,b}, G. Zumerle^{a,b}

INFN Sezione di Pavia^a, Università di Pavia^b, Pavia, Italy

A. Braghieri^a, A. Magnani^a, P. Montagna^{a,b}, S.P. Ratti^{a,b}, V. Re^a, M. Ressegotti^{a,b}, C. Riccardi^{a,b}, P. Salvini^a, I. Vai^{a,b}, P. Vitulo^{a,b}

INFN Sezione di Perugia^a, Università di Perugia^b, Perugia, Italy

M. Biasini^{a,b}, G.M. Bilei^a, C. Cecchi^{a,b}, D. Ciangottini^{a,b}, L. Fanò^{a,b}, P. Lariccia^{a,b}, R. Leonardi^{a,b}, E. Manoni^a, G. Mantovani^{a,b}, V. Mariani^{a,b}, M. Menichelli^a, A. Rossi^{a,b}, A. Santocchia^{a,b}, D. Spiga^a

INFN Sezione di Pisa^a, Università di Pisa^b, Scuola Normale Superiore di Pisa^c, Pisa, Italy

K. Androsov^a, P. Azzurri^a, G. Bagliesi^a, L. Bianchini^a, T. Boccali^a, L. Borrello, R. Castaldi^a, M.A. Ciocci^{a,b}, R. Dell'Orso^a, G. Fedi^a, F. Fiori^{a,c}, L. Giannini^{a,c}, A. Giassi^a, M.T. Grippo^a, F. Ligabue^{a,c}, E. Manca^{a,c}, G. Mandorli^{a,c}, A. Messineo^{a,b}, F. Palla^a, A. Rizzi^{a,b}, G. Rolandi³⁰, P. Spagnolo^a, R. Tenchini^a, G. Tonelli^{a,b}, A. Venturi^a, P.G. Verdini^a

INFN Sezione di Roma ^a, Sapienza Università di Roma ^b, Rome, Italy

L. Barone^{a,b}, F. Cavallari^a, M. Cipriani^{a,b}, D. Del Re^{a,b}, E. Di Marco^{a,b}, M. Diemoz^a, S. Gelli^{a,b}, E. Longo^{a,b}, B. Marzocchi^{a,b}, P. Meridiani^a, G. Organtini^{a,b}, F. Pandolfi^a, R. Paramatti^{a,b}, F. Preiato^{a,b}, S. Rahatlou^{a,b}, C. Rovelli^a, F. Santanastasio^{a,b}

INFN Sezione di Torino ^a, Università di Torino ^b, Torino, Italy, Università del Piemonte Orientale ^c, Novara, Italy

N. Amapane^{a,b}, R. Arcidiacono^{a,c}, S. Argiro^{a,b}, M. Arneodo^{a,c}, N. Bartosik^a, R. Bellan^{a,b}, C. Biino^a, A. Cappati^{a,b}, N. Cartiglia^a, F. Cenna^{a,b}, S. Cometti^a, M. Costa^{a,b}, R. Covarelli^{a,b}, N. Demaria^a, B. Kiani^{a,b}, C. Mariotti^a, S. Maselli^a, E. Migliore^{a,b}, V. Monaco^{a,b}, E. Monteil^{a,b}, M. Monteno^a, M.M. Obertino^{a,b}, L. Pacher^{a,b}, N. Pastrone^a, M. Pelliccioni^a, G.L. Pinna Angioni^{a,b}, A. Romero^{a,b}, M. Ruspa^{a,c}, R. Sacchi^{a,b}, R. Salvatico^{a,b}, K. Shchelina^{a,b}, V. Sola^a, A. Solano^{a,b}, D. Soldi^{a,b}, A. Staiano^a

INFN Sezione di Trieste ^a, Università di Trieste ^b, Trieste, Italy

S. Belforte^a, V. Candelise^{a,b}, M. Casarsa^a, F. Cossutti^a, A. Da Rold^{a,b}, G. Della Ricca^{a,b}, F. Vazzoler^{a,b}, A. Zanetti^a

Kyungpook National University, Daegu, Korea

D.H. Kim, G.N. Kim, M.S. Kim, J. Lee, S. Lee, S.W. Lee, C.S. Moon, Y.D. Oh, S.I. Pak, S. Sekmen, D.C. Son, Y.C. Yang

Chonnam National University, Institute for Universe and Elementary Particles, Kwangju, Korea

H. Kim, D.H. Moon, G. Oh

Hanyang University, Seoul, Korea

B. Francois, J. Goh³¹, T.J. Kim

Korea University, Seoul, Korea

S. Cho, S. Choi, Y. Go, D. Gyun, S. Ha, B. Hong, Y. Jo, K. Lee, K.S. Lee, S. Lee, J. Lim, S.K. Park, Y. Roh

Sejong University, Seoul, Korea

H.S. Kim

Seoul National University, Seoul, Korea

J. Almond, J. Kim, J.S. Kim, H. Lee, K. Lee, K. Nam, S.B. Oh, B.C. Radburn-Smith, S.h. Seo, U.K. Yang, H.D. Yoo, G.B. Yu

University of Seoul, Seoul, Korea

D. Jeon, H. Kim, J.H. Kim, J.S.H. Lee, I.C. Park

Sungkyunkwan University, Suwon, Korea

Y. Choi, C. Hwang, J. Lee, I. Yu

Vilnius University, Vilnius, Lithuania

V. Dudenas, A. Juodagalvis, J. Vaitkus

National Centre for Particle Physics, Universiti Malaya, Kuala Lumpur, Malaysia

I. Ahmed, Z.A. Ibrahim, M.A.B. Md Ali³², F. Mohamad Idris³³, W.A.T. Wan Abdullah, M.N. Yusli, Z. Zolkapli

Universidad de Sonora (UNISON), Hermosillo, Mexico

J.F. Benitez, A. Castaneda Hernandez, J.A. Murillo Quijada

Centro de Investigacion y de Estudios Avanzados del IPN, Mexico City, Mexico

H. Castilla-Valdez, E. De La Cruz-Burelo, M.C. Duran-Osuna, I. Heredia-De La Cruz³⁴, R. Lopez-Fernandez, J. Mejia Guisao, R.I. Rabadan-Trejo, M. Ramirez-Garcia, G. Ramirez-Sanchez, R. Reyes-Almanza, A. Sanchez-Hernandez

Universidad Iberoamericana, Mexico City, Mexico

S. Carrillo Moreno, C. Oropeza Barrera, F. Vazquez Valencia

Benemerita Universidad Autonoma de Puebla, Puebla, Mexico

J. Eysermans, I. Pedraza, H.A. Salazar Ibarquen, C. Uribe Estrada

Universidad Autónoma de San Luis Potosí, San Luis Potosí, Mexico

A. Morelos Pineda

University of Auckland, Auckland, New Zealand

D. Krofcheck

University of Canterbury, Christchurch, New Zealand

S. Bheesette, P.H. Butler

National Centre for Physics, Quaid-I-Azam University, Islamabad, Pakistan

A. Ahmad, M. Ahmad, M.I. Asghar, Q. Hassan, H.R. Hoorani, A. Saddique, M.A. Shah, M. Shoaib, M. Waqas

National Centre for Nuclear Research, Swierk, Poland

H. Bialkowska, M. Bluj, B. Boimska, T. Frueboes, M. Górski, M. Kazana, M. Szleper, P. Traczyk, P. Zalewski

Institute of Experimental Physics, Faculty of Physics, University of Warsaw, Warsaw, Poland

K. Bunkowski, A. Byszuk³⁵, K. Doroba, A. Kalinowski, M. Konecki, J. Krolikowski, M. Misiura, M. Olszewski, A. Pyskir, M. Walczak

Laboratório de Instrumentação e Física Experimental de Partículas, Lisboa, Portugal

M. Araujo, P. Bargassa, C. Beirão Da Cruz E Silva, A. Di Francesco, P. Faccioli, B. Galinhas, M. Gallinaro, J. Hollar, N. Leonardo, J. Seixas, G. Strong, O. Toldaiev, J. Varela

Joint Institute for Nuclear Research, Dubna, Russia

S. Afanasiev, P. Bunin, M. Gavrilenko, I. Golutvin, I. Gorbunov, A. Kamenev, V. Karjavine, A. Lanev, A. Malakhov, V. Matveev^{36,37}, P. Moisezenz, V. Palichik, V. Perelygin, S. Shmatov, S. Shulha, N. Skatchkov, V. Smirnov, N. Voytishin, A. Zarubin

Petersburg Nuclear Physics Institute, Gatchina (St. Petersburg), Russia

V. Golovtsov, Y. Ivanov, V. Kim³⁸, E. Kuznetsova³⁹, P. Levchenko, V. Murzin, V. Oreshkin, I. Smirnov, D. Sosnov, V. Sulimov, L. Uvarov, S. Vavilov, A. Vorobyev

Institute for Nuclear Research, Moscow, Russia

Yu. Andreev, A. Dermenev, S. Gninenko, N. Golubev, A. Karneyeu, M. Kirsanov, N. Krasnikov, A. Pashenkov, D. Tlisov, A. Toropin

Institute for Theoretical and Experimental Physics, Moscow, Russia

V. Epshteyn, V. Gavrilov, N. Lychkovskaya, V. Popov, I. Pozdnyakov, G. Safronov, A. Spiridonov, A. Steppenov, V. Stolin, M. Toms, E. Vlasov, A. Zhokin

Moscow Institute of Physics and Technology, Moscow, Russia

T. Aushv

National Research Nuclear University 'Moscow Engineering Physics Institute' (MEPhI), Moscow, Russia

M. Chadeeva⁴⁰, P. Parygin, D. Philippov, S. Polikarpov⁴⁰, E. Popova, V. Rusinov

P.N. Lebedev Physical Institute, Moscow, Russia

V. Andreev, M. Azarkin, I. Dremin³⁷, M. Kirakosyan, A. Terkulov

Skobeltsyn Institute of Nuclear Physics, Lomonosov Moscow State University, Moscow, Russia

A. Baskakov, A. Belyaev, E. Boos, M. Dubinin⁴¹, L. Dudko, A. Ershov, A. Gribushin, V. Klyukhin, O. Kodolova, I. Lokhtin, I. Miagkov, S. Obraztsov, S. Petrushanko, V. Savrin, A. Snigirev

Novosibirsk State University (NSU), Novosibirsk, Russia

A. Barnyakov⁴², V. Blinov⁴², T. Dimova⁴², L. Kardapoltsev⁴², Y. Skovpen⁴²

Institute for High Energy Physics of National Research Centre 'Kurchatov Institute', Protvino, Russia

I. Azhgirey, I. Bayshev, S. Bitiukov, V. Kachanov, A. Kalinin, D. Konstantinov, P. Mandrik, V. Petrov, R. Ryutin, S. Slabospitskii, A. Sobol, S. Troshin, N. Tyurin, A. Uzunian, A. Volkov

National Research Tomsk Polytechnic University, Tomsk, Russia

A. Babaev, S. Baidali, V. Okhotnikov

University of Belgrade, Faculty of Physics and Vinca Institute of Nuclear Sciences, Belgrade, Serbia

P. Adzic⁴³, P. Cirkovic, D. Devetak, M. Dordevic, J. Milosevic

Centro de Investigaciones Energéticas Medioambientales y Tecnológicas (CIEMAT), Madrid, Spain

J. Alcaraz Maestre, A. Álvarez Fernández, I. Bachiller, M. Barrio Luna, J.A. Brochero Cifuentes, M. Cerrada, N. Colino, B. De La Cruz, A. Delgado Peris, C. Fernandez Bedoya, J.P. Fernández Ramos, J. Flix, M.C. Fouz, O. Gonzalez Lopez, S. Goy Lopez, J.M. Hernandez, M.I. Josa, D. Moran, A. Pérez-Calero Yzquierdo, J. Puerta Pelayo, I. Redondo, L. Romero, M.S. Soares, A. Triossi

Universidad Autónoma de Madrid, Madrid, Spain

C. Albajar, J.F. de Trocóniz

Universidad de Oviedo, Oviedo, Spain

J. Cuevas, C. Erice, J. Fernandez Menendez, S. Folgueras, I. Gonzalez Caballero, J.R. González Fernández, E. Palencia Cortezon, V. Rodríguez Bouza, S. Sanchez Cruz, J.M. Vizan Garcia

Instituto de Física de Cantabria (IFCA), CSIC-Universidad de Cantabria, Santander, Spain

I.J. Cabrillo, A. Calderon, B. Chazin Quero, J. Duarte Campderros, M. Fernandez, P.J. Fernández Manteca, A. García Alonso, J. Garcia-Ferrero, G. Gomez, A. Lopez Virto, J. Marco, C. Martinez Rivero, P. Martinez Ruiz del Arbol, F. Matorras, J. Piedra Gomez, C. Prieels, T. Rodrigo, A. Ruiz-Jimeno, L. Scodellaro, N. Trevisani, I. Vila, R. Vilar Cortabitarte

University of Ruhuna, Department of Physics, Matara, Sri Lanka

N. Wickramage

CERN, European Organization for Nuclear Research, Geneva, Switzerland

D. Abbaneo, B. Akgun, E. Auffray, G. Auzinger, P. Baillon, A.H. Ball, D. Barney, J. Bendavid,

M. Bianco, A. Bocci, C. Botta, E. Brondolin, T. Camporesi, M. Cepeda, G. Cerminara, E. Chapon, Y. Chen, G. Cucciati, D. d'Enterria, A. Dabrowski, N. Daci, V. Daponte, A. David, A. De Roeck, N. Deelen, M. Dobson, M. Dünser, N. Dupont, A. Elliott-Peisert, P. Everaerts, F. Fallavollita⁴⁴, D. Fasanella, G. Franzoni, J. Fulcher, W. Funk, D. Gigi, A. Gilbert, K. Gill, F. Glege, M. Gruchala, M. Guilbaud, D. Gulhan, J. Hegeman, C. Heidegger, V. Innocente, A. Jafari, P. Janot, O. Karacheban¹⁹, J. Kieseler, A. Kornmayer, M. Krammer¹, C. Lange, P. Lecoq, C. Lourenço, L. Malgeri, M. Mannelli, A. Massironi, F. Meijers, J.A. Merlin, S. Mersi, E. Meschi, P. Milenovic⁴⁵, F. Moortgat, M. Mulders, J. Ngadiuba, S. Nourbakhsh, S. Orfanelli, L. Orsini, F. Pantaleo¹⁶, L. Pape, E. Perez, M. Peruzzi, A. Petrilli, G. Petrucciani, A. Pfeiffer, M. Pierini, F.M. Pitters, D. Rabady, A. Racz, T. Reis, M. Rovere, H. Sakulin, C. Schäfer, C. Schwick, M. Selvaggi, A. Sharma, P. Silva, P. Sphicas⁴⁶, A. Stakia, J. Steggemann, D. Treille, A. Tsirou, V. Veckalns⁴⁷, M. Verzetti, W.D. Zeuner

Paul Scherrer Institut, Villigen, Switzerland

L. Caminada⁴⁸, K. Deiters, W. Erdmann, R. Horisberger, Q. Ingram, H.C. Kaestli, D. Kotlinski, U. Langenegger, T. Rohe, S.A. Wiederkehr

ETH Zurich - Institute for Particle Physics and Astrophysics (IPA), Zurich, Switzerland

M. Backhaus, L. Bäni, P. Berger, N. Chernyavskaya, G. Dissertori, M. Dittmar, M. Donegà, C. Dorfer, T.A. Gómez Espinosa, C. Grab, D. Hits, T. Klijnsma, W. Lustermaan, R.A. Manzoni, M. Marionneau, M.T. Meinhard, F. Micheli, P. Musella, F. Nessi-Tedaldi, J. Pata, F. Pauss, G. Perrin, L. Perrozzi, S. Pigazzini, M. Quittnat, C. Reissel, D. Ruini, D.A. Sanz Becerra, M. Schönenberger, L. Shchutska, V.R. Tavolaro, K. Theofilatos, M.L. Vesterbacka Olsson, R. Wallny, D.H. Zhu

Universität Zürich, Zurich, Switzerland

T.K. Aarrestad, C. AMSler⁴⁹, D. Brzhechko, M.F. Canelli, A. De Cosa, R. Del Burgo, S. Donato, C. Galloni, T. Hreus, B. Kilminster, S. Leontsinis, I. Neutelings, G. Rauco, P. Robmann, D. Salerno, K. Schweiger, C. Seitz, Y. Takahashi, A. Zucchetta

National Central University, Chung-Li, Taiwan

T.H. Doan, R. Khurana, C.M. Kuo, W. Lin, A. Pozdnyakov, S.S. Yu

National Taiwan University (NTU), Taipei, Taiwan

P. Chang, Y. Chao, K.F. Chen, P.H. Chen, W.-S. Hou, Arun Kumar, Y.F. Liu, R.-S. Lu, E. Paganis, A. Psallidas, A. Steen

Chulalongkorn University, Faculty of Science, Department of Physics, Bangkok, Thailand

B. Asavapibhop, N. Srimanobhas, N. Suwonjandee

Çukurova University, Physics Department, Science and Art Faculty, Adana, Turkey

M.N. Bakirci⁵⁰, A. Bat, F. Boran, S. Cerci⁵¹, S. Damarseckin, Z.S. Demiroglu, F. Dolek, C. Dozen, I. Dumanoglu, E. Eskut, S. Girgis, G. Gokbulut, Y. Guler, E. Gurpinar, I. Hos⁵², C. Isik, E.E. Kangal⁵³, O. Kara, A. Kayis Topaksu, U. Kiminsu, M. Oglakci, G. Onengut, K. Ozdemir⁵⁴, A. Polatoz, U.G. Tok, S. Turkcapar, I.S. Zorbakir, C. Zorbilmez

Middle East Technical University, Physics Department, Ankara, Turkey

B. Isildak⁵⁵, G. Karapinar⁵⁶, M. Yalvac, M. Zeyrek

Bogazici University, Istanbul, Turkey

I.O. Atakisi, E. Gülmez, M. Kaya⁵⁷, O. Kaya⁵⁸, S. Ozkorucuklu⁵⁹, S. Tekten, E.A. Yetkin⁶⁰

Istanbul Technical University, Istanbul, Turkey

M.N. Agaras, A. Cakir, K. Cankocak, Y. Komurcu, S. Sen⁶¹

Institute for Scintillation Materials of National Academy of Science of Ukraine, Kharkov, Ukraine

B. Grynyov

National Scientific Center, Kharkov Institute of Physics and Technology, Kharkov, Ukraine

L. Levchuk

University of Bristol, Bristol, United Kingdom

F. Ball, J.J. Brooke, D. Burns, E. Clement, D. Cussans, O. Davignon, H. Flacher, J. Goldstein, G.P. Heath, H.F. Heath, L. Kreczko, D.M. Newbold⁶², S. Paramesvaran, B. Penning, T. Sakuma, D. Smith, V.J. Smith, J. Taylor, A. Titterton

Rutherford Appleton Laboratory, Didcot, United Kingdom

K.W. Bell, A. Belyaev⁶³, C. Brew, R.M. Brown, D. Cieri, D.J.A. Cockerill, J.A. Coughlan, K. Harder, S. Harper, J. Linacre, K. Manolopoulos, E. Olaiya, D. Petyt, C.H. Shepherd-Themistocleous, A. Thea, I.R. Tomalin, T. Williams, W.J. Womersley

Imperial College, London, United Kingdom

R. Bainbridge, P. Bloch, J. Borg, S. Breeze, O. Buchmuller, A. Bundock, D. Colling, P. Dauncey, G. Davies, M. Della Negra, R. Di Maria, G. Hall, G. Iles, T. James, M. Komm, C. Laner, L. Lyons, A.-M. Magnan, S. Malik, A. Martelli, J. Nash⁶⁴, A. Nikitenko⁷, V. Palladino, M. Pesaresi, D.M. Raymond, A. Richards, A. Rose, E. Scott, C. Seez, A. Shtipliyski, G. Singh, M. Stoye, T. Strebler, S. Summers, A. Tapper, K. Uchida, T. Virdee¹⁶, N. Wardle, D. Winterbottom, J. Wright, S.C. Zenz

Brunel University, Uxbridge, United Kingdom

J.E. Cole, P.R. Hobson, A. Khan, P. Kyberd, C.K. Mackay, A. Morton, I.D. Reid, L. Teodorescu, S. Zahid

Baylor University, Waco, USA

K. Call, J. Dittmann, K. Hatakeyama, H. Liu, C. Madrid, B. McMaster, N. Pastika, C. Smith

Catholic University of America, Washington, DC, USA

R. Bartek, A. Dominguez

The University of Alabama, Tuscaloosa, USA

A. Buccilli, S.I. Cooper, C. Henderson, P. Rumerio, C. West

Boston University, Boston, USA

D. Arcaro, T. Bose, D. Gastler, D. Pinna, D. Rankin, C. Richardson, J. Rohlf, L. Sulak, D. Zou

Brown University, Providence, USA

G. Benelli, X. Coubez, D. Cutts, M. Hadley, J. Hakala, U. Heintz, J.M. Hogan⁶⁵, K.H.M. Kwok, E. Laird, G. Landsberg, J. Lee, Z. Mao, M. Narain, S. Sagir⁶⁶, R. Syarif, E. Usai, D. Yu

University of California, Davis, Davis, USA

R. Band, C. Brainerd, R. Breedon, D. Burns, M. Calderon De La Barca Sanchez, M. Chertok, J. Conway, R. Conway, P.T. Cox, R. Erbacher, C. Flores, G. Funk, W. Ko, O. Kukral, R. Lander, M. Mulhearn, D. Pellett, J. Pilot, S. Shalhout, M. Shi, D. Stolp, D. Taylor, K. Tos, M. Tripathi, Z. Wang, F. Zhang

University of California, Los Angeles, USA

M. Bachtis, C. Bravo, R. Cousins, A. Dasgupta, A. Florent, J. Hauser, M. Ignatenko, N. Mccoll, S. Regnard, D. Saltzberg, C. Schnaible, V. Valuev

University of California, Riverside, Riverside, USA

E. Bouvier, K. Burt, R. Clare, J.W. Gary, S.M.A. Ghiasi Shirazi, G. Hanson, G. Karapostoli, E. Kennedy, F. Lacroix, O.R. Long, M. Olmedo Negrete, M.I. Paneva, W. Si, L. Wang, H. Wei, S. Wimpenny, B.R. Yates

University of California, San Diego, La Jolla, USA

J.G. Branson, P. Chang, S. Cittolin, M. Derdzinski, R. Gerosa, D. Gilbert, B. Hashemi, A. Holzner, D. Klein, G. Kole, V. Krutelyov, J. Letts, M. Masciovecchio, D. Olivito, S. Padhi, M. Pieri, M. Sani, V. Sharma, S. Simon, M. Tadel, A. Vartak, S. Wasserbaech⁶⁷, J. Wood, F. Würthwein, A. Yagil, G. Zevi Della Porta

University of California, Santa Barbara - Department of Physics, Santa Barbara, USA

N. Amin, R. Bhandari, C. Campagnari, M. Citron, V. Dutta, M. Franco Sevilla, L. Gouskos, R. Heller, J. Incandela, H. Mei, A. Ovcharova, H. Qu, J. Richman, D. Stuart, I. Suarez, S. Wang, J. Yoo

California Institute of Technology, Pasadena, USA

D. Anderson, A. Bornheim, J.M. Lawhorn, N. Lu, H.B. Newman, T.Q. Nguyen, M. Spiropulu, J.R. Vlimant, R. Wilkinson, S. Xie, Z. Zhang, R.Y. Zhu

Carnegie Mellon University, Pittsburgh, USA

M.B. Andrews, T. Ferguson, T. Mudholkar, M. Paulini, M. Sun, I. Vorobiev, M. Weinberg

University of Colorado Boulder, Boulder, USA

J.P. Cumalat, W.T. Ford, F. Jensen, A. Johnson, E. MacDonald, T. Mulholland, R. Patel, A. Perloff, K. Stenson, K.A. Ulmer, S.R. Wagner

Cornell University, Ithaca, USA

J. Alexander, J. Chaves, Y. Cheng, J. Chu, A. Datta, K. Mcdermott, N. Mirman, J.R. Patterson, D. Quach, A. Rinkevicius, A. Ryd, L. Skinnari, L. Soffi, S.M. Tan, Z. Tao, J. Thom, J. Tucker, P. Wittich, M. Zientek

Fermi National Accelerator Laboratory, Batavia, USA

S. Abdullin, M. Albrow, M. Alyari, G. Apollinari, A. Apresyan, A. Apyan, S. Banerjee, L.A.T. Bauerdick, A. Beretvas, J. Berryhill, P.C. Bhat, K. Burkett, J.N. Butler, A. Canepa, G.B. Cerati, H.W.K. Cheung, F. Chlebana, M. Cremonesi, J. Duarte, V.D. Elvira, J. Freeman, Z. Gecse, E. Gottschalk, L. Gray, D. Green, S. Grünendahl, O. Gutsche, J. Hanlon, R.M. Harris, S. Hasegawa, J. Hirschauer, Z. Hu, B. Jayatilaka, S. Jindariani, M. Johnson, U. Joshi, B. Klima, M.J. Kortelainen, B. Kreis, S. Lammel, D. Lincoln, R. Lipton, M. Liu, T. Liu, J. Lykken, K. Maeshima, J.M. Marraffino, D. Mason, P. McBride, P. Merkel, S. Mrenna, S. Nahn, V. O'Dell, K. Pedro, C. Pena, O. Prokofyev, G. Rakness, L. Ristori, A. Savoy-Navarro⁶⁸, B. Schneider, E. Sexton-Kennedy, A. Soha, W.J. Spalding, L. Spiegel, S. Stoynev, J. Strait, N. Strobbe, L. Taylor, S. Tkaczyk, N.V. Tran, L. Uplegger, E.W. Vaandering, C. Vernieri, M. Verzocchi, R. Vidal, M. Wang, H.A. Weber, A. Whitbeck

University of Florida, Gainesville, USA

D. Acosta, P. Avery, P. Bortignon, D. Bourilkov, A. Brinkerhoff, L. Cadamuro, A. Carnes, D. Curry, R.D. Field, S.V. Gleyzer, B.M. Joshi, J. Konigsberg, A. Korytov, K.H. Lo, P. Ma, K. Matchev, G. Mitselmakher, D. Rosenzweig, K. Shi, D. Sperka, J. Wang, S. Wang, X. Zuo

Florida International University, Miami, USA

Y.R. Joshi, S. Linn

Florida State University, Tallahassee, USA

A. Ackert, T. Adams, A. Askew, S. Hagopian, V. Hagopian, K.F. Johnson, T. Kolberg, G. Martinez, T. Perry, H. Prosper, A. Saha, C. Schiber, R. Yohay

Florida Institute of Technology, Melbourne, USA

M.M. Baarmand, V. Bhopatkar, S. Colafranceschi, M. Hohlmann, D. Noonan, M. Rahmani, T. Roy, F. Yumiceva

University of Illinois at Chicago (UIC), Chicago, USA

M.R. Adams, L. Apanasevich, D. Berry, R.R. Betts, R. Cavanaugh, X. Chen, S. Dittmer, O. Evdokimov, C.E. Gerber, D.A. Hangal, D.J. Hofman, K. Jung, J. Kamin, C. Mills, M.B. Tonjes, N. Varelas, H. Wang, X. Wang, Z. Wu, J. Zhang

The University of Iowa, Iowa City, USA

M. Alhousseini, B. Bilki⁶⁹, W. Clarida, K. Dilsiz⁷⁰, S. Durgut, R.P. Gandrajula, M. Haytmyradov, V. Khristenko, J.-P. Merlo, A. Mestvirishvili, A. Moeller, J. Nachtman, H. Ogul⁷¹, Y. Onel, F. Ozok⁷², A. Penzo, C. Snyder, E. Tiras, J. Wetzel

Johns Hopkins University, Baltimore, USA

B. Blumenfeld, A. Cocoros, N. Eminizer, D. Fehling, L. Feng, A.V. Gritsan, W.T. Hung, P. Maksimovic, J. Roskes, U. Sarica, M. Swartz, M. Xiao, C. You

The University of Kansas, Lawrence, USA

A. Al-bataineh, P. Baringer, A. Bean, S. Boren, J. Bowen, A. Bylinkin, J. Castle, S. Khalil, A. Kropivnitskaya, D. Majumder, W. Mcbrayer, M. Murray, C. Rogan, S. Sanders, E. Schmitz, J.D. Tapia Takaki, Q. Wang

Kansas State University, Manhattan, USA

S. Duric, A. Ivanov, K. Kaadze, D. Kim, Y. Maravin, D.R. Mendis, T. Mitchell, A. Modak, A. Mohammadi

Lawrence Livermore National Laboratory, Livermore, USA

F. Rebassoo, D. Wright

University of Maryland, College Park, USA

A. Baden, O. Baron, A. Belloni, S.C. Eno, Y. Feng, C. Ferraioli, N.J. Hadley, S. Jabeen, G.Y. Jeng, R.G. Kellogg, J. Kunkle, A.C. Mignerey, S. Nabili, F. Ricci-Tam, M. Seidel, Y.H. Shin, A. Skuja, S.C. Tonwar, K. Wong

Massachusetts Institute of Technology, Cambridge, USA

D. Abercrombie, B. Allen, V. Azzolini, A. Baty, G. Bauer, R. Bi, S. Brandt, W. Busza, I.A. Cali, M. D'Alfonso, Z. Demiragli, G. Gomez Ceballos, M. Goncharov, P. Harris, D. Hsu, M. Hu, Y. Iiyama, G.M. Innocenti, M. Klute, D. Kovalskyi, Y.-J. Lee, P.D. Luckey, B. Maier, A.C. Marini, C. Mcginn, C. Mironov, S. Narayanan, X. Niu, C. Paus, C. Roland, G. Roland, Z. Shi, G.S.F. Stephans, K. Sumorok, K. Tatar, D. Velicanu, J. Wang, T.W. Wang, B. Wyslouch

University of Minnesota, Minneapolis, USA

A.C. Benvenuti[†], R.M. Chatterjee, A. Evans, P. Hansen, J. Hiltbrand, Sh. Jain, S. Kalafut, M. Krohn, Y. Kubota, Z. Lesko, J. Mans, N. Ruckstuhl, R. Rusack, M.A. Wadud

University of Mississippi, Oxford, USA

J.G. Acosta, S. Oliveros

University of Nebraska-Lincoln, Lincoln, USA

E. Avdeeva, K. Bloom, D.R. Claes, C. Fangmeier, F. Golf, R. Gonzalez Suarez, R. Kamalieddin, I. Kravchenko, J. Monroy, J.E. Siado, G.R. Snow, B. Stieger

State University of New York at Buffalo, Buffalo, USA

A. Godshalk, C. Harrington, I. Iashvili, A. Kharchilava, C. Mclean, D. Nguyen, A. Parker, S. Rappoccio, B. Roozbahani

Northeastern University, Boston, USA

G. Alverson, E. Barberis, C. Freer, Y. Haddad, A. Hortiangtham, D.M. Morse, T. Orimoto, T. Wamorkar, B. Wang, A. Wisecarver, D. Wood

Northwestern University, Evanston, USA

S. Bhattacharya, J. Bueghly, O. Charaf, T. Gunter, K.A. Hahn, N. Mucia, N. Odell, M.H. Schmitt, K. Sung, M. Trovato, M. Velasco

University of Notre Dame, Notre Dame, USA

R. Bucci, N. Dev, M. Hildreth, K. Hurtado Anampa, C. Jessop, D.J. Karmgard, N. Kellams, K. Lannon, W. Li, N. Loukas, N. Marinelli, F. Meng, C. Mueller, Y. Musienko³⁶, M. Planer, A. Reinsvold, R. Ruchti, P. Siddireddy, G. Smith, S. Taroni, M. Wayne, A. Wightman, M. Wolf, A. Woodard

The Ohio State University, Columbus, USA

J. Alimena, L. Antonelli, B. Bylsma, L.S. Durkin, S. Flowers, B. Francis, C. Hill, W. Ji, T.Y. Ling, W. Luo, B.L. Winer

Princeton University, Princeton, USA

S. Cooperstein, P. Elmer, J. Hardenbrook, S. Higginbotham, A. Kalogeropoulos, D. Lange, M.T. Lucchini, J. Luo, D. Marlow, K. Mei, I. Ojalvo, J. Olsen, C. Palmer, P. Piroué, J. Salfeld-Nebgen, D. Stickland, C. Tully, Z. Wang

University of Puerto Rico, Mayaguez, USA

S. Malik, S. Norberg

Purdue University, West Lafayette, USA

A. Barker, V.E. Barnes, S. Das, L. Gutay, M. Jones, A.W. Jung, A. Khatiwada, B. Mahakud, D.H. Miller, N. Neumeister, C.C. Peng, S. Piperov, H. Qiu, J.F. Schulte, J. Sun, F. Wang, R. Xiao, W. Xie

Purdue University Northwest, Hammond, USA

T. Cheng, J. Dolen, N. Parashar

Rice University, Houston, USA

Z. Chen, K.M. Ecklund, S. Freed, F.J.M. Geurts, M. Kilpatrick, W. Li, B.P. Padley, R. Redjimi, J. Roberts, J. Rorie, W. Shi, Z. Tu, A. Zhang

University of Rochester, Rochester, USA

A. Bodek, P. de Barbaro, R. Demina, Y.t. Duh, J.L. Dulemba, C. Fallon, T. Ferbel, M. Galanti, A. Garcia-Bellido, J. Han, O. Hindrichs, A. Khukhunaishvili, E. Ranken, P. Tan, R. Taus

Rutgers, The State University of New Jersey, Piscataway, USA

J.P. Chou, Y. Gershtein, E. Halkiadakis, A. Hart, M. Heindl, E. Hughes, S. Kaplan, R. Kunnawalkam Elayavalli, S. Kyriacou, I. Laflotte, A. Lath, R. Montalvo, K. Nash, M. Osherson, H. Saka, S. Salur, S. Schnetzer, D. Sheffield, S. Somalwar, R. Stone, S. Thomas, P. Thomassen, M. Walker

University of Tennessee, Knoxville, USA

A.G. Delannoy, J. Heideman, G. Riley, S. Spanier

Texas A&M University, College Station, USA

O. Bouhali⁷³, A. Celik, M. Dalchenko, M. De Mattia, A. Delgado, S. Dildick, R. Eusebi, J. Gilmore, T. Huang, T. Kamon⁷⁴, S. Luo, D. Marley, R. Mueller, D. Overton, L. Perniè, D. Rathjens, A. Safonov

Texas Tech University, Lubbock, USA

N. Akchurin, J. Damgov, F. De Guio, P.R. Duderov, S. Kunori, K. Lamichhane, S.W. Lee, T. Mengke, S. Muthumuni, T. Peltola, S. Undleeb, I. Volobouev, Z. Wang

Vanderbilt University, Nashville, USA

S. Greene, A. Gurrola, R. Janjam, W. Johns, C. Maguire, A. Melo, H. Ni, K. Padeken, F. Romeo, J.D. Ruiz Alvarez, P. Sheldon, S. Tuo, J. Velkovska, M. Verweij, Q. Xu

University of Virginia, Charlottesville, USA

M.W. Arenton, P. Barria, B. Cox, R. Hirosky, M. Joyce, A. Ledovskoy, H. Li, C. Neu, T. Sinthuprasith, Y. Wang, E. Wolfe, F. Xia

Wayne State University, Detroit, USA

R. Harr, P.E. Karchin, N. Poudyal, J. Sturdy, P. Thapa, S. Zaleski

University of Wisconsin - Madison, Madison, WI, USA

M. Brodski, J. Buchanan, C. Caillol, D. Carlsmith, S. Dasu, I. De Bruyn, L. Dodd, B. Gomber, M. Grothe, M. Herndon, A. Hervé, U. Hussain, P. Klabbers, A. Lanaro, K. Long, R. Loveless, T. Ruggles, A. Savin, V. Sharma, N. Smith, W.H. Smith, N. Woods

†: Deceased

1: Also at Vienna University of Technology, Vienna, Austria

2: Also at IRFU, CEA, Université Paris-Saclay, Gif-sur-Yvette, France

3: Also at Universidade Estadual de Campinas, Campinas, Brazil

4: Also at Federal University of Rio Grande do Sul, Porto Alegre, Brazil

5: Also at Université Libre de Bruxelles, Bruxelles, Belgium

6: Also at University of Chinese Academy of Sciences, Beijing, China

7: Also at Institute for Theoretical and Experimental Physics, Moscow, Russia

8: Also at Joint Institute for Nuclear Research, Dubna, Russia

9: Also at Fayoum University, El-Fayoum, Egypt

10: Now at British University in Egypt, Cairo, Egypt

11: Now at Helwan University, Cairo, Egypt

12: Also at Department of Physics, King Abdulaziz University, Jeddah, Saudi Arabia

13: Also at Université de Haute Alsace, Mulhouse, France

14: Also at Skobeltsyn Institute of Nuclear Physics, Lomonosov Moscow State University, Moscow, Russia

15: Also at Tbilisi State University, Tbilisi, Georgia

16: Also at CERN, European Organization for Nuclear Research, Geneva, Switzerland

17: Also at RWTH Aachen University, III. Physikalisches Institut A, Aachen, Germany

18: Also at University of Hamburg, Hamburg, Germany

19: Also at Brandenburg University of Technology, Cottbus, Germany

20: Also at Institute of Physics, University of Debrecen, Debrecen, Hungary

21: Also at Institute of Nuclear Research ATOMKI, Debrecen, Hungary

22: Also at MTA-ELTE Lendület CMS Particle and Nuclear Physics Group, Eötvös Loránd University, Budapest, Hungary

- 23: Also at Indian Institute of Technology Bhubaneswar, Bhubaneswar, India
- 24: Also at Institute of Physics, Bhubaneswar, India
- 25: Also at Shoolini University, Solan, India
- 26: Also at University of Visva-Bharati, Santiniketan, India
- 27: Also at Isfahan University of Technology, Isfahan, Iran
- 28: Also at Plasma Physics Research Center, Science and Research Branch, Islamic Azad University, Tehran, Iran
- 29: Also at Università degli Studi di Siena, Siena, Italy
- 30: Also at Scuola Normale e Sezione dell'INFN, Pisa, Italy
- 31: Also at Kyunghee University, Seoul, Korea
- 32: Also at International Islamic University of Malaysia, Kuala Lumpur, Malaysia
- 33: Also at Malaysian Nuclear Agency, MOSTI, Kajang, Malaysia
- 34: Also at Consejo Nacional de Ciencia y Tecnología, Mexico City, Mexico
- 35: Also at Warsaw University of Technology, Institute of Electronic Systems, Warsaw, Poland
- 36: Also at Institute for Nuclear Research, Moscow, Russia
- 37: Now at National Research Nuclear University 'Moscow Engineering Physics Institute' (MEPhI), Moscow, Russia
- 38: Also at St. Petersburg State Polytechnical University, St. Petersburg, Russia
- 39: Also at University of Florida, Gainesville, USA
- 40: Also at P.N. Lebedev Physical Institute, Moscow, Russia
- 41: Also at California Institute of Technology, Pasadena, USA
- 42: Also at Budker Institute of Nuclear Physics, Novosibirsk, Russia
- 43: Also at Faculty of Physics, University of Belgrade, Belgrade, Serbia
- 44: Also at INFN Sezione di Pavia ^a, Università di Pavia ^b, Pavia, Italy
- 45: Also at University of Belgrade, Faculty of Physics and Vinca Institute of Nuclear Sciences, Belgrade, Serbia
- 46: Also at National and Kapodistrian University of Athens, Athens, Greece
- 47: Also at Riga Technical University, Riga, Latvia
- 48: Also at Universität Zürich, Zurich, Switzerland
- 49: Also at Stefan Meyer Institute for Subatomic Physics (SMI), Vienna, Austria
- 50: Also at Gaziosmanpasa University, Tokat, Turkey
- 51: Also at Adiyaman University, Adiyaman, Turkey
- 52: Also at Istanbul Aydin University, Istanbul, Turkey
- 53: Also at Mersin University, Mersin, Turkey
- 54: Also at Piri Reis University, Istanbul, Turkey
- 55: Also at Ozyegin University, Istanbul, Turkey
- 56: Also at Izmir Institute of Technology, Izmir, Turkey
- 57: Also at Marmara University, Istanbul, Turkey
- 58: Also at Kafkas University, Kars, Turkey
- 59: Also at Istanbul University, Faculty of Science, Istanbul, Turkey
- 60: Also at Istanbul Bilgi University, Istanbul, Turkey
- 61: Also at Hacettepe University, Ankara, Turkey
- 62: Also at Rutherford Appleton Laboratory, Didcot, United Kingdom
- 63: Also at School of Physics and Astronomy, University of Southampton, Southampton, United Kingdom
- 64: Also at Monash University, Faculty of Science, Clayton, Australia
- 65: Also at Bethel University, St. Paul, USA
- 66: Also at Karamanoğlu Mehmetbey University, Karaman, Turkey
- 67: Also at Utah Valley University, Orem, USA

68: Also at Purdue University, West Lafayette, USA

69: Also at Beykent University, Istanbul, Turkey

70: Also at Bingol University, Bingol, Turkey

71: Also at Sinop University, Sinop, Turkey

72: Also at Mimar Sinan University, Istanbul, Istanbul, Turkey

73: Also at Texas A&M University at Qatar, Doha, Qatar

74: Also at Kyungpook National University, Daegu, Korea